Neuroscience

Somatotopic organization among parallel sensory pathways that promote a grooming sequence in *Drosophila*

Katharina Eichler, Stefanie Hampel, Adrián Alejandro-García, Steven A. Calle-Schuler, Alexis Santana-Cruz, Lucia Kmecova, Jonathan M. Blagburn, Eric D. Hoopfer, Andrew M. Seeds

Institute of Neurobiology, University of Puerto Rico-Medical Sciences Campus, San Juan, Puerto Rico • Neuroscience Program, Carleton College, Northfield, Minnesota

https://en.wikipedia.org/wiki/Open_access

Copyright information

Reviewed Preprint

Revised by authors after peer review.

About eLife's process

Reviewed preprint version 2
March 22, 2024 (this version)

Reviewed preprint version 1
May 31, 2023

Posted to preprint server
April 4, 2023

Sent for peer review
March 29, 2023

Abstract

Mechanosensory neurons located across the body surface respond to tactile stimuli and elicit diverse behavioral responses, from relatively simple stimulus location-aimed movements to complex movement sequences. How mechanosensory neurons and their postsynaptic circuits influence such diverse behaviors remains unclear. We previously discovered that *Drosophila* perform a body location-prioritized grooming sequence when mechanosensory neurons at different locations on the head and body are simultaneously stimulated by dust (Hampel et al., 2017; Seeds et al., 2014). Here, we identify nearly all mechanosensory neurons on the *Drosophila* head that individually elicit aimed grooming of specific head locations, while collectively eliciting a whole head grooming sequence. Different tracing methods were used to reconstruct the projections of these neurons from different locations on the head to their distinct arborizations in the brain. This provides the first synaptic resolution somatotopic map of a head, and defines the parallel-projecting mechanosensory pathways that elicit head grooming.

eLife assessment

This **valuable** work provides a near-complete description of the mechanosensory bristles on the *Drosophila melanogaster* head and the anatomy and projection patterns of the bristle mechanosensory neurons that innervate them. The data presented are **solid**. The study has generated numerous resources for the community that will be of interest to neuroscientists in the field of circuits and behaviour, particularly those interested in mechanosensation and behavioural sequence generation.

Introduction

The ability to produce complex behaviors by assembling sequences of different movements is essential for purposeful behavior and survival. One prominent model that describes how the brain produces movement sequences is called a “parallel model”. This model proposes that the premotor elements of different movements to be executed in sequence are activated (or readied) in parallel and then selected sequentially through a mechanism where movements occurring earlier in the sequence suppress later ones (Bohland et al., 2010; Bullock, 2004; Houghton and Hartley, 1995; Lashley, 1951). A hallmark feature of this model is a parallel circuit architecture that ensures all mutually exclusive actions to be performed in sequence are simultaneously readied and competing for output. Performance order is established by hierarchical suppression among the parallel circuits, where earlier actions suppress later actions. This architecture is supported by physiological and behavioral evidence from the movement sequences of different animals (Averbeck et al., 2002; Mushiake et al., 2006; Seeds et al., 2014). Yet, despite some movement sequences exhibiting features consistent with the parallel model, we lack an organizational and mechanistic understanding of the underlying neural circuits.

The grooming behavior of fruit flies (*Drosophila melanogaster*) can be studied to define the circuit mechanisms that produce movement sequences. Making flies dirty by coating them in dust elicits a grooming sequence that starts with the cleaning of different locations on the head, such as the eyes, antennae, and proboscis, and proceeds to body locations, such as the abdomen, wings, and thorax (Mueller et al., 2019; Phillis et al., 1993; Seeds et al., 2014). We previously determined that the sequence is produced by a mechanism that is consistent with a parallel model (Seeds et al., 2014). The sequence begins when different aimed grooming movements that clean specific locations of the head or body become activated in parallel by dust. The resulting competition among mutually exclusive grooming movements is resolved through hierarchical suppression. For example, grooming of the eyes occurs first because eye grooming suppresses grooming of other locations on the head and body. This parallel model of hierarchical suppression provides a conceptual framework for dissecting the neural circuit architecture that produces *Drosophila* grooming (**Figure 1 – figure supplement 1A,B**). Here, we focus on the organization of the sensory inputs in the hypothesized architecture (Seeds et al., 2014), the parallel mechanosensory neurons that detect dust at different locations and elicit aimed grooming movements.

Different mechanosensory structures are distributed across the head and body surface that respond to mechanical stimuli and elicit grooming. The most abundant of these structures are mechanosensory bristles (aka hairs or setae). Tactile displacement of individual bristles elicits grooming movements in which the legs are precisely aimed at the stimulus location (Corfas and Dudai, 1989; Page and Matheson, 2004; Vandervorst and Ghysen, 1980). Each bristle is innervated by a single *bristle mechanosensory neuron* (BMN) that is excited by displacement of that bristle (Corfas and Dudai, 1990; Tuthill and Wilson, 2016a; Walker, 2000). Thus, bristles and their corresponding BMNs can be ascribed to specific, aimed leg grooming movements. Other mechanosensory structures, including chordotonal organs and stretch receptors, also elicit stimulus location-aimed grooming (Hampel et al., 2017; Zhang et al., 2020). Simultaneous (parallel) optogenetic activation of mechanosensory neurons across the body elicits a grooming sequence that proceeds in the same order as the “natural” dust-induced sequence (Hampel et al., 2017; Zhang et al., 2020). Thus, the sequence is elicited by parallel mechanosensory pathways that each produce a movement that grooms a specific location on the head or body (**Figure 1 – figure supplement 1A,B**).

BMNs project their axons from different locations on the head or body, through different nerves, and into the *central nervous system* (CNS). Previous studies of BMNs from different body locations demonstrated that they show somatotopic organization in their CNS projections (Johnson and Murphey, 1985; Murphey et al., 1989b; Newland, 1991; Newland et al., 2000; Tsubouchi et

al., 2017). That is, particular projection zones in the CNS correspond to specific body locations. Somatotopic organization among mechanosensory neurons and their postsynaptic circuits is consistent with the parallel model that underlies the body grooming sequence (Seeds et al., 2014). In this model, parallel-projecting mechanosensory neurons that respond to stimuli at specific locations on the head or body could connect with somatotopically-organized parallel circuits that elicit grooming of those locations (**Figure 1 – figure supplement 1A-C**). The previous discovery of a mechanosensory-connected circuit that elicits aimed grooming of the antennae provides evidence of this organization (Hampel 2015). However, the extent to which distinct circuits elicit grooming of other locations is unknown, in part, because the somatotopic projections of the mechanosensory neurons have not been comprehensively defined for the head or body.

Here, we comprehensively map the somatotopic organization among BMNs that elicit grooming of different locations on the head. *Drosophila* use their front legs to groom their heads in a sequence that starts with the eyes and proceeds to other locations, such as the antennae and proboscis (Seeds et al., 2014). Two mechanosensory structures on the head (i.e. chordotonal organs and bristles) are implicated in grooming. The antennal *Johnston's organ* (JO) is a chordotonal organ containing mechanosensory neurons called *JO neurons* (JONs) that detect stimulations of the antennae and elicit aimed grooming (Hampel et al., 2015, 2020a). There are over 1,000 bristles located on the head whose stimulation we postulated could also elicit aimed grooming of different head locations. In support of this, BMNs innervating bristles on the eyes were previously shown to elicit grooming of the eyes (Hampel et al., 2017; Zhang et al., 2020). Here, we use optogenetic tools to show that activation of subsets of BMNs at other head locations also elicits aimed grooming. We use transgenic expression, dye fills, and electron microscopy (EM) reconstructions to trace the projections of nearly all BMNs on the head, from their bristles, through their respective nerves, and into the CNS. This reveals somatotopic organization, where BMNs innervating neighboring head bristles project to overlapping zones in the CNS while those innervating distant bristles project to distinct zones. Analysis of head BMN postsynaptic connectivity reveals that neighboring BMNs show higher connectivity similarity than distant BMNs, providing evidence of somatotopically organized postsynaptic circuit pathways. This provides a comprehensive synaptic resolution projection map of head mechanosensory neurons, and further defines the organization of parallel mechanosensory pathways that elicit sequential grooming.

Results

Classification and quantification of the head bristles

A prerequisite for determining the somatotopy of head BMNs was to define the locations of their respective bristles on the head. Different populations of bristles are located on the eyes, antennae, proboscis, and other areas on the head. While the identities of most of these populations were known (Bodenstein et al., 1994), some were poorly described and their bristle numbers were not reported. Therefore, we imaged the bristles on the head and then classified and quantified each population. We developed a unified nomenclature for the different bristle populations that was based partially on published nomenclature. Most of the bristles were easily observed by imaging white light-illuminated heads (**Figure 1A-D**), and color-coded depth maps further helped to distinguish between bristles while they were being counted (**Figure 1 – figure supplement 2A-H**). Some bristles could not be counted from these images because of their small size, position on the head, or because they could not be distinguished from one another (**Figure 1E**, asterisk with bristle number range). Therefore, we used confocal microscopy images, or referred to published work to estimate or obtain the numbers of bristles in these populations (see Materials and methods).

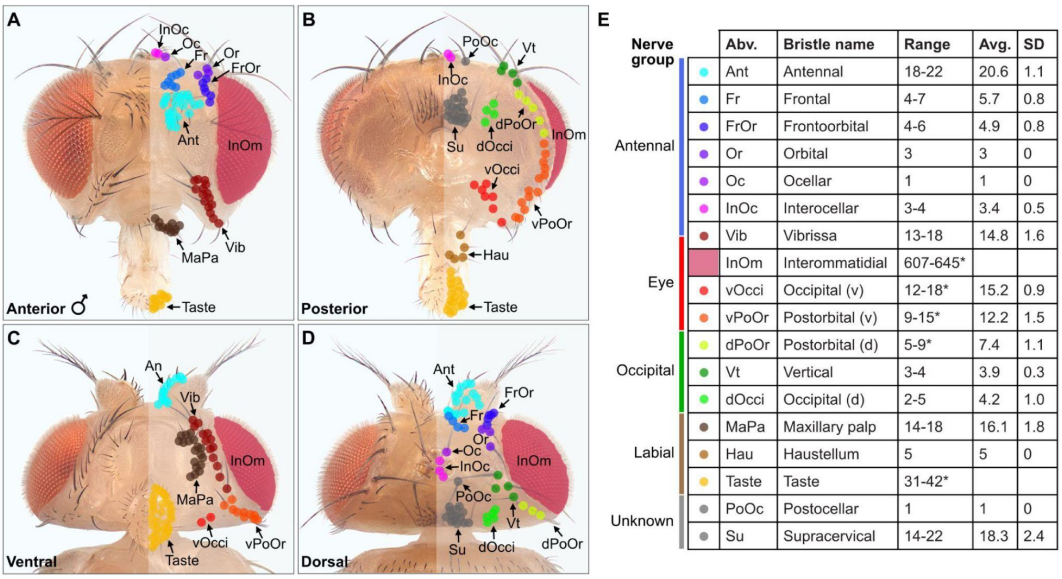

	Abv.	Bristle name	Range	Avg.	SD
Antennal	Ant	Antennal	18-22	20.6	1.1
	Fr	Frontal	4-7	5.7	0.8
	FrOr	Frontoorbital	4-6	4.9	0.8
	Or	Orbital	3	3	0
	Oc	Ocellar	1	1	0
	InOc	Interocellar	3-4	3.4	0.5
	Vib	Vibrissa	13-18	14.8	1.6
Eye	InOm	Interommatidial	607-645*		
	vOcci	Occipital (v)	12-18*	15.2	0.9
	vPoOr	Postorbital (v)	9-15*	12.2	1.5
Occipital	dPoOr	Postorbital (d)	5-9*	7.4	1.1
	Vt	Vertical	3-4	3.9	0.3
	dOcci	Occipital (d)	2-5	4.2	1.0
Labial	MaPa	Maxillary palp	14-18	16.1	1.8
	Hau	Haustellum	5	5	0
	Taste	Taste	31-42*		
Unknown	PoOc	Postocellar	1	1	0
	Su	Supracervical	14-22	18.3	2.4

Figure 1.

Classification and quantification of *Drosophila melanogaster* head bristles.

(**A-D**) Bristles on the anterior (**A**), posterior (**B**), ventral (**C**), and dorsal (**D**) male head. The bristles on the right half are marked with color-coded dots to indicate their classification. Bristle names are abbreviated (Abv.), and full names and color codes are listed in (**E**). (**E**) Quantification of bristle populations on the male head (per half). Range indicates the lowest and highest number of bristles counted across individuals for each population (N=8). Bristle number average (Avg.) and standard deviation (SD) across individuals for each population are shown. Bristle counting was facilitated using color-coded depth maps (examples shown in **Figure 1 – figure supplement 2**). Quantification of bristles on female heads and male/female comparisons are shown in **Figure 1 – figure supplement 3**. See **Supplementary file 1** for bristle counts for each head and **Supplementary file 2** for image stack download links for each head. *InOm and Taste bristle number ranges are based on published data while dPoOr, vPoOr, and vOcci bristles were counted using confocal microscopy (see Materials and methods). Bristles are organized into nerve groups based on the nerve each bristle's corresponding bristle mechanosensory neuron (BMN) projects through to enter the brain (evidence shown in **Figure 2**). Dorsal (d) and Ventral (v).

We next produced a map of the different bristles at their stereotyped locations on the head, and determined how the numbers of bristles in each population varied across individual flies (**Figure 1A-E**). By counting the bristles on both male and female heads, we found no significant gender-based differences in their numbers (**Figure 1 – figure supplement 3A-E**, see **Supplementary file 1** for bristle counts for each head, see **Supplementary file 2** for head image downloads). Given that the bristles are singly innervated (Tuthill and Wilson, 2016b), we could use the bristle counts to estimate the number of BMNs for each bristle population. This provided a framework for us to define the somatotopic projections of BMNs that innervate particular bristles.

Light microscopy-based reconstruction of BMNs innervating the head bristles

BMNs project from bristles at specific head locations and then through their respective nerves to enter the brain. While the nerve projections of BMNs innervating bristles on the eyes, proboscis, and antennae were previously reported (Hampel et al., 2017; Homberg et al., 1989; Melzig et al., 1996; Singh and Nayak, 1985; Stocker, 1994), the projections of BMNs innervating other head bristles were unknown. We determined these projections using a transgenic driver line (R52A06-GAL4) that labels BMNs on the head (Hampel et al., 2017). R52A06-GAL4 was used to express membrane-targeted *green fluorescent protein* (mCD8::GFP), and the anterior and posterior head was imaged with a confocal microscope (see **Supplementary file 2** for confocal Z-stack downloads). The GFP-labeled neurons had all the characteristic morphological features of BMNs (Tuthill and Wilson, 2016b), including a dendrite innervating a bristle, a cell body, and an axon (**Figure 2A,B**). R52A06-GAL4 labeled almost all BMNs on the head, but did not label any associated with the *postocellar* (PoOc) or *supracervical* (Su) bristles (**Figure 2 – figure supplement 1A-H**). We used the software neuTube (Feng et al., 2015) to reconstruct the GFP-labeled projections of head BMNs from confocal Z-stacks (**Figure 2C-H**). The reconstructions enabled us to classify the BMNs into 'nerve groups', based on the nerves they project through to enter the brain (**Figure 2I,J**, groups listed in **Figure 1E**). This revealed that BMNs innervating bristles at different locations on the head project through specific nerves, including the antennal, eye, occipital, and labial nerves. Below we introduce the BMNs in each nerve group and the bristles that they innervate.

Head BMNs project to the brain through specific nerves

BMNs innervating the 18-22 *antennal* (Ant) bristles were previously reported to project through the *antennal nerve* (AntNv) that also carries the axons of JONs and olfactory neurons (Homberg et al., 1989; Melzig et al., 1996). We identified additional BMNs projecting through the AntNv that innervate bristles located on the anterior and dorsal head (**Figure 2E,I**, blue). These include 4-7 *frontal* (Fr) bristles located medially, 3 *orbital* (Or) and 4-6 *frontoorbital* (FrOr) bristles located laterally, and 1 *ocellar* (Oc) and 3-4 *interocellar* (InOc) bristles located on the dorsal head. BMNs projecting from these bristles form a bundle below the cuticle that projects ventrally to join the AntNv. We also identified BMNs that innervate 1-3 of the small anterior *vibrissae* (Vib) on the ventral head whose axons project dorsally to join the AntNv.

BMNs innervating bristles on the dorsal half of the posterior head project through a previously undescribed nerve that we named the *occipital nerve* (OcciNv) (**Figure 2F,J**, green). This includes the 3-4 *vertical* (Vt), 2-5 *dorsal occipital* (dOcci), and 5-9 *dorsal postorbital* (dPoOr) bristles. BMNs that innervate these different bristles form the OcciNv that projects under the cuticle ventromedially towards the brain.

Each eye contains between 645 and 828 regularly spaced ommatidia, many of which have an associated *interommatidial* (InOm) bristle (Ready et al., 1976). We estimated that there are between 607 and 645 InOm bristles on each eye based on published data (see Materials and methods). BMNs that innervate the InOm bristles were previously found to form a nerve that

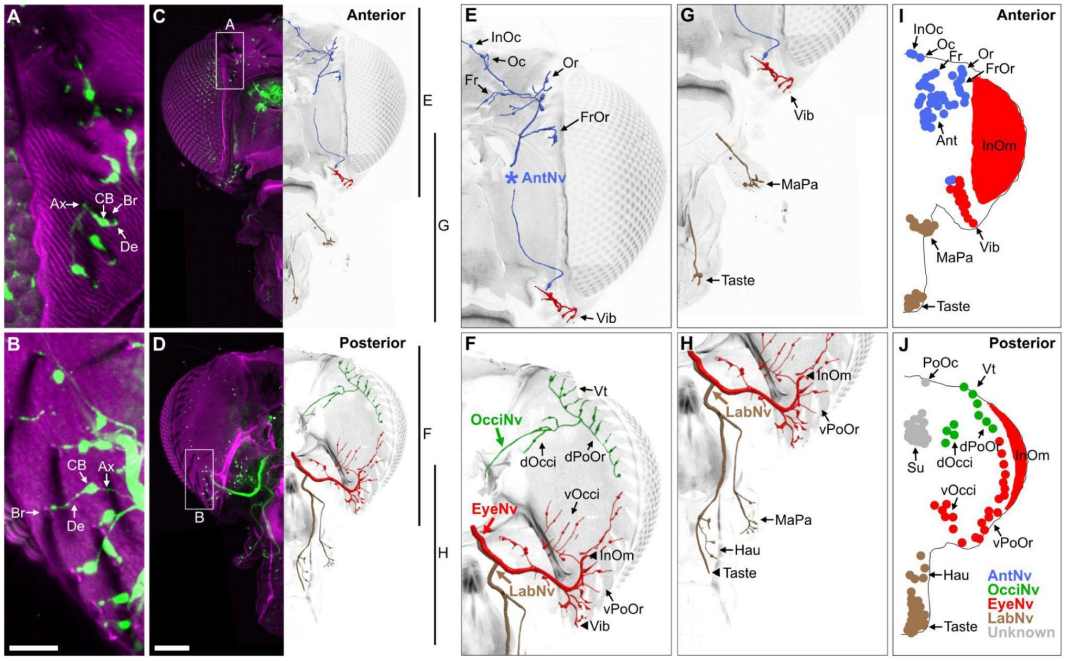

Figure 2.

BMNs on the head project through specific nerves.

(**A-D**) Confocal Z-stack maximum intensity projections of the anterior (**A,C**) and posterior (**B,D**) head in which the driver line R52A06-GAL4 drives expression of GFP in BMNs (green). Cuticle is magenta. (**A,B**) Magnified views of the boxed areas indicated in **C** and **D**. The *dendrite* (De), *axon* (Ax), *cell body* (CB), and innervated *bristle* (Br) of a BMN are indicated in each panel. (**C,D**) The left half of the head is shown as a maximum projection, while Z-stack-reconstructed BMNs are shown for the right half. Maximum projections of the right half of the head is shown in **Figure 2 – figure supplement 1A-F**. (**E-H**) Magnified images of the reconstructions. The magnified areas are indicated by vertical lines on the right in **C** and **D**. Reconstructed BMNs are color-coded and labeled according to the nerve that they project through: AntNv (blue); OcciNv (green); EyeNv (red); LabNv (brown). Unreconstructed portion of the antennal nerve is indicated by an asterisk. Innervated bristles are indicated with black arrows. Black arrowheads in **F** and **H** indicate partially reconstructed axons of BMNs innervating the InOm, Vib, and Taste bristles. Scale bars: 25 μm (**B**), 100 μm (**D**). (**I,J**) Summary of bristles innervated by BMNs that belong to particular nerve groups on the anterior (**I**) and posterior (**J**) head. Nerve groups also listed in **Figure 1E**. **Supplementary file 2** provides confocal Z-stack download links.

projects to the brain from the posterior head (Hampel et al., 2017). Because this nerve was not previously named, it is referred to here as the *eye nerve* (EyeNv). We found that the EyeNv also carries the projections of BMNs innervating bristles on the posterior and ventral head (**Figure 2E-J**, red). Those on the posterior head innervate the 12-18 *ventral occipital* (vOcci) and 9-15 *ventral postorbital* (vPoOr) bristles. Those on the ventral head innervate most of the 13-18 Vib bristles.

The proboscis has bristles on the labellum, haustellum, and maxillary palps. Each half of the labellum has 31-42 *Taste* bristles whose associated BMNs project through the *labial nerve* (LabNv) (Falk et al., 1976; Jeong et al., 2016; Nayak and Singh, 1983; Shanbhag et al., 2001; Stocker, 1994). The LabNv also carries mechanosensory neurons innervating the labellar taste pegs, along with gustatory neurons innervating either the taste pegs or taste bristles (Stocker and Schorderet, 1981). We found that BMNs innervating the 5 *haustellum* (Hau) bristles also project through the LabNv (**Figure 2H,J**, brown). BMNs that innervate the 14-18 *maxillary palp* (MaPa) bristles project through the *maxillary nerve* (MaxNv) that also carries the axons of olfactory neurons (Singh and Nayak, 1985). The Lab- and MaxNvs merge as they approach the head, and in this work we refer to the merged nerve as the LabNv. The LabNv then merges with the EyeNv in the ventral head, suggesting that these nerves project into the brain at the same location (**Figure 2H**).

Head BMNs project into discrete zones in the ventral brain

BMNs in the Ant-, Eye-, and LabNvs were previously reported to project into a region of the ventral brain called the *subesophageal zone* (SEZ) (**Figure 3A,B**) (Hampel et al., 2017; Jeong et al., 2016; Kamikouchi et al., 2006; Mitchell et al., 1999; Singh and Nayak, 1985; Stocker, 1994). To determine if all head BMNs project into the SEZ, we used R52A06-GAL4 to label their projections in a dissected brain (**Figure 3C**, see **Supplementary file 2** for confocal Z-stack download). The AntNv was identified in the R52A06-GAL4 pattern based on its reported dorsal-arriving projection into the SEZ (Kamikouchi et al., 2006; Stocker, 1994), while the Eye- and LabNvs were identified based on their reported ventral-arriving projections (Hampel et al., 2017; Stocker, 1994). We found that the Eye- and LabNvs project into the ventral SEZ at the same location (**Figure 3C**), consistent with the observation that they merge as they approach the brain (**Figure 2F,H**). We tentatively identified the OcciNv projecting into the SEZ from a lateral direction, revealing that all head BMN nerves project into the SEZ (**Figure 3C**). R52A06-GAL4 also labels the antennal chordotonal JONs that are known to project through the AntNv into a dorsal region of the SEZ (Hampel et al., 2017, 2020a; Kamikouchi et al., 2006; Kim et al., 2020). Visualization of JONs and BMNs in the same expression pattern revealed that most of the BMNs project into more ventral regions of the SEZ than the JONs (**Figure 3C**).

We next used different transgenic driver lines that express in specific populations of head BMNs to independently label and visualize the different nerves (**Figure 3D-I**, **Figure 3 – figure supplement 1A-D**, see **Supplementary file 2** for confocal Z-stack downloads). The EyeNv was labeled using a previously identified driver line (VT017251-LexA) that expresses in BMNs innervating the InOm bristles (**Figure 3D**) (Hampel et al., 2017). Here, we refer to this line as InOmBMN-LexA. We also used a screening approach to produce three new Split GAL4 (spGAL4) combinations that express in BMNs innervating bristles at other locations on the head (see Materials and methods). One line named dBMN-spGAL4 labels BMNs innervating some dorsally located bristles (InOc, Vt, and dPoOr) that project through the Ant- and OcciNvs (**Figure 3E**). Another line named pBMN-spGAL4 labels BMNs innervating bristles on the posterior head (Vt, dOcci, dPoOr, and vOcci) that project through the Occi- and EyeNvs (**Figure 3F**). The third line named TasteBMN-spGAL4 labels BMNs innervating Taste bristles on the labellum that project through the LabNv (**Figure 3G**). These driver lines each provided independent labeling of one or two different nerves (**Figure 3H**).

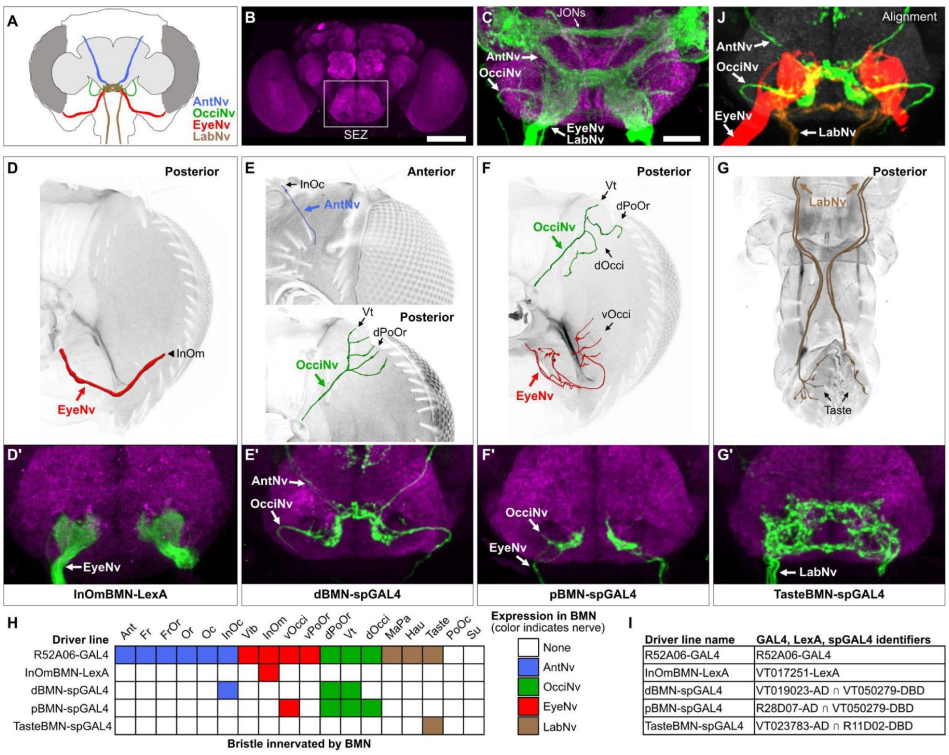

Figure 3.

Head BMNs project into the ventral brain region called the subesophageal zone (SEZ).

(**A**) Schematic of BMNs projecting from different nerves into the SEZ. (**B**) Anterior view of the brain immunostained for Bruchpilot (magenta) to visualize the neuropile. White box indicates the SEZ. Scale bar, 100 µm. (**C**) Image of the SEZ in which R52A06-GAL4 expressed GFP in BMNs and JONs. Brains were immunostained for GFP (green) and Bruchpilot (magenta). BMN nerves and JONs are labeled. Scale bar, 25 µm. (**D-G**) Driver lines that label BMNs from different nerves. Reconstructed BMNs on half of the head that are labeled by the following driver lines: InOmBMN-LexA (**D**), dBMN-spGAL4 (**E**), pBMN-spGAL4 (**F**), and TasteBMN-spGAL4 (whole proboscis shown) (**G**). Images of the heads used for each reconstruction are shown in **Figure 3 – figure supplement 1A-D**. Reconstructed neurons are color-coded and labeled as described in **Figure 2**. (**D'-G'**) SEZ projections of BMNs from both halves of the head that are labeled by InOmBMN-LexA (**D'**), dBMN-spGAL4 (**E'**), pBMN-spGAL4 (**F'**), and TasteBMN-spGAL4 (**G'**). (**H**) Table of BMNs innervating specific bristles that are labeled by each driver line, indicated by box shading (numbers of labeled BMNs innervating different bristles shown in **Figure 3 – figure supplement 1E**). Shade color indicates the nerve that each BMN projects through. (**I**) Driver line names and identifiers. (**J**) Shown in the upper right corner of the figure are the aligned expression patterns of InOmBMN-LexA (red), dBMN-spGAL4 (green), and TasteBMN-spGAL4 (brown). **Supplementary file 2** provides confocal Z-stack download links.

Consistent with what we observed using R52A06-GAL4, each driver line labeled BMNs that projected into the SEZ and no other regions of the brain or *ventral nerve cord* (VNC) (**Figure 3D'-G'**, **Figure 3 – figure supplement 1A'-D'**, see **Supplementary file 2** for confocal Z-stack downloads). dBMN-spGAL4 and pBMN-spGAL4 both labeled the OcciNv that was found to project into the SEZ from a lateral direction (**Figure 3E',F'**), in agreement with what we observed in the R52A06-GAL4 pattern (**Figure 3C**). A comparison of the nerves labeled by the different driver lines revealed that each nerve has morphologically distinct projections. To further visualize the spatial relationships between these projections, we computationally aligned the expression patterns of the different driver lines into the same brain space (**Figure 3J**, upper right corner). Indeed, BMNs from different nerves were found to project into distinct zones of the ventral SEZ. However, we also observed potential zones where overlap could occur between the projections of BMNs from different nerves (discussed more below).

Brain projections of BMNs that innervate specific head bristles

Our results suggested that different BMN "types" innervate specific populations of bristles on the head and project into distinct zones in the SEZ. However, it was unclear to what extent BMNs of the same type projected to the same zones, and if other BMN types had distinct or overlapping projections. Therefore, we next compared the projections of individual BMNs from different populations of bristles.

The head contains different sized bristles, ranging from large Vt bristles on the dorsal head, to small vOcci bristles on the posterior head. We performed dye fills to label individual BMNs that innervate the largest bristles. This was done by modifying a previously published method for filling BMNs innervating bristles on the thorax (Kays et al., 2014). In the modified method, a particular bristle was plucked from the head and a small volume of dye (DiD) pipetted into the exposed socket containing the dendrite of the associated BMN. The dye then diffused into the neuron, and its projection morphology in the brain was imaged using a confocal microscope (experiment schematic and example fills shown in **Figure 4 – figure supplement 1A-E**). This method was particularly amenable to large bristles that were relatively easy to pluck. We successfully filled individual BMNs that innervate the Oc, Or, Ant, Vib, and Vt bristles (**Figure 4A-Q**, see **Supplementary file 2** for confocal Z-stack downloads). The BMNs were named based on the bristle populations that they innervate. For example, BMNs that innervate the Ant bristles were named *bristle mechanosensory Ant neurons* (BM-Ant neurons).

The large bristles are invariant in number and location across individuals (**Figure 1A-E**). For example, all flies have one Oc bristle on each half of the head that is always in the same location. We therefore performed dye fills on the same bristles from multiple different heads. This revealed that BMNs innervating the same bristle have the same general projection morphology across individual flies (**Figure 4 – figure supplements 2-5**). We also performed dye fills on different bristles from the same population, such as the Ant 1, Ant 2, Ant 3, and Ant 4 bristles (**Figure 4 – figure supplement 3A-M**). BMNs innervating the same populations were found to have similar projections. For example, BM-Ant neurons all showed similar ipsilateral and midline projecting branches (**Figure 4G-J**). Morphological similarity among BMNs innervating the same bristle populations was also observed for the BM-Or (**Figure 4D-F**), -Vib (**Figure 4K-N**), and -Vt (**Figure 4O-Q**) neurons.

While BMNs innervating the largest bristles could be labeled using dye fills, we could not label BMNs innervating small bristles using this method. Therefore, we used the *multicolor flipout* (MCFO) method (Nern et al., 2015) to stochastically label individual BMNs innervating bristles within the expression patterns of the driver lines shown in **Figure 3E'-G'**. This enabled us to determine the morphologies of BMNs that innervate the InOc, dOcci, dPoOr, vOcci, and Taste bristles (**Figure 4R-V**, see **Supplementary file 2** for confocal Z-stack downloads). Unlike the dye-filled BMNs, the MCFO-labeled BMNs could not be matched to specific bristles within a population (e.g. Ant 1 or Ant 2), but only to a specific population (e.g. Ant). In agreement with what we

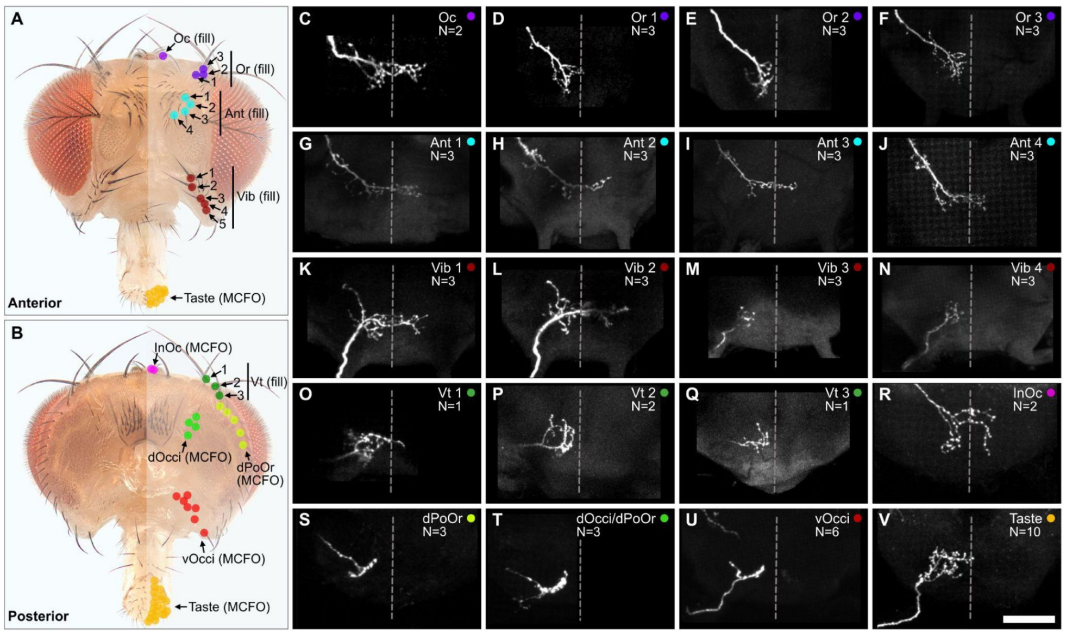

Figure 4.

Projections of BMNs that innervate specific head bristles.

(**A,B**) Bristles on the anterior (**A**) and posterior (**B**) head whose associated BMNs were labeled using dye fill (**C-Q**, fill) or multicolor flipout (**R-V**, MCFO) techniques. (**C-V**) SEZ projections of individual BMNs that innervate the bristle indicated in the upper right corner (anterior view). BMNs are oriented as if they are projecting from the right side of the head. Dotted line indicates approximate SEZ midline. Scale bar, 50 µm. (**C-Q**) BMNs labeled by dye filling. Schematic of the filling technique and whole brain examples shown in **Figure 4 – figure supplement 1**. Filled BMNs innervate the Oc (**C**), Or (**D-F**), Ant (**G-J**), Vib (**K-N**), and Vt (**O-Q**) bristles. All fill trials for the different bristles are shown in **Figure 4 – figure supplement 2**, **Figure 4 – figure supplement 3**, **Figure 4 – figure supplement 4**, and **Figure 4 – figure supplement 5**. (**R-V**) MCFO-labeled BMNs innervate the InOc (**R**), dPoOr (**S**), dOcci/dPoOr (**T**), vOcci (**U**), and Taste (**V**) bristles. BMNs were MCFO labeled using the following driver lines: dBMN-spGAL4 (**R,S**), pBMN-spGAL4 (**T,U**), and TasteBMN-spGAL4 (**V**). All MCFO trials for the different bristles are shown in **Figure 4 – figure supplement 6**, **Figure 4 – figure supplement 7**, and **Figure 4 – figure supplement 8**. The number (N) of fill or MCFO trials obtained for each BMN is indicated in the upper right corner. **Supplementary file 2** provides confocal Z-stack download links.

observed with dye-filled BMNs innervating the same populations of large bristles, the MCFO-labeled BMNs innervating the same populations of small bristles also showed similar projection morphologies (**Figure 4 – figure supplements 6-8**).

We next compared the projections of the dye-filled and MCFO-labeled BMNs (**Figure 4C-V**). This revealed that some BMNs innervating neighboring bristle populations have similar morphologies. For example, BM-InOc and -Oc neurons have similar morphology, including ipsilateral and midline-crossing projections (**Figure 4C,R**), while BM-dPoOr, -dOcci, and -vOcci neurons show similar ipsilateral projections. This suggested that BMNs innervating neighboring head bristle populations show similar morphology and project into overlapping zones in the SEZ.

EM-based reconstruction of the head BMN projections in a full adult brain

We next used a previously reported serial-section EM volume of a *full adult fly brain* (FAFB) to reconstruct the SEZ projections of all head BMNs and produce a comprehensive map of their organization (Zheng et al., 2018). FAFB consists of a brain that was dissected from the head capsule, making it impossible to reconstruct BMNs all the way from their bristles. Instead, the severed Ant-, Occi-, Eye-, and LabNvs were identified in FAFB at the same anatomical locations that we had observed using light microscopy (**Figure 3C,J**, **Figure 5 – figure supplement 1A**). We used the FlyWire.ai platform (Dorkenwald et al., 2023, 2022) to seed all automatically-segmented neurons within the different nerve bundles as they entered the neuropil (left brain hemisphere nerves, **Figure 5 – figure supplement 1B-D**), and the neurons were then fully proofread and edited by human experts to identify their individual morphologies. The morphologies of the majority of the reconstructed neurons matched those of mechanosensory neurons, including BMNs (discussed below), JONs (Hampel et al., 2020a; Kamikouchi et al., 2006; Kim et al., 2020), and labellar taste peg mechanosensory neurons (TPMNs) (Jeong et al., 2016; Miyazaki and Ito, 2010; Zhou et al., 2019) (**Figure 5 – figure supplement 1E**). The remaining neurons included gustatory neurons (Engert et al., 2022), unidentified sensory neurons (**Figure 5 – figure supplement 2A-Y**), and interneurons (not shown).

We identified 705 BMNs among the EM-reconstructed neurons by comparing their SEZ projection morphologies with light microscopy imaged BMNs (**Figure 3C,J**, **Figure 4C-V**). In agreement with the light microscopy data, the reconstructed BMNs project through different nerves into distinct zones in the SEZ (**Figure 5A,B**). For example, BMNs from the Eye- and LabNv have distinct ventral and anterior projections, respectively. This shows how the BMNs are somatotopically organized, as their distinct projections correspond to different bristle locations on the head (**Figure 5B,C**, see *FlyWire.ai link 1* to view the BMN projections in three dimensions).

Matching the reconstructed head BMNs with their bristles

The reconstructed BMN projections were next matched with their specific bristle populations. The projections were clustered based on morphological similarity using the NBLAST algorithm (example clustering at cut height 5 shown in **Figure 6 – figure supplement 1A,B**, **Supplementary file 3**, *FlyWire.ai link 2*) (Costa et al., 2016). Clusters could be assigned as BMN types based on their similarity to light microscopy images of BMNs known to innervate specific bristles. 10 types were matched with dye-filled or MCFO-labeled BMNs (BM-InOc, -Oc, -Ant, -Or, -Vib, -Vt, -dPoOr, -dOcci, vOcci, and -Taste neurons, BM-InOc example shown in **Figure 6A**, all shown in **Figure 6 – figure supplement 2A-M**). BM-MaPa neurons were matched using published images of labeled MaxNv projections (Singh and Nayak, 1985). 4 types were matched by comparison with BMNs innervating neighboring bristles that showed similar morphology (BM-Fr, -FrOr, -vPoOr, and -Hau neurons). Among these, the BM-vPoOr neurons were so morphologically similar to the MCFO matched BM-vOcci neurons that they could not be distinguished from each other, and were therefore treated as a single group (BM-vOcci/vPoOr

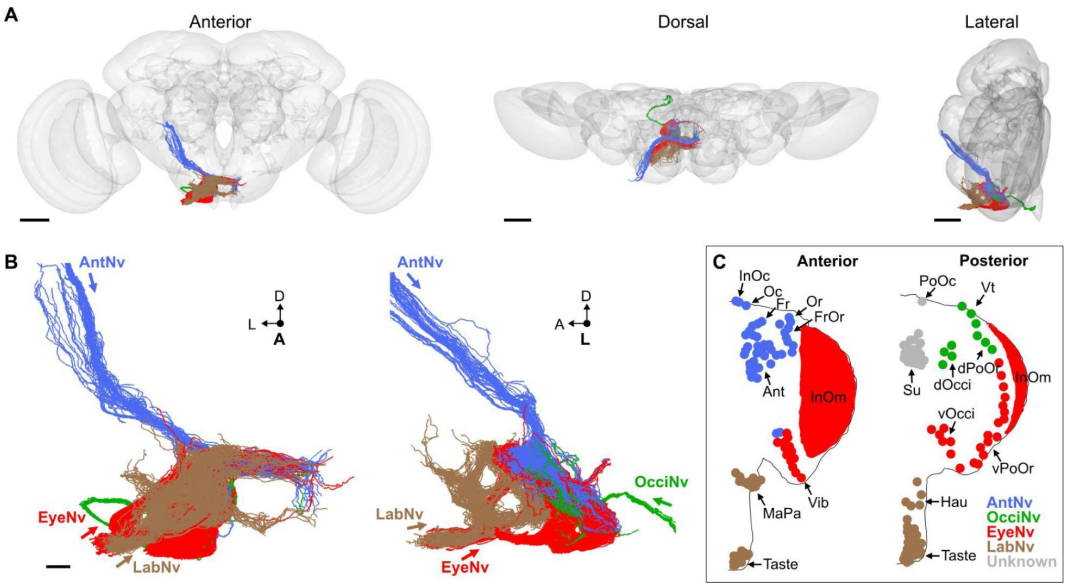

Figure 5.

Electron microscopy-based reconstruction of head BMNs.

(**A**) All reconstructed BMNs projecting into the brain from the left side of the head (anterior, dorsal, and lateral views shown). BMN colors correspond to the nerves that they project through, including the AntNv (blue), EyeNv (red), OcciNv (green), and LabNv (brown). Scale bars, 50 µm. (**B**) Zoomed anterior (left) and lateral (right) views of the BMNs in the SEZ. Labeled arrows for each incoming nerve indicate BMN projection direction. Scale bars, 10 µm. (**C**) Bristles on the anterior (left) and posterior (right) head that are innervated by BMNs in the nerve groups indicated by their color. **Figure 5 – figure supplement 1** summarizes the EM reconstruction strategy. Sensory neurons that could not be assigned an identity are shown in **Figure 5 – figure supplement 2**.

neurons). The collective projections of the 555 reconstructed BM-InOm neurons were matched with BMNs labeled using the InOmBMN-LexA driver line (**Figure 6B**, **Figure 6 – figure supplement 2N**). This matching involved combining 11 different NBLAST clusters (**Figure 6 – figure supplement 1A,B**) and revealed morphological diversity among the BM-InOm neurons.

Additional evidence was used to support our BMN type assignments (**Figure 6 – figure supplement 3A**), including a comparison of the morphology and numbers of reconstructed BMNs on both sides of the brain (for the small OcciNv, **Figure 6 – figure supplement 4A-D**), and determining that BMNs of the same type show common postsynaptic connectivity (described below). Finally, we verified that the numbers of BMNs for each type were consistent with their corresponding bristle numbers (**Figure 6 – figure supplement 3B-F**). This consistency of the BMN/bristle numbers, and completeness of sensory neuron proofreading in each nerve suggested that nearly all BMNs were reconstructed. Thus, we produced a near complete brain projection map of 15 BMN types that innervate the different bristle populations on the head (**Figure 6C-T**, listed in **Supplementary file 3**).

BMN somatotopic map

The projection map defined above revealed three features of somatotopic organization among the BMN types (**Figure 6E-T**, see *FlyWire.ai link 3* to better view the BMN projections in three dimensions). First, each type has a unique branch morphology that defines its projections into distinct zones in the SEZ. Second, types that innervate neighboring bristle populations have branches that project into partially overlapping zones. For example, BMNs that innervate bristles on the dorsal head all have a common ipsilateral projection (**Figure 6F-K,Q**, lateral branch in each panel). In contrast, BMNs that innervate bristles at distant locations (e.g. dorsal and ventral head) show little or no projection overlap. Third, the projections of BMNs either remain in the ipsilateral brain hemisphere or cross the midline to the contralateral side, depending on the locations of their corresponding bristle populations (**Figure 7A-E**). That is, BMNs innervating populations located medially on the anterior head have midline-crossing projections, whereas BMNs innervating lateral, eye, and posterior head populations have ipsilateral-only projections. BMNs innervating bristles on the proboscis showed mixtures of ipsilateral-only and midline-crossing projections. These somatotopic features reveal how BMNs have distinct and overlapping SEZ projections that reflect their relative locations and proximities on the head.

The BMN somatotopic organization was further defined using NBLAST and connectomic data. NBLAST calculates similarity scores based on neuron morphology and spatial location (Costa et al., 2016). BMNs innervating neighboring bristle populations showed high similarity, indicating that their projections are morphologically similar and in close proximity (**Figure 6 – figure supplement 1A,B**). We confirmed this close proximity through analysis of BMN/BMN interconnectivity. All neurons in FlyWire.ai were previously linked to their corresponding automatically detected synapses in FAFB (Buhmann et al., 2021; Dorkenwald et al., 2022), which revealed that the BMN axons have both pre- and postsynaptic sites (**Figure 8 – figure supplement 1A**). Analysis of all-to-all connectivity among the BMNs revealed that some of these sites corresponded to BMN/BMN synaptic connections (**Figure 8 – figure supplement 1B**). The highest connectivity was among BMNs of the same type, but types innervating neighboring bristles were also connected. In contrast, BMNs innervating bristles at distant locations showed low NBLAST similarity and were not connected, consistent with these BMNs projecting into distinct zones. Interestingly, the different BMN projection zones defined by the NBLAST and connectivity data correspond roughly to the eye, ventral, dorsal, and posterior head.

Somatotopically-organized parallel BMN pathways

The map of somatotopically organized BMN projection zones provided evidence of the parallel sensory pathways predicted by the model of hierarchical suppression underlying grooming (Hampel et al., 2017; Seeds et al., 2014). In the model, mechanosensory neurons detect dust at

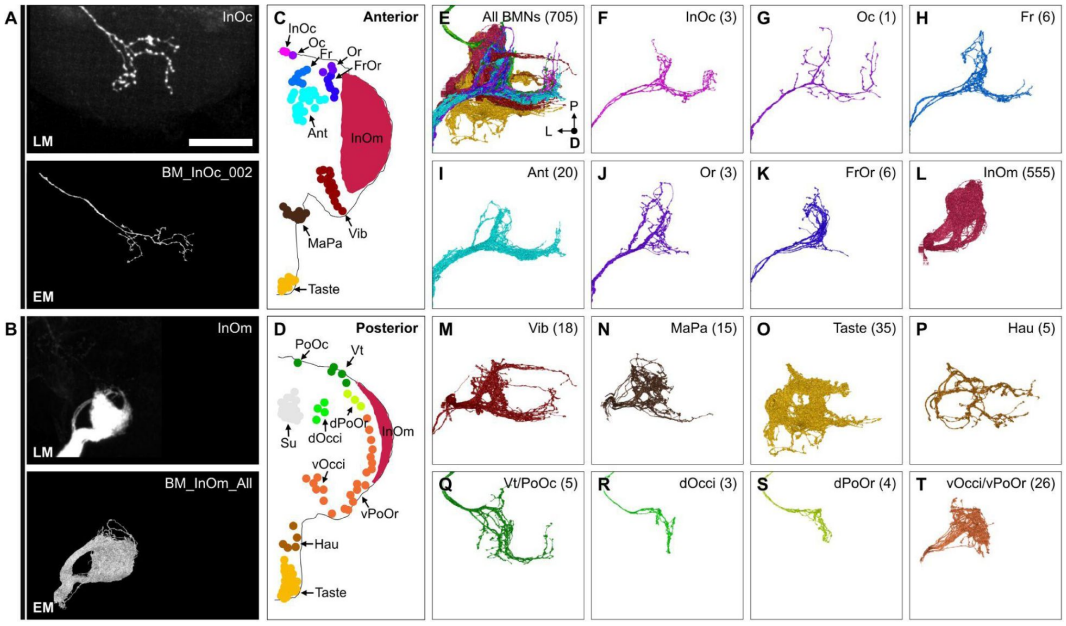

Figure 6.

BMN types that innervate specific head bristles.

(**A-B**) Examples of matching light microscopy (LM) imaged BMN projections with their corresponding EM reconstructed BMNs, including BM-InOc neurons (**A**) and BM-InOm neurons (**B**). Top panels show representative LM images of labeled BMNs that innervate the bristle indicated in the top right corner (anterior SEZ views as shown in **Figure 4**). The individual BM-InOc neuron was labeled by dye filling using DiD while the collective projections of the BM-InOm neurons were labeled using the driver line InOmBMN-LexA expressing GFP. Bottom panels show the EM-reconstructed BMN types indicated in the top right corner. Shown is a representative example of a BM-InOc neuron (**A**) and all reconstructed BM-InOm neurons (**B**). Scale bar, 50 µm. Examples for all LM and EM matched BMNs are shown in **Figure 6 – figure supplement 2**. Additional evidence used for assigning the different BMN types is shown in **Figure 6 – figure supplement 1**, **Figure 6 – figure supplement 3**, and **Figure 6 – figure supplement 4**. (**C-D**) Different bristle populations indicated by labeled and colored dots are innervated by BMNs shown in **E-T**. The anterior (**C**) and posterior (**D**) head are shown. (**E-T**) Reconstructed SEZ projections of BMN types that are labeled and plotted in colors indicating the bristles that they innervate. Shown are the dorsal views of all BMNs (**E**), BM-InOc (**F**), BM-Oc (**G**), BM-Fr (**H**), BM-Ant (**I**), BM-Or (**J**), BM-FrOr (**K**), BM-InOm (**L**), BM-Vib (**M**), BM-MaPa (**N**), BM-Taste (**O**), BM-Hau (**P**), BM-Vt/PoOc (**Q**), BM-dOcci (**R**), BM-dPoOr (**S**), and BM-vOcci/vPoOr (**T**) neurons. The number of reconstructed BMNs for each type is indicated.

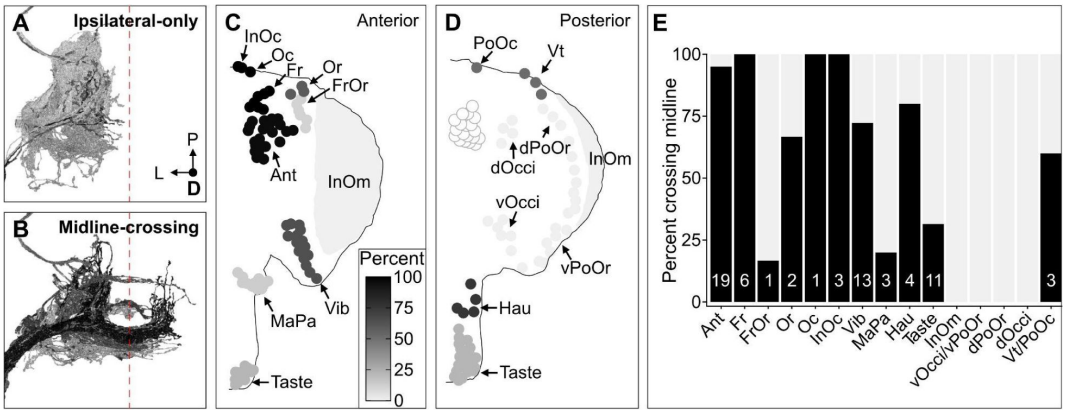

Figure 7.

Some head BMNs have projections that cross the midline to the contralateral brain hemisphere.

(**A-B**) BMNs that remain in the ipsilateral brain hemisphere (**A**) versus those with midline-crossing projections (**B**), shaded by percent midline-crossing for each type (scale in **C**). Red dashed line indicates the brain midline. (**C,D**) Shaded dots on the anterior (**C**) and posterior (**D**) head indicate the percent of BMNs innervating each bristle population that are midline-crossing. (**E**) Bar plots of midline crossing percentages (numbers of midline-crossing BMNs indicated).

different head locations and elicit aimed grooming through distinct postsynaptic circuits that function in parallel (**Figure 1 – figure supplement 1A,C**). The projection zones could be where BMNs synapse with these circuits. Therefore, we examined the postsynaptic connectivity of the different BMN types to test if they form parallel connections with distinct partners. Nearly all neurons postsynaptic to the BMNs were first proofread in FlyWire.ai by our group and the wider proofreading community (Dorkenwald et al., 2023, 2022). We then compared the connectivity of the BMNs with their postsynaptic partners using cosine similarity-based clustering (**Figure 8 – figure supplement 2**). The 555 BM-InOm neurons were excluded from this analysis because they were present in higher numbers and with fewer presynaptic sites than the 150 BMNs of other types, and clustering all BMNs together resulted in obscured clustering (presynaptic site counts in **Figure 8 – figure supplement 1A**). The BMN/BMN connections shown in **Figure 8 – figure supplement 1B** were also excluded from the cluster analysis.

Cosine similarity clustering revealed that BMNs formed parallel postsynaptic connections that reflected their head somatotopy. The lowest level clusters at the lowest cut heights shown in the **Figure 8A** dendrogram contained BMNs of the same type (colored bars next to dendrogram), demonstrating that BMNs innervating the same bristle populations had the highest connectivity similarity. Higher dendrogram cut heights (larger cluster sizes) uncovered connectivity similarity among BMN types innervating neighboring bristle populations. For example, a cut height of 4.5 identified five clusters that captured connectivity similarity among both same and neighboring BMN types (**Figure 8A,B**, colored circles 1-5, *FlyWire.ai link 4*). Clusters 1 and 4 contained exclusively BMNs of the same type, including BM-Vib (Cluster 1) and a subset of BM-Taste neurons (Cluster 4). The other subset of BM-Taste neurons is represented in Cluster 3, showing connectivity similarity with neighboring BMNs on the ventral head. This intratype differential clustering observed with the BM-Taste neurons was also found with other BMN types, including the morphologically diverse BM-InOm neurons (**Figure 8 – figure supplement 3A,B**, *FlyWire.ai link 5*). Thus, while BMNs of the same type tend to show high connectivity similarity, we also find evidence that there are BMN subtypes with distinct postsynaptic partners. Clusters 2, 3, and 5 contained BMNs innervating neighboring bristle populations that were located roughly on the dorsal, ventral, and posterior head areas (**Figure 8A-C**). Clusters 2 and 3 contained exclusively dorsal or ventral BMNs, respectively, while Cluster 5 contained 77% posterior head BMNs and 23% anterior. The posterior and anterior BMNs in Cluster 5 showed relatively low postsynaptic connectivity similarity with each other (**Figure 8 – figure supplement 2**), thus maintaining a mostly anterior versus posterior spatial distinction in their postsynaptic connectivity. However, the presence of both anterior and posterior head BMNs in Cluster 5 also indicates that some postsynaptic partners receive BMN inputs that are not head location specific.

Our results reveal head bristle proximity-based organization among the BMN projections and their postsynaptic partners to form parallel mechanosensory pathways. BMNs innervating neighboring bristles project into overlapping zones in the SEZ, whereas those innervating distant bristles project to distinct zones (example of BM-Fr, -Ant, and -MaPa neurons shown in **Figure 8D,E**). Cosine similarity analysis of BMN postsynaptic connectivity revealed that BMNs innervating the same bristle populations (same types) have the highest connectivity similarity. **Figure 8F** shows example parallel connections for BM-Fr, -Ant, and -MaPa neurons (vertical arrows), where the edge width indicates the number of synapses from each BMN type to their major postsynaptic partners. Additionally, BMNs innervating neighboring bristle populations showed postsynaptic connectivity similarity, while BMNs innervating distant bristles show little or none. For example, BM-Fr and -Ant neurons have connections to common postsynaptic partners, whereas BM-MaPa neurons show only weak connections with the main postsynaptic partners of BM-Fr or -Ant neurons (**Figure 8F**, connections under 5% of total BMN output omitted). These results suggest that BMN somatotopy could have different possible levels of head spatial resolution, from specific bristle populations (e.g. Ant bristles), to general head areas (e.g. dorsal head bristles).

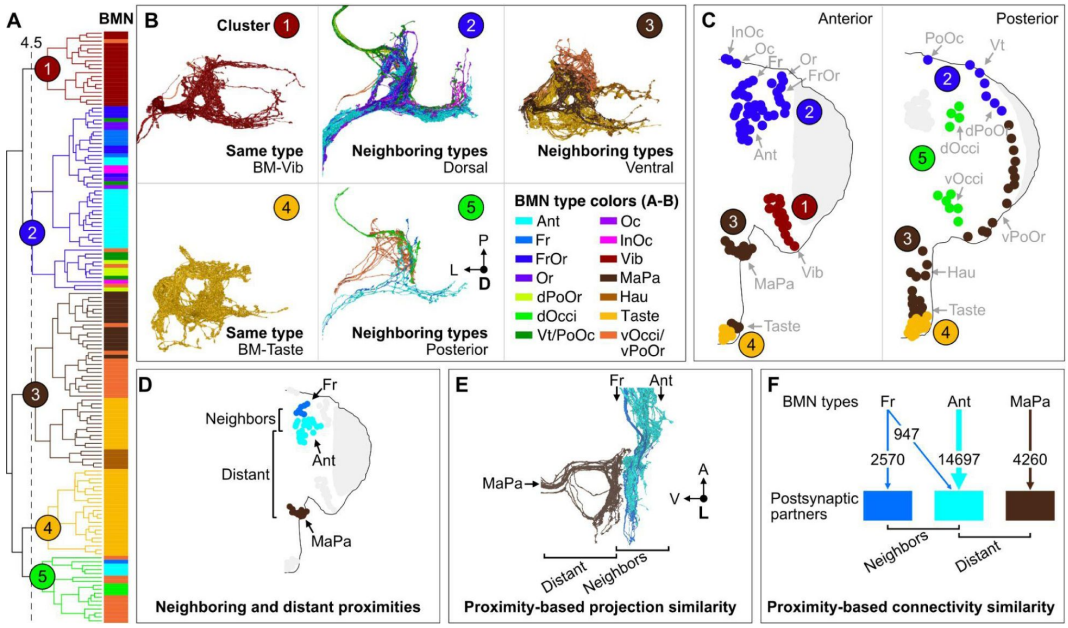

Figure 8.

Somatotopy-based postsynaptic connectivity similarity among BMN types.

(**A**) Dendrogram of cosine similarity clustering of BMNs by postsynaptic connectivity similarity. Analysis excludes postsynaptic partners with fewer than 6 synapses, and the BMN/BMN connections shown in **Figure 8 – figure supplement 1**. Individual BMNs are shown as bars and their types correspond to the colors indicated in **B** (bottom right). The five clusters are from cut height 4.5 on the dendrogram (dotted line) derived from the comparisons shown in **Figure 8 – figure supplement 2**. (**B**) Morphologies of BMNs in the indicated clusters (upper right) whose types correspond to the colors shown in the bottom right. (**C**) Spatial relationships among the clustered BMNs are shown by coloring their bristles (dots) by cluster number on the anterior and posterior head. BMN types in more than one cluster are colored accordingly if at least 20% of that type was in a given cluster (e.g. BM-Taste neurons are in clusters 3 (37%, brown) and 4 (63%, orange)). Note: the positioning of the colored dots indicating different clusters for Taste and vOcci/vPoOr bristles is hypothesized based on their proximity to other BMNs in the same cluster. The clusters exemplify different levels of connectivity similarity shown by the dendrogram (**A**). BMNs showing the highest connectivity similarity innervate the same bristle populations, as exemplified by BM-Vib (Cluster 1) and BM-Taste (Cluster 4) neurons. BMNs that innervate neighboring bristle populations also show high connectivity similarity, including BMNs on the dorsal (Cluster 2), ventral (Cluster 3), and posterior head (Cluster 5). Note: Cluster 5 consists mostly of posterior head BMNs, but also BM-Ant and -Fr neurons on the anterior head, although these BMNs show relatively low cosine similarity with the posterior head BMNs. BM-InOm neurons were analyzed separately (**Figure 8 – figure supplement 3**). (**D-F**) Summary of BMN somatotopic features. (**D**) Different BMN types innervate bristles at neighboring and distant proximities. (**E,F**) BMNs that innervate neighboring bristles project into overlapping zones (**E**, example of EM reconstructed BM-Fr and -Ant neuron SEZ projections with non-overlapping -MaPa neuron projections) and can show postsynaptic connectivity similarity (**F**, edge widths based on number of total synapses from a given BMN type to its major postsynaptic partners, edges under 5% of BMN output omitted). Labeled arrows for each BMN type shown in **E** indicate projection direction.

Activation of subsets of head BMNs elicits aimed grooming of specific locations

We next tested the extent to which the parallel-projecting BMNs elicited aimed grooming of specific head locations. The driver lines described above (**Figure 3D-I**) were used to express the light-gated neural activator CsChrimson (Klapoetke et al., 2014) in different subsets of BMNs (**Figure 9A**). Flies were placed in chambers where they could move freely and then exposed to red light to activate the CsChrimson-expressing BMNs. We manually annotated the movements elicited by optogenetic activation of BMNs from recorded video (**Figure 9 – figure supplement 1**, **Videos 1-4**).

Optogenetic activation of BMN types labeled by each driver line elicited grooming by the front legs that was aimed at specific head locations (**Figure 9B,C**). For example, a line that expressed in different BMN types on the dorsal head elicited aimed dorsal head grooming (dBMN-spGAL4; BM-InOc, -Vt, and -dPoOr neurons, blue trace, **Video 1**). Two lines expressed exclusively in specific BMN types, which enabled us to test the extent to which grooming was aimed specifically at those BMNs (i.e. BM-Taste and -InOm neurons). Indeed, BM-Taste neurons on the labellum elicited labellar grooming, but also grooming of neighboring locations on the proboscis and ventral head (TasteBMN-spGAL4, yellow trace includes proboscis and ventral head grooming, **Video 2**). Activation of BM-InOm neurons (InOmBMN-LexA, **Video 3**) elicited eye grooming (red trace), but also grooming of the neighboring dorsal head (blue trace). This suggested that head BMNs elicit aimed grooming of their corresponding bristle locations, but also neighboring locations. This result is consistent with our anatomical and connectomic data indicating that BMNs innervating neighboring bristles show overlapping projections and postsynaptic connectivity similarity (see Discussion).

Activation of BMNs on the posterior head elicited low levels of dorsal head grooming (blue trace), but mostly a forward head nodding movement (**Figure 9A-C**, pBMN-spGAL4; BM-Vt, -dOcci, -dPoOr, and -vOcci neurons, **Video 4**). Nodding was an apparent avoidance response to posterior touches of the head, and occurred while the flies either stood in place or walked around. However, nodding was also observed during dorsal head grooming. Such nodding movements during head grooming were previously shown to help the legs reach particular locations (Honegger et al., 1979). Nodding also occurred with the dorsal head grooming elicited using the dBMN-spGAL4 and InOmBMN-LexA driver lines, but these lines did not elicit nodding in the absence of grooming as we observed with pBMN-spGAL4. This suggested that BMN-activated nodding occurs in two different behavioral contexts: during dorsal head grooming and as an avoidance response. Different evidence led us to hypothesize that nodding in these contexts was elicited by distinct BMN types. First, pBMN- and dBMN-spGAL4 driver lines show overlapping expression in BM-Vt and -dPoOr neurons, and both elicit dorsal head grooming accompanied by nodding. Second, pBMN-spGAL4 is the only tested line that expressed in BM-dOcci and -vOcci neurons and also the only line that elicited nodding in the absence of grooming. When taken together, our experiments suggest that nodding-only movements are elicited by BM-dOcci and -vOcci neurons and dorsal head grooming is elicited by BM-InOc, -Vt, -dPoOr, and -InOm neurons.

In addition to grooming, BMNs on the dorsal head and eyes elicited backwards motions that appeared as if flies were avoiding something that touched the head (dBMN-spGAL4 and InOmBMN-LexA). The backward motion and grooming were mutually exclusive and sequential, as the backward motion occurred transiently at the stimulus onset and was followed by grooming. As we reported previously (Hampel et al., 2020a), the red-light stimulus also elicited backward motions with control flies (**Figure 9B,C**, control, black trace, **Video 5**). However, control flies only responded in 33% of trials, whereas BMN activation flies responded with backward motions in most trials (73% for dorsal head BMNs, 100% BM-InOm neurons). Taken together, this study reveals that the somatotopically organized head BMNs elicit both aimed grooming and avoidance-like responses.

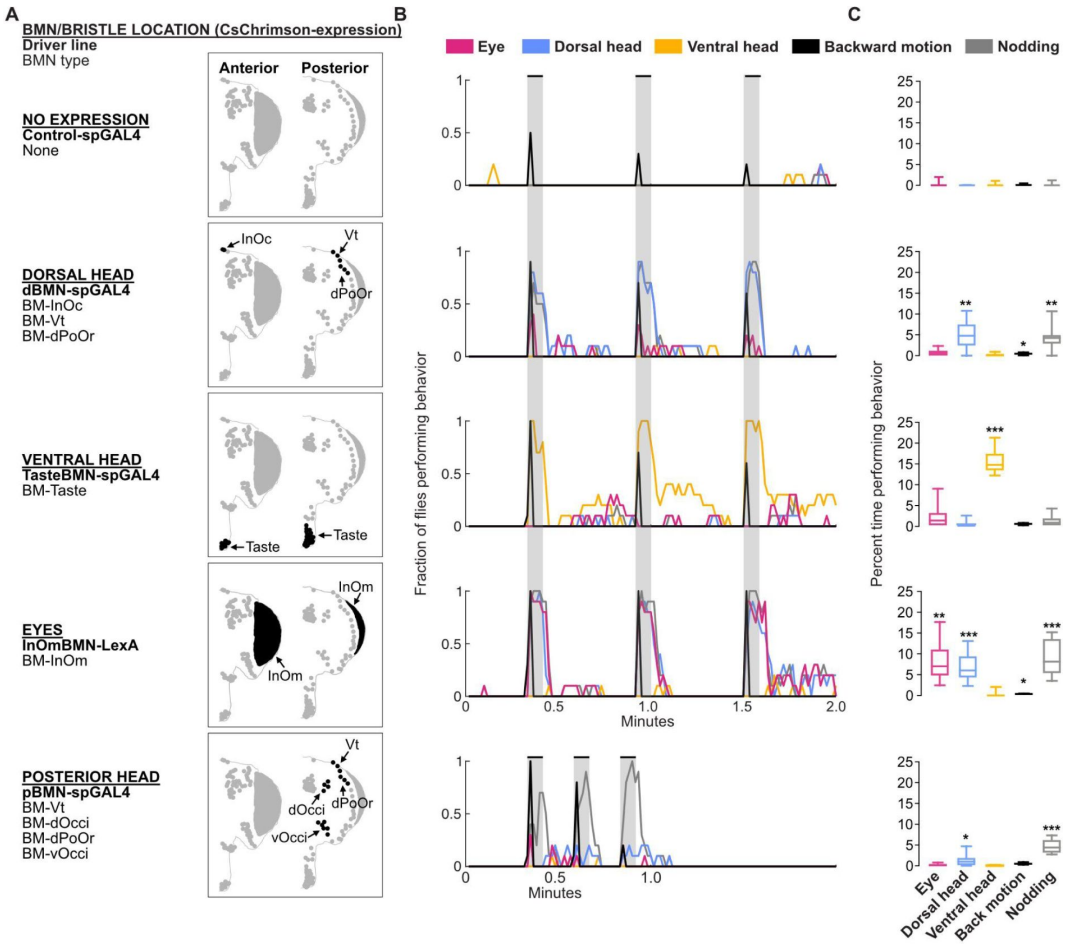

Figure 9.

Optogenetic activation of BMNs at specific head locations elicits aimed grooming.

(**A**) Bristles shaded black on the anterior (left) and posterior (right) head are innervated by BMNs that express CsChrimson under control of the indicated driver lines. Control-spGAL4 shows no expression. (**B**) Histograms of manually annotated video for each line show movements elicited with red-light induced optogenetic activation. The fraction of flies performing each movement are plotted in one second bins (N = 10 flies per line). Grooming movements are indicated by different colors, including eye (magenta), dorsal head (blue), and ventral head (orange) grooming. Other elicited movements include backward motion (black) and head nodding (gray). Gray bars indicate a 5 second red-light stimulus. Most driver lines were tested using 30 second interstimulus intervals, while pBMN-spGAL4 elicited more reliable behavior using 10 second intervals. Movements are mutually exclusive except head nodding. Representative experimental trials shown in **Video 1**, **Video 2**, **Video 3**, **Video 4**, and **Video 5**. **Figure 9 – figure supplement 1** shows additional controls and ethograms for individual flies tested. (**C**) Box plots show the percent time that flies spent performing each movement during the experiment shown in **B**. Bottom and top of the boxes indicate the first and third quartiles, respectively; median is shown in each box; whiskers show the minimum and maximum values. Asterisks indicate *p,0.05, **p,0.001, ***p,0.0001 from Mann-Whitney U pairwise tests between each experimental line and its corresponding control after application of Bonferroni correction. **Figure 9 – source data 1** contains numerical data used for producing each box plot.

Discussion

Comprehensive definition of head BMNs

A major outcome of this work was the definition of nearly all BMNs on the *Drosophila* head. Although there were previous descriptions of the BMNs from different body parts, there were no comprehensive descriptions of all BMNs for any part. Furthermore, the head BMNs were among the least well described. Here, we modified a previously reported BMN dye fill method and produced new transgenic driver lines to define the projection morphologies of the different head BMN types that innervate specific bristle populations on the head. We then identified and reconstructed these types in the FAFB EM dataset. This provides the most comprehensive definition of the BMNs for any body part of *Drosophila* (or any other insect), and an essential resource for future studies. The annotated neurons can be linked to the ongoing neural circuit reconstructions in FAFB (Dorkenwald et al., 2023, 2022), or identified in anticipated new EM reconstructions of the brains of other individuals using available and emerging tools (Galili et al., 2022).

While nearly all head BMNs were reconstructed in this work, different knowledge gaps remain. First, it is unclear if the PoOc and Su bristles are innervated by BMNs because they could not be observed using transgenic driver lines or dye filling methods. We proposed that one of the BM-Vt/PoOc neurons innervates the PoOc bristle, based on proximity and presumed morphological similarity to the neighboring BM-Vt, -InOc, and -Oc neurons. For the Su bristles, one possibility is that they are innervated by some of the 25 unknown sensory neurons reconstructed in this work (**Figure 5 – figure supplement 2A-Y**). Second, it remains unclear what neurotransmitter(s) are used by the BMNs. A machine learning approach was recently developed that can predict whether a neuron in FAFB uses any of 6 major neurotransmitters with high accuracy (Eckstein et al., 2020). Given that the neurotransmitter predictions for the BMNs were overwhelmingly cholinergic (not shown), and a previous study indicated that leg BMNs are sensitive to a nicotinic acetylcholine receptor antagonist (Tuthill and Wilson, 2016a), the parsimonious explanation is that the BMNs are cholinergic. However, other studies suggest that BMNs could use histamine as a neurotransmitter (Melzig et al., 1996; Salvaterra and Kitamoto, 2001; Yasuyama and Salvaterra, 1999). Thus, the extent to which head BMNs use acetylcholine, histamine, or other neurotransmitters remains unresolved.

Resource: nearly all head mechanosensory neurons reconstructed and annotated in FAFB

In conjunction with two previous studies, work presented here contributes to the FAFB reconstruction and annotation of neurons associated with the major head mechanosensory structures, including the bristles (BMNs), JO (JONs), and taste pegs (TPMNs). The BMNs and TPMNs were reconstructed using the FlyWire.ai platform in the present work, and the JONs were previously reconstructed using the CATMAID platform (Hampel et al., 2020a; Kim et al., 2020). The TPMNs (38 reconstructed) respond to tactile displacements of the taste pegs and are implicated in feeding behavior (Jeong et al., 2016; Sánchez-Alcañiz et al., 2017; Zhou et al., 2019). Subpopulations of ~480 JONs have been previously defined that respond to diverse mechanical forces that move the antennae (JO-A, -B, -C, -D, -E, -F, and -mz neurons), including sound, gravity, wind, and tactile displacements (Hampel et al., 2015, 2020a; Ishikawa et al., 2017; Kamikouchi et al., 2009; Mamiya and Dickinson, 2015; Matsuo et al., 2014; Patella and Wilson, 2018). The JONs are implicated in different behaviors including courtship, flight, locomotion, gravitaxis, wind-guided orientation, escape, and head grooming (Hampel et al., 2015, 2020a; Kamikouchi et al., 2009; Lehnert et al., 2013; Mamiya et al., 2011; Mamiya and Dickinson, 2015; Suver et al., 2019; Tootoonian et al., 2012; Vaughan et al., 2014; Yorozu et al., 2009). The reconstruction and annotation of head mechanosensory neurons in FAFB provides an important resource for connectomics-based studies of mechanosensory

processing (**Supplementary file 3**). While the majority of mechanosensory neurons on the head are now identified in FAFB, some remain unknown, such as multidendritic and pharyngeal mechanosensory neurons on the proboscis (Yang et al., 2021; Zhang et al., 2016).

The reconstructed JONs, BMNs, and TPMNs project into distinct regions in the SEZ (**Figure 5 – figure supplement 1A,E**), and therefore show modality-specific projections. For example, the JONs (chordotonal neurons) define a region of the SEZ called the antennal mechanosensory and motor center (AMMC) while the BMNs project more ventrally. While the BMN projections are based on head location (somatotopic), the JON projections are based on mechanical stimulus modality, such as their responses to vibrational or tonic antennal movements (tonotopic) (Hampel et al., 2020a; Kamikouchi et al., 2006; Kim et al., 2020; Patella and Wilson, 2018). However, there are potential overlapping projections between the most ventral projecting JONs (JO-F neurons) and some BMNs projecting through the AntNv (**Figure 5 – figure supplement 1**). Among the BMNs that appear to overlap with the JO-F neurons are the BM-Ant neurons that are located on the same antennal segment as the JONs (pedicel). This overlap suggests that the JO-F neuron projections are somatotopic like the BMNs. Modality-specific mechanosensory projections are also reported in the VNC of *Drosophila* and other insects (e.g. BMNs, hair plates, campaniform sensilla, and chordotonal neurons), revealing this organization to be fundamental in insects (Merritt and Murphey, 1992; Murphey et al., 1989a; Phelps et al., 2021; Smith and Shepherd, 1998; Tsubouchi et al., 2017; Tuthill and Wilson, 2016a).

A synaptic resolution somatotopic map of the head BMNs

This work defines the somatotopic organization of the head BMNs. Somatotopy was previously reported for BMNs innervating bristles on the bodies of *Drosophila* and other insects (Johnson and Murphey, 1985; Murphey et al., 1989b; Newland, 1991; Newland et al., 2000; Tsubouchi et al., 2017). However, these studies only produced partial somatotopic maps using dye fills or transgenic driver lines. Furthermore, there were no previous descriptions of somatotopy among the head BMNs. Here, we use EM reconstructions to produce a comprehensive synaptic resolution somatotopic map of head BMNs in the same brain.

All reconstructed *Drosophila* head BMN types terminate their projections in the SEZ. This indicates that the first layers of BMN processing for the head occur in the SEZ. In contrast, head BMNs reported in other insects project into both the SEZ and thoracic ganglia, including BMNs innervating the InOm bristles of the praying mantis and cricket (Honegger, 1977; Zack and Bacon, 1981) and wind sensitive head bristles of the locust (Tyrer et al., 1979).

Head BMNs that innervate the same bristle populations (same types) project into the same zones in the SEZ, show the highest morphological similarity, and their morphology is stereotyped across individual flies. These characteristics likely apply to most BMNs, as numerous studies have identified the stereotyped projections of BMNs innervating specific bristles on the bodies of *Drosophila* and other insects (Burg and Wu, 1986, 1989; Burg et al., 1993; Chen et al., 2006; Ghysen, 1980; Honegger, 1977; Kays et al., 2014; Murphey et al., 1989b; Zack and Bacon, 1981). Head BMNs of the same type also show the highest postsynaptic connectivity similarity. However, some BMN types fall into multiple different NBLAST and cosine similarity clusters, revealing that there are BMN subtypes with differing morphology and postsynaptic connectivity. One notable example of such intratype diversity are the BM-InOm neurons that show differential clustering (**Figure 8 – figure supplement 3**). This could reflect the large surface area of the eyes that spans from the dorsal to ventral head, and the differentially clustered BM-InOm neurons may innervate bristles at different locations on the eyes. Future studies will address the organizational and functional logic of such intratype diversity.

We also find that BMN types innervating neighboring bristle populations have overlapping projections (example shown in **Figure 8E**) into zones that correspond roughly to the dorsal, ventral, and posterior head. The overlap is likely functionally significant, as cosine similarity

analysis revealed that neighboring head BMN types can have common postsynaptic partners (example shown in **Figure 8F**). However, overlap between neighboring BMN types is only partial, as they show differing projections and postsynaptic connectivity. The extent of overlap likely reflects the proximity between bristles and enables postsynaptic partners to respond to mechanosensory stimulations of neighboring bristles whose corresponding BMNs are likely to show correlated activity (Tuthill and Wilson, 2016b). BMN projection overlap has also been observed with other parts of the body in *Drosophila*. For example, BMNs innervating bristles on the anterior and posterior leg compartments show overlapping projections in the VNC leg neuromere anterior and posterior zones, respectively (Murphey et al., 1989b). Similarly, BMNs innervating neighboring bristles on the thorax show overlap in their projections into the accessory mesothoracic neuropil (Ghysen, 1980; Kays et al., 2014). This overlap may have implications for aimed grooming behavior. For example, neighboring BMNs could connect with common neural circuits to elicit grooming of overlapping locations (discussed more below).

The somatotopic map reveals that some head BMNs have projections that remain in the ipsilateral brain hemisphere, while others have midline-crossing projections to the contralateral hemisphere (**Figure 7A-E**). Interestingly, BMNs innervating bristles located medially on the anterior head show midline-crossing projections, whereas those innervating more lateral populations have ipsilateral-only projections. Previous studies found that BMNs innervating medial bristles on the thorax have midline-crossing projections, while those innervating more lateral bristles have ipsilateral-only projections (Ghysen, 1980; Kays et al., 2014). Similarly, BMNs that innervate bristles located on the leg segment most medial to the body (coxa) have midline-crossing projections (Murphey et al., 1989b; Phelps et al., 2021). This is also the case for BMNs on the legs of other insects, such as the cricket (Johnson and Murphey, 1985) and hawkmoth (Kent and Levine, 1988). Why do some BMNs have ipsilateral and midline-crossing projections? One possibility is that these BMNs can excite postsynaptic circuitry in both brain hemispheres to elicit bilateral leg grooming responses, which could be appropriate for medial stimuli. In contrast, BMNs on the proboscis have mixtures of ipsilateral-only and midline-crossing projections, while those on the posterior head show ipsilateral-only projections. Thus, the organizational logic of midline-crossing BMNs described above may not be universal.

First synaptic resolution somatotopic map of the head

This work provides the first synaptic resolution somatotopic map of a head (or body) for any species. Previous studies identified somatotopic maps across species, such as the vertebrate maps of head and body (Abraira and Ginty, 2013; Adibi, 2019; Brown et al., 1977). Somatotopic organization has been found to be preserved at different layers of the nervous system and is thought to be of fundamental importance, although the full functional significance of this organization is unclear (Kaas, 1997; Thivierge and Marcus, 2007). Therefore, it remains important to produce anatomical and functional maps and define how this somatotopy interfaces with postsynaptic circuits. It has previously not been possible to obtain a comprehensive description of a somatotopic map, as most studies were limited to sparse labeling experiments and extrapolation across different animals. Thus, the spatial relationships among mechanosensory neurons that make up particular maps could not be definitively determined. We overcame this through the first complete EM reconstruction of a somatotopic map of a head in the same brain. This enables future work that will define the postsynaptic connectome of this complete map. Thus, the synaptic resolution map provided here has important implications for expanding our understanding of somatotopic neural circuit organization and function.

Circuits that elicit aimed grooming of specific head locations

We report here that activation of the head BMNs elicits aimed grooming. Flies groom specific head locations, including the eyes, antennae, dorsal head, ventral head, and proboscis (Dawkins and Dawkins, 1976; Hampel et al., 2015, 2017, 2020a; Seeds et al., 2014; Szebenyi, 1969; Zhang et al., 2020). With the exception of the BM-InOm neurons, little was known about the

roles of the other BMNs in eliciting head grooming. The BM-InOm neurons were originally identified as necessary for grooming in response to mechanical stimulation of the eyes in the praying mantis (Zack and Bacon, 1981). Mechanical stimulation of the *Drosophila* InOm bristles (Melzig et al., 1996) and optogenetic activation of the BM-InOm neurons (Hampel et al., 2017; Zhang et al., 2020) were later reported to elicit eye grooming. Here, we used optogenetic activation to further define the movements elicited by BM-InOm neurons, and show that other BMN types elicit grooming of the dorsal and ventral head. Previous studies in *Drosophila* and other insects showed that stimulations of bristles on the legs, wings, and thorax also elicit aimed grooming (Corfas and Dudai, 1989; Li et al., 2016; Matheson, 1997; Page and Matheson, 2004; Usui-Ishihara et al., 1995; Vandervorst and Ghysen, 1980). Thus, the BMNs are important for eliciting aimed grooming of specific locations on the head and body.

While we show that the parallel-projecting head BMNs elicit grooming of specific locations (i.e. eyes, dorsal and ventral head), the full range of aimed grooming movements that can be elicited was not explored. For example, antennal grooming was previously shown to be elicited by JON activation (Hampel et al., 2015, 2020a; Zhang et al., 2020), and we hypothesize here that BM-Ant neuron activation also elicits antennal grooming. However, we did not identify a transgenic driver line that labels BM-Ant neurons that would enable us to test this hypothesis. Previous studies of the legs, wings, and thorax used mechanical stimulation of specific bristles, rather than BMN optogenetic activation to test the ranges of grooming movements that could be elicited. This was done by delivering mechanical stimuli directly to the bristles of decapitated flies that do not move unless stimulated. In contrast, stimulating the head bristles is relatively challenging, as it requires delivering precise mechanical stimulations to specific bristles in intact and tethered flies. We have used optogenetic analysis in this study, as it was previously demonstrated that BMN optogenetic activation elicits grooming that is comparable to mechanically stimulating their corresponding bristles (Hampel et al., 2017; Zhang et al., 2020). However, our ability to test the full range of grooming movements elicited with BMN activation was limited by the driver lines produced in this study (**Figure 3D-G**).

How do the parallel-projecting head BMNs interface with postsynaptic neural circuits to elicit aimed grooming of specific head locations? Different evidence supports the hypothesis that the BMNs connect with parallel circuits that each elicit a different aimed grooming movement (Seeds et al., 2014). First, cosine similarity analysis revealed parallel connectivity at the first postsynaptic layer. However, this analysis revealed partial convergence of neighboring BMN types onto common postsynaptic partners. Thus, the resolution of the hypothesized parallel circuits and the specificity of the aimed grooming that they elicit remains to be determined. Second, previous studies showed that optogenetic activation of different sensory and interneuron types elicits grooming of specific head locations, suggesting that they are components of putative parallel circuits (Cande et al., 2018; Guo et al., 2022; Hampel et al., 2015; Seeds et al., 2014; Zhang et al., 2020). Third, we identified different neuron types whose activation elicit grooming of the antennae and showed that they are connected to form a neural circuit (Hampel et al., 2020b, 2015). The inputs to this circuit are JONs that detect tactile stimulations of the antennae and project to the SEZ where they excite two interneuron types (aBN1 and aBN2) and a descending neuron type (aDN) to elicit grooming. The aDNs project to a zone in the VNC where circuitry for generating antennal grooming leg movement patterns is thought to reside (Berkowitz and Laurent, 1996). While this circuit is postsynaptic to the JONs (Hampel et al., 2020b, 2015), preliminary connectomic analysis reveals that it is also postsynaptic to BMNs (not shown). Future studies will define the BMN connectivity with the antennal grooming circuit, and other neurons (and circuits) whose activation elicit aimed grooming of different head locations.

We find that activation of specific BMN types elicits both aimed grooming of their corresponding bristle locations and neighboring locations. This suggests overlap in the locations that are groomed with the activation of different BMN types. Such overlap provides a means of cleaning the area surrounding the stimulus location. Interestingly, our NBLAST and cosine similarity analysis

indicates that neighboring BMNs project into overlapping zones in the SEZ and show common postsynaptic connectivity. Thus, we hypothesize that neighboring BMNs connect with common neural circuits (e.g. antennal grooming circuit) to elicit overlapping aimed grooming of common head locations.

BMN involvement in multiple distinct behaviors

In addition to grooming, this work identifies other movements that are elicited by the head BMNs and their corresponding bristles. Previous studies implicated the InOm bristles in an avoidance response (Melzig et al., 1996), although this response was not described in detail. Here, we demonstrate that activation of the BM-InOm neurons elicits an avoidance-like response in the form of backward motions. This response was also elicited by activating BMN types on the dorsal head. Another putative avoidance-like behavior, head nodding, was found to be elicited by posterior head BMNs. Avoidance responses to bristle stimulation have been previously reported in *Drosophila* and other insects, such as limb withdrawal and postural changes (Melzig et al., 1996; Newland and Burrows, 1997; Pflüger, 1980; Vandervorst and Ghysen, 1980). Thus, BMNs across the head and body elicit grooming and possibly avoidance responses.

Parallel circuit architecture underlying the grooming sequence

This study examines the mechanosensory layer of the parallel model of hierarchical suppression that produces the head to body grooming sequence (Hampel et al., 2017; Mueller et al., 2019; Seeds et al., 2014). This layer consists of mechanosensory neurons at specific locations on the head and body that elicit aimed grooming of those locations (Hampel et al., 2020a, 2017, 2015; Zhang et al., 2020). The aimed movements are performed in a prioritized sequence when mechanosensory neurons detect dust at different locations and become simultaneously activated (i.e. head and body completely dirty). In support of this, simultaneous optogenetic activation of mechanosensory neurons across the head and body elicits a grooming sequence that resembles the dust-induced sequence (Hampel et al., 2017; Zhang et al., 2020). Among the different mechanosensory neurons, the BMNs are particularly important, as their activation alone is sufficient to elicit a grooming sequence (Zhang et al., 2020). Thus, activation of individual BMN types elicits aimed grooming, while their simultaneous activation elicits a sequence.

Here we define the parallel architecture of BMN types that elicit the head grooming sequence that starts with the eyes and proceeds to other locations, such as the antennae and ventral head. The different BMN types are hypothesized to connect with parallel circuits that elicit grooming of specific locations (described above and shown in **Figure 1 – figure supplement 1A,C**). Indeed, we identify distinct projections and connectivity among BMNs innervating distant bristles on the head, providing evidence supporting this parallel architecture (**Figure 8D-F**). However, we also find partially overlapping projections and connectivity among BMNs innervating neighboring bristles. Further, optogenetic activation of BMNs at specific head locations elicits grooming of both those locations and neighboring locations (**Figure 9**). These findings raise questions about the resolution of the parallel architecture underlying grooming. Are BMN types connected with distinct postsynaptic circuits that elicit aimed grooming of their corresponding bristle populations (e.g. Ant bristles)? Or are neighboring BMN types that innervate bristles in particular head areas connected with circuits that elicit grooming of those areas (e.g. dorsal or ventral head)? Future studies of the BMN postsynaptic circuits will be required to define the resolution of the parallel pathways that elicit aimed grooming.

The parallel-projecting head BMNs are also hypothesized to connect with postsynaptic circuits that perform additional functions to produce the sequence (Seeds et al., 2014). Simultaneous activation of the parallel architecture by dust causes competition among all movements to be performed in the sequence. This competition is resolved through a hierarchical suppression mechanism whereby earlier movements suppress later ones (**Figure 1 – figure supplement 1B**). Performance order is established by an activity gradient among the parallel circuits where earlier

movements have the highest activity and later ones have the lowest. This gradient was proposed to be produced by controlling sensory gain among the BMNs, or through putative lateral inhibitory connections between the parallel circuits. A winner-take-all network selects the movement with the highest activity and suppresses the others. Our work here provides the foundation for studies that will examine how the BMN postsynaptic circuitry is organized to drive these different functions and produce the grooming sequence.

The BMNs are hypothesized to have roles in both eliciting and terminating the different movements in the grooming sequence through dust detection (Hampel et al., 2017; Seeds et al., 2014; Zhang et al., 2020). That is, dust on particular body parts would be detected by BMNs that are activated with displacement of their corresponding bristles and elicit aimed grooming. While a completely dirty body part would cause strong BMN activation, the level of activation would decrease as a consequence of the decreased dust levels that occur with grooming. This reduced activity would terminate the selected movement in the sequence, allowing a new round of competition among the remaining movements and selection of the next movement through hierarchical suppression. However, it has not been directly demonstrated that the BMNs elicit or terminate the sequence through dust sensing. For example, blocking BM-InOm neurons does not reduce dust-induced grooming of the head (Zhang et al., 2020). However, this may be due to compensation from neighboring mechanosensory neurons. Thus, the presumed role of the BMNs in detecting dust remains to be directly demonstrated.

Materials and methods

Key resources table

Reagent type (species) or resource	Designation	Source or reference	Identifiers	Additional information
Genetic reagent (*D. melanogaster*)	R52A06-GAL4	Jenett *et al.*, 2012	RRID:BDSC_38810	
Genetic reagent (*D. melanogaster*)	VT017251-LexA	Hampel *et al.*, 2017		aka InOmBMN-LexA
Genetic reagent (*D. melanogaster*)	VT019023-AD	Tirian *et al.*, 2017	RRID:BDSC_71430	

Genetic reagent (*D. melanogaster*)	VT050279-DBD	Tirian *et al*., 2017	RRID:BDSC_72433	
Genetic reagent (*D. melanogaster*)	R28D07-AD	Dionne *et al*., 2017	RRID:BDSC_70168	
Genetic reagent (*D. melanogaster*)	VT023783-AD	Tirian *et al*., 2017	RRID:BDSC_73261	
Genetic reagent (*D. melanogaster*)	R11D02-DBD	Dionne *et al*., 2017	RRID:BDSC_68554	
Genetic reagent (*D. melanogaster*)	dBMN-spGAL4	This paper		Stock contains VT019023-AD and VT050279-DBD
Genetic reagent (*D. melanogaster*)	pBMN-spGAL4	This paper		Stock contains R28D07-AD and VT050279-DBD
Genetic reagent (*D. melanogaster*)	TasteBMN-spGAL4	This paper		Stock contains VT023783-AD and R11D02-DBD
Genetic reagent (*D. melanogaster*)	*20XUAS-IVS-mCD8::GFP*	Pfeiffer *et al*., 2010	RRID:BDSC_32194	
Genetic reagent (*D. melanogaster*)	*13XLexAop2-IVS-myr::GFP*		RRID:BDSC_32209	
Genetic reagent (*D. melanogaster*)	C155-GAL4, UAS-nSyb.eGFP	Kendal Broadie	RRID:BDSC_6920	
Genetic reagent (*D. melanogaster*)	BPADZp; BPZpGDBD	Hampel *et al*., 2015	RRID:BDSC_79603	spGAL4 control
Genetic reagent (*D. melanogaster*)	BDPLexA	Pfeiffer *et al*., 2010	RRID:BDSC_77691	

Genetic reagent (*D. melanogaster*)	*20XUAS-IVS-CsChrimson-mVenus*	Klapoetke *et al*., 2014	RRID:BDSC_55134	
Genetic reagent (*D. melanogaster*)	MCFO-5	Nern *et al*., 2015	RRID:BDSC_64089	
Genetic reagent (*D. melanogaster*)	MCFO-3	Nern *et al*., 2015	RRID:BDSC_64087	
Genetic reagent (*D. melanogaster*)	*13XLexAop2-IVS-CsChrimson-mVenus*		RRID:BDSC_55137	
Antibody	anti-GFP (Rabbit polyclonal)	Thermo Fisher Scientific	Cat# A-11122, RRID:AB_221569	IF(1:500)
Antibody	anti-Brp (Mouse monoclonal)	DSHB	Cat# nc82, RRID:AB_2314866	IF(1:50)
Antibody	anti-FLAG (Rat monoclonal)	Novus Biologicals	Cat# NBP1-06712, RRID:AB_1625981	IF(1:300)
Antibody	anti-HA (Rabbit monoclonal)	Cell Signaling Technology	Cat# 3724, RRID:AB_1549585	IF(1:500)
Antibody	anti-V5 (Mouse monoclonal)	BIO-RAD	Cat# MCA1360, RRID:AB_322378	IF(1:300)
Antibody	anti-Rabbit AF488 (Goat polyclonal)	Thermo Fisher Scientific	Cat# A-11034, RRID:AB_2576217	IF(1:500)
Antibody	anti-Mouse AF568 (Goat polyclonal)	Thermo Fisher Scientific	Cat# A-11031, RRID:AB_144696	IF(1:500)
Antibody	anti-Rat AF633 (Goat polyclonal)	Thermo Fisher Scientific	Cat# A-21094, RRID:AB_2535749	IF(1:500)

Chemical compound, drug	Paraformaldehyde 20%	Electron Microscopy Sciences	Cat# 15713	
Chemical compound, drug	DiD solid	Thermo Fisher Scientific	Cat# 07757	
Chemical compound, drug	all-*trans*-Retinal	Toronto Research Chemicals	Cat# R240000	
Software, algorithm	neuTube	Feng *et al*., 2015		https://www.neutracing.com/
Software, algorithm	Vcode	Hagedorn *et al*., 2008		http://social.cs.uiuc.edu/projects/vcode.html
Software, algorithm	Fiji	Schindelin *et al*., 2012		http://fiji.sc/
Software, algorithm	R			https://www.r-project.org/
Software, algorithm	CMTK	Jefferis *et al*. 2007		https://www.nitrc.org/projects/cmtk/
Software, algorithm	FluoRender	Wan *et al*., 2012		http://www.sci.utah.edu/software/fluorender.html
Software, algorithm	Blender version 2.79			https://www.blender.org/download/releases/2-79/
Software, algorithm	MATLAB	MathWorks Inc., Natick, MA		
Software, algorithm	natverse	Bates *et al*. 2020		http://natverse.org/
Software, algorithm	Cytoscape	Shannon et al. 2003		https://cytoscape.org/

Rearing conditions and fly stocks

GAL4, LexA, and *Split GAL4* (spGAL4) lines were generated by the labs of Gerald Rubin and Barry Dickson, and most lines are available from the Bloomington *Drosophila* Stock Center (Dionne et al., 2017; Jenett et al., 2012; Pfeiffer et al., 2008; Tirián and Dickson, 2017). Canton S flies were obtained from Martin Heisenberg's lab in Wurzburg, Germany. Other stocks used in this study are listed in the key resources table.

GAL4, spGAL4, and LexA lines were crossed to either UAS or LexAop driver lines as described below. Flies were reared on Fisherbrand Jazz-Mix *Drosophila* food (Fisher Scientific, Fair Lawn, NJ) containing corn meal, brown sugar, yeast, agar, benzoic acid, methyl paraben, and propionic acid. The flies were kept in an incubator at 21°C and 55-65% relative humidity. Flies that were not used for optogenetic experiments were kept on a 16/8 hour light/dark cycle. Flies used for optogenetic experiments were reared on food containing 0.4 mM all-*trans*-retinal (Toronto Research Chemicals, Toronto, Canada) in vials that were wrapped in aluminum foil and kept in a box to keep them in the dark. Unless stated otherwise, the flies used for experiments were 5 to 8 day-old males.

Imaging the head bristles

1-2 mm was cut off the tip of an Eppendorf 200 µL pipette tip, then an approximately 6 mm length was cut off and the remainder discarded. A freeze-killed (> 1 hour) male or female Canton S fly was then gently pushed in with a piece of wire, until the head protruded from the tip. The tip was then mounted in a small piece of soft wax. An observation chamber was constructed on a microscope slide, by cutting a 5 mm square hole in 3 layers of Highland electrical insulation tape (3M, Saint Paul, Minnesota) and covering the bottom with a translucent white plastic square (cut from a Farmland Traditions dog treat bag). The fly, held in the tube, was mounted over the chamber using the wax, first dorsal side up (imaged), then ventral side up (imaged). The head was carefully cut off using sharpened iridectomy scissors, falling into the chamber where it was arranged anterior side up, held in place with a piece of coverslip, imaged, flipped posterior side up, and imaged again.

Imaging was done with a Zeiss Axio Examiner D1 microscope equipped with a 10x Achroplan objective (0.25 NA) (Karl Zeiss, Oberkochen, Germany). The objective was surrounded with a cylinder of the same translucent white plastic in order to diffuse the light source and to avoid air movements that could move the antennae. The cylinder was illuminated from both sides at 2-3 cm distance by a Dolan-Jenner Fiber-lite (Dolan-Jenner Industries, Boxborough, Massachusetts). A small amount of additional back-lighting was provided by the microscope light source (20% power) with a blue filter. Images were captured with a Zeiss Axiocam 512 at 60 ms exposure. The focal plane was advanced in small increments manually, resulting in approximately 50 images per head.

The image Sequence function of Fiji software (*http://fiji.sc/*) was used to combine all the images into a stack. The pixel size was adjusted to 0.3125 micron and calibrated with an image of a slide micrometer. The stack was down-sized to 2048 pixels minimum dimension (usually the height), and an Unsharp Mask filter applied (3 pixel radius, 0.6 mask weight), then the sides of the stack were cropped to remove unnecessary space.

The Fiji *extended depth of field* (EDF) plugin (Alex Prudencio, EPFL, École polytechnique fédérale de Lausanne) was used to superimpose in-focus areas from the stacks. For acceptable processing times, the stack was down-sized to 1024 pixels minimum dimension. The EDF process requires square images, so to avoid excessive cropping the canvas size was increased to 2048 pixels square, resulting in a black surround. The best results were obtained by averaging (with Image Calculator) (1) the result of EDF Easy Mode Fast setting, Gaussian-blurred by 1 pixel radius, with (2) the result of EDF Easy Mode High setting. The resulting image was cropped to 1024 minimum dimension, sharpened with Unsharp Mask, radius 1 pixel, and adjusted for optimal contrast.

With anterior views of the head, the EDF algorithm has difficulties separating the aristae from the underlying eye facets. Thus, for presentation images of the front view of the head, the EDF process was carried out separately on an anterior stack with the aristae present, and a more posterior stack with the antennae absent. These results were imported as layers into GIMP (GNU Image Manipulation Program) and manually combined by masking.

To facilitate bristle identification, a color-coded depth map was constructed from the downsized 1024-height stack, sharpened with Unsharp-mask (1 pixel). The color channels were split, and G and B channels discarded. The R channel was Inverted (Edit menu), the contrast was adjusted, and a Gamma correction of 1.34 was applied to the stack. A lookup table (LUT) had been previously created ranging from light blue, through white and yellow to dark red ("Stellar"). The Image: Hyperstacks: Temporal-Color Code function (LUT Stellar) was applied to the stack, giving a depth-coded image. Finally, an Enhanced Local Contrast (CLAHE, blocksize 63) was applied, followed by a gamma adjustment (1.5-1.8).

Bristle nomenclature

Published names for the different bristles were used when possible. However, bristle abbreviations are from the present work unless otherwise indicated. Some bristle names were from (Bodenstein et al., 1994), including the *frontal* (Fr), *frontoorbital* (FrOr), *orbital* (Or), *ocellar* (Oc), *interocellar* (InOc), *vertical* (Vt), *postorbital* (PoOr), and *vibrissae* (Vib). We deviated from this nomenclature in the following cases. First, although the PoOr bristles form a continuous row along the back margin of each eye (**Figure 1B**), we subdivided them into *dorsal* (dPoOr) and *ventral* (vPoOr) populations based on whether their associated BMNs project through the OcciNv or EyeNv, respectively (**Figure 2F,J**). Second, we did not use the bristle name *postvertical*, but instead used *postocellar* (PoOc) that was previously proposed to better describe the location of these bristles as posterior to the other ocellar bristles (Steyskal, 1976). Third, instead of occipital, we used the name *supracervical* (Su) for the bristles located immediately above the cervical connective on the back of the head (Steyskal, 1976). This is because we named two populations of small bristles on the back of the head the *dorsal* and *ventral occipital* (dOcci and vOcci) bristles. This name was previously proposed for these bristles in other species of flies (Steyskal, 1976). The abbreviation (Occi) was taken from the blowfly literature (Thei, 1979). Given that the Occi bristles are found as two distinct populations in *Drosophila melanogaster*, we refer to them in this work as the *dorsal* (dOcci) and *ventral* (vOcci) bristles (**Figure 1B**).

Our abbreviation for the *vertical* (Vt) bristles describes all vertical bristles. The largest two have been referred to as *Vt inner* (Vti) and *exterior* (Vte) bristles in different fly species (Steyskal, 1976), and were named in the present work Vt 1 and Vt 2, respectively (**Figure 4 – figure supplement 5A**). The other previously described Vt bristle (named Vt 3) is posterior to Vt 2. Medial to the Vt 2 bristle is a newly categorized fourth Vt bristle that we could not find a previous description of in *Drosophila* (labeled Vt 4 in **Figure 4 – figure supplement 5A**). This bristle could be the paravertical bristle that was previously described (Steyskal, 1976).

The bristles on the eyes were referred to as *interommatidial* (InOm) bristles (Honegger et al., 1979; Zack and Bacon, 1981). For the bristles on the outer labellum, we used the common name, *taste* (Taste) bristles (Stocker, 1994). We refer to the other bristles on the proboscis as *maxillary palp* (MaPa) and *haustellum* (Hau) bristles. Note: while most of the bristles on the head are termed trichoid sensilla that are innervated by a single BMN, the Taste bristles are mostly basiconic sensilla that are each innervated by a BMN and multiple gustatory neurons. The bristles on the first and second segments of the antennae are referred to as *antennal* (Ant) bristles.

Bristle quantification

We counted the bristle populations that are defined above and shown in **Figure 1A-D**. Most bristles were counted using color-coded depth maps (described above) that aided the identification of the bristles within each population (**Figure 1 – figure supplement 2A-H**). The Ant, Fr, FrOr, Or, Oc, InOc, Vt, dOcci, PoOr, Vib, MaPa, Hau, PoOc, and Su bristles were counted using this method on eight male and four female heads (**Figure 1E**, **Figure 1 – figure supplement 3A-E**, **Supplementary file 1** (Table 1)). Bristles on each half of the head were counted using the Fiji Cell Counter plugin (Kurt De Vos, University of Sheffield) and then averaged. These averages were used to calculate average and standard deviation for each bristle population from all counted male and

female heads. Two tailed t-tests were performed to compare male and female bristle numbers for each population. Although in this manuscript we make a distinction between the dPoOr and vPoOr bristles (**Figure 1B**), we counted all PoOr bristles together when comparing their numbers between males and females (**Figure 1 – figure supplement 3E**). We used other approaches to obtain or estimate the numbers of dPoOr, vPoOr, InOm, vOcci, and Taste bristles (described below).

BMNs that innervate the PoOr bristles project through two different nerves, the Occi- and EyeNvs (**Figure 2F**). Specifically, BMNs innervating *dorsal PoOr* (dPoOr) bristles project through the OcciNv, while those innervating *ventral PoOr* (vPoOr) bristles project through the EyeNv. We determined the average number of dPoOr or vPoOr bristles based on whether they were innervated by an Occi- or EyeNv-projecting BMN. The BMNs were labeled using R52A06-GAL4 to express membrane-targeted *green fluorescent protein* (mCD8::GFP) and imaged using a confocal microscope (imaging method described below). We then counted the dPoOr and vPoOr bristles from confocal images (example shown in **Figure 2 – figure supplement 1D**). Multiple different heads were counted to determine the average number of dPoOr and vPoOr bristles (N = 10, **Supplementary file 1** (Table 2)).

The InOm bristles were too small and numerous to be counted, and it was only necessary to estimate their numbers in this work. The eyes contain the majority of bristles on the head and the numbers of these bristles can vary. Data from a previous study indicated that each eye contains between 745 and 828 regularly spaced ommatidia (776 average), and most ommatidia have an associated bristle (Ready et al., 1976). However, some ommatidia around the eye edges are not associated with bristles. Based on one example of an eye from a Canton S fly (Ready et al., 1976), we calculated that 78% of the ommatidia had an associated bristle for that eye. This percentage was used to estimate that there are between 607 and 645 bristles on each eye from the above counted bristle ranges. This estimate was sufficient for identifying the EM reconstructed BMNs that innervate the InOm bristles (described below) based on their overwhelming number relative to other head BMNs.

In this work we identified the vOcci bristles that were not previously described. These bristles were too small to be reliably observed at the level of resolution of the images shown in **Figure 1A-D**. To help visualize and count these bristles, we used a transgenic driver line pBMN-spGAL4 (R28D07-AD ⋂ VT050279-DBD) that labels BMNs innervating these bristles (shown in **Figure 3F,F'**). pBMN-spGAL4 was used to express mCD8::GFP, and the ventral posterior head was imaged with a confocal microscope (see below for imaging method). The bristles could be counted by using the labeled BMN dendrites to highlight their locations (shown in **Figure 3 – figure supplement 1C**). pBMN-spGAL4 labeled almost all of the visible vOcci bristles, but in some heads, we could see bristles that did not have an labeled BMN (not shown). Therefore, it is possible that the counts of these bristles using the GFP-labeled BMNs are lower than the actual number. We determined the average number of Occi bristles by counting different heads (N = 13, **Supplementary file 1** (Table 3)).

Most of the heads that we imaged had their proboscises oriented such that we could not observe and count all of the Taste bristles. However, Taste bristles have been counted in previous studies (Falk et al., 1976; Jeong et al., 2016; Nayak and Singh, 1983; Shanbhag et al., 2001). See **Supplementary file 1** (Table 4) for Taste bristle counts from different publications (published counts for Ant and MaPa bristles are also shown). One of these studies also determined that there were no differences in the numbers of Taste bristles between males and females (Shanbhag et al., 2001). We took the highest and lowest numbers from these different references for the range that is shown in **Figure 1E**.

Head immunostaining and nerve reconstructions

R52A06-GAL4 (RRID:BDSC_38810), dBMN-spGAL4, pBMN-spGAL4, and TasteBMN-spGAL4 were crossed to *20XUAS-IVS-mCD8::GFP* (RRID:BDSC_32194) while VT017251-LexA (InOmBMN-LexA) was crossed to *13XLexAop2-IVS-myr::GFP* (RRID:BDSC_32209). Anesthetized male progeny were decapitated using a standard razor blade and heads were placed in phosphate-buffered saline (PBS). To facilitate antibody penetration for staining, we used #5 Dumoxel forceps (Fine Science Tools, Foster City, California) to tear small holes in the cuticle and pull off the antennae or proboscis. Heads were fixed in PBS with 2% paraformaldehyde for 1 hour at room temperature, and then washed with PAT (PBS, 1% Bovine Serum Albumin, 0.5 % TritonX) six times within 2 hours. Heads were blocked overnight at 4 °C in PAT with 3% normal goat serum (PAT-NGS), then incubated for 3 days (room temperature during the day and 4 °C at night) in PAT-NGS containing rabbit anti-GFP (Thermo Fisher Scientific, Waltham, MA, RRID:AB_221569). Heads were washed with PAT for 5 hours and then incubated for 3 days in PAT-NGS with goat anti-rabbit AlexaFluor-488 (Thermo Fisher Scientific, Waltham, MA, RRID:AB_2576217). Heads were washed for 2 days with several exchanges of PAT, and then in PBS for 2 hours at room temperature. A standard slide was used for mounting with a small “well” created by stacking five Avery reinforcement labels (Avery products corporation, Brea, California). A drop of Vectashield (Vector Laboratories, Inc. Burlingame, California) was added to the well and the heads were positioned either anteriorly or dorsally. The well was then covered with a circular cover slip (Electron Microscopy Sciences, Hatfield, Pennsylvania, 1.5 Micro Coverglass 12 mm diameter, Cat# 72230-01).

Heads were imaged using a Zeiss LSM800 confocal microscope (Carl Zeiss, Oberkochen, Germany) equipped with a 20x objective (Plan-Apochromat 20x/0.8). Fiji software (*http://fiji.sc/*) was used for examining the morphology of the imaged BMNs and for image processing steps, including adjustment of brightness and contrast, stitching, and image inversion. Reconstructions of the labeled head BMNs and their respective nerves from the confocal Z-stacks (**Figure 2** and **Figure 3**) were performed using the software neuTube (Feng et al., 2015). Image stacks of the heads are displayed as maximum intensity projections (**Figure 2** and **Figure 3**).

CNS immunostaining and analysis

The different GAL4, spGAL4, and LexA driver lines described above were crossed to either *20XUAS-IVS-mCD8::GFP* or *13XLexAop2-IVS-myr::GFP*. Brains and ventral nerve cords were dissected and stained as previously described (Hampel et al., 2015, 2011). The following primary and secondary antibodies were used for staining GFP and the neuropil: rabbit anti-GFP, mouse anti-nc82 (Developmental Studies Hybridoma Bank, University of Iowa, RRID:AB_2314866) to stain Bruchpilot, goat anti-rabbit AlexaFluor-488, and goat anti-mouse AlexaFluor-568 (Thermo Fisher Scientific, RRID:AB_144696). The stained CNSs were imaged, and confocal stacks processed as described above for heads.

To display the GFP expression patterns of different spGAL4 and LexA lines together as shown in **Figure 3J** we used the Computational Morphometry Toolkit (CMTK) (*https://www.nitrc.org/projects/cmtk/*) (Jefferis et al., 2007) to computationally register individual confocal stacks of each line to the JFRC-2010 standard brain (*www.virtualflybrain.org*). The PIC file of each registered stack was loaded into Fiji and merged to display each in a different color channel.

For multicolor flipout (MCFO) experiments, dBMN-spGAL4, pBMN-spGAL4, and TasteBMN-spGAL4 were crossed to the MCFO-5 stock (RRID:BDSC_64089) (Nern et al., 2015). 9-12 day-old fly brains were dissected for pBMN-spGAL4 and dBMN-spGAL4, while 4-6 day-old brains were dissected for Taste-spGAL4. Brains were stained using rat anti-FLAG (Novus Biologicals, LLC, Littleton, Colorado, RRID:AB_1625981), rabbit anti-HA (Cell Signaling Technology, Danvers, Massachusetts, RRID:AB_1549585), mouse anti-V5 (Bio-Rad, Hercules, California, RRID:AB_322378), goat anti-rabbit AlexaFluor-488, goat anti-mouse AlexaFluor-568, goat anti-rat AlexaFluor-633 (Thermo Fisher Scientific, RRID:AB_2535749). Stained brains were imaged, and confocal stacks processed as

described above. Individually labeled neurons from each line are shown as maximum projections in **Figure 4** and **Figure 4 – figure supplements 6-8**. Given that very few flipout events occurred using the MCFO-5 stock in combination with the dBMN-spGAL4 and pBMN-spGAL4, we used a different MCFO stock (MCFO-3, RRID:BDSC_64087) to obtain a higher number of individually labeled neurons. Using dBMN-spGAL4 crossed with MCFO-3, we aged males for 9-12 days and obtained approximately 1-2 individually labeled neurons in 7 dissected brains. Crossing pBMN-spGAL4 with MCFO-3, we obtained about 1-4 labeled neurons in each dissected brain when we aged males 4-6 days.The flipout events in the latter cross occurred in much higher frequency given that most brains labeled more than a single neuron with the MCFO-3 stock.

Identification of driver lines that express in different subsets of head BMNs

We used the spGAL4 system to produce driver lines that expressed in different subsets of head BMNs (Luan et al., 2006; Pfeiffer et al., 2010). spGAL4 allows for independent expression of the GAL4 DNA binding domain (DBD) and activation domain (AD). When DBD and AD are expressed in the overlapping neurons, these domains reconstitute into a transcriptionally active protein. To label specific subpopulations of head BMNs, we visually screened through an image collection of the CNS expression patterns of enhancer-driven lines and identified candidate lines that were predicted to express in different subsets of head BMNs (Dionne et al., 2017; Jenett et al., 2012; Tirián and Dickson, 2017). We selected two candidate lines to express the DBD in subsets of head BMNs: VT050279 (VT050279-DBD, RRID:BDSC_72433) and R11D02 (R11D02-DBD, RRID:BDSC_68554). VT050279-DBD or R11D02-DBD flies carrying the *20XUAS-IVS-CsChrimson-mVenus* transgene (RRID:BDSC_55134) (Klapoetke et al., 2014) were crossed to 55 different candidate-ADs. The progeny were placed in behavioral chambers and exposed to red light for optogenetic activation (described below). We tested three flies for each DBD/AD combination to identify those that expressed in neurons whose activation could elicit grooming. Grooming “hits” were stained using a GFP antibody to detect CsChrimson-mVenus expression in the CNS and anti-NC82 to mark the neuropil as described above. We identified three different combinations that expressed in restricted subsets of BMNs, that included the ADs R28D07-AD (RRID:BDSC_70168), VT019023-AD (RRID:BDSC_71430), and VT023783-AD (RRID:BDSC_73261). We generated stable lines containing both the AD and DBD, including dBMN-spGAL4 (VT019023-AD ⋂ VT050279-DBD), pBMN-spGAL4 (R28D07-AD ⋂ VT050279-DBD), and TasteBMN-spGAL4 (VT023783-AD ⋂ R11D02-DBD).

Behavioral analysis procedures

For behavioral experiments, dBMN-spGAL4, pBMN-spGAL4, TasteBMN-spGAL4, and BPADZp; BPZpGDBD (spGAL4 control, RRID:BDSC_79603) were crossed to *20XUAS-CsChrimson-mVenus*. InOmBMN-LexA and BPADZp and BDPLexA (LexA control, RRID:BDSC_77691) were crossed to *13XLexAop2-IVS-CsChrimson-mVenus* (RRID:BDSC_55137). The controls used with the spGAL4 and LexA lines contain the vector backbone that was used to produce each line (including the coding regions for each spGAL4 half or LexA), but lack any enhancer to drive spGAL4 or LexA expression (Hampel et al., 2015; Pfeiffer et al., 2010, 2008).

We used a previously reported behavioral optogenetic rig, camera setup, and methods for the recording of freely moving flies (Hampel et al., 2017, 2015; Seeds et al., 2014). The stimulus parameters used were 656 nm red light at 27 mW/cm^2 intensity delivered at 5 Hz for 5 s (0.1 s on/off) with 10 or 30 second interstimulus intervals (total of 3 stimulations). While most of the driver lines were recorded using 30 second interstimulus intervals, pBMN-spGAL4 was recorded using 10 second intervals. This was because the elicited head nodding behavior occurred more robustly when stimulated every 10 seconds rather than 30 seconds.

Manual scoring of behavior from prerecorded video was performed using VCode software (Hagedorn et al., 2008) and analyzed in MATLAB (MathWorks Incorporated, Natick, MA). Some grooming and avoidance-like movements were annotated as previously described, including antennal, eye, ventral head, proboscis, and backward motion (Hampel et al., 2020a, 2017, 2015; Seeds et al., 2014). In this work, ventral head and proboscis grooming were combined and referred to as ventral head grooming. Head nodding was annotated when the fly tilted its head downward by any amount until it returned its head back in its original position. This movement often occurred in repeated cycles. Therefore, the "start" was scored at the onset of the first forward movement and the "stop" when the head returned to its original position on the last nod. Dorsal head grooming was scored when the fly used one or both legs to touch its dorsal head, which included the dorsal part of the eye. During dorsal head grooming, flies sometimes nodded, rotated, or kept their heads in their original position to groom the outer dorsal areas of the head (dorsal eye and posterior dorsal eye). The start of dorsal head grooming was scored when the legs reached their farthest posterior position on the head, before sweeping in the opposite direction. The movement was scored as stopped three frames after the legs last touched the head.

Behavioral data was analyzed using nonparametric statistical tests as previously reported (Hampel et al., 2020a, 2017, 2015). The percent time flies spent performing each behavior was calculated. To compare the behavior performed by each experimental genotype with its corresponding genetic control, we performed pairwise comparisons for each behavior using a Mann-Whitney U test and applied Bonferroni correction. Note that we tested both male and female flies for optogenetic activation of behavior. Although only males are presented in this manuscript, optogenetic activation was found to elicit similar behaviors in both males and females (not shown).

Dye filling of BMNs that innervate large bristles

The dye filling protocol used in this study was adapted from one that was previously published (Kays et al., 2014). C155-GAL4, *UAS-nSyb.eGFP* flies (RRID:BDSC_6920) were used for the dye fill experiments to label the neuropil. Flies were decapitated with a standard razor blade and their heads glued to a microscope cover glass (Fisher Scientific, Pittsburgh, Pennsylvania) using TOA 400 UV cured glue (Kemxert, York, Pennsylvania). Heads were submerged in 3.7% w/v paraformaldehyde in 0.2 M carbonate-bicarbonate buffer at pH 9.5 overnight at 4°C. Heads were washed 24 hours later by dipping in 0.2 M carbonate-bicarbonate buffer at pH 9.5 for 30 seconds, and subsequently in ddH2O for 30 seconds. Heads were gently blotted dry to prevent dye from spilling over the cuticle, and the selected bristles on the head were plucked with #5 Dumoxel forceps. Bristles were selected from either the left or right side of the head, depending on which bristle was in the most optimal orientation for plucking and filling.

Micropipettes for dye filling were prepared from Borosilicate Thin Wall capillaries (Warner Instruments, Holliston, Massachusetts, G100T-4). Capillaries were filled with 5-10 µL of dye solution of 10 µg/µL DiD (Thermo Fisher Scientific) in 100% ethanol and the tip was approached to the bristle socket with a micromanipulator. The tip of the capillary was made to contact the edge of the bristle socket such that the dye diffused into the socket until a stable bubble of solution formed. Heads were then dried for 5 minutes and then submerged in a 0.2 M carbonate-bicarbonate buffer at pH 9.5, in the dark, and at room temperature for 48 hours. The brains were then dissected and imaged immediately without fixation. Dissected brains were placed on a microscope slide with two Avery circular reinforcement labels and a circular cover slip. The brains were imaged immediately using a Zeiss LSM 800 confocal microscope. The native fluorescence of nSyb.eGFP was preserved enough at the conclusion of the experiment to image the brain neuropil (**Figure 4 – figure supplement 1B-E**).

We attempted to fill BMNs innervating the following head bristles: PoOc, Oc, Or, Ant, Vib, and Vt. Many attempts to fill particular bristles resulted in unfilled or partially filled BMNs. Anecdotally, there also seemed to be a difference in how well the filling method worked for the different bristle

populations. For example, multiple attempts to fill the Vt bristles only resulted in one successful fill of a BMN from Vt 1 and Vt 3 bristles. Additionally, we were unable to fill a BMN with multiple attempts of the PoOc bristle. Successful fill trials and the locations of specific bristles that were filled are shown in **Figure 4C-Q** and **Figure 4 – figure supplements 2-5**.

Light microscopy image stack storage and availability

The Z-stacks used to produce panels for **Figure 1**, **Figure 2**, **Figure 3**, and **Figure 4** and their figure supplements are all available for download at the Brain Image Library (RRID:SCR_017272). Links for each image Z-stack can be found in **Supplementary file 2**. The group DOI for all these Z-stacks is *https://doi.org/10.35077/g.1144*.

Reconstruction and analysis of bristle mechanosensory neurons from an EM volume

BMNs were reconstructed in a complete EM volume of the adult female brain (FAFB) dataset (Zheng et al., 2018) using the FlyWire.ai platform (Dorkenwald et al., 2023, 2022). We first identified the locations of the Ant-, Occi-, and merged Eye/LabNvs in the EM volume based on their identified locations from light microscopy data. We then chose a cross section of each nerve, close to where they enter brain neuropil, and where segmentation was available for all neurons in the nerve (**Figure 5 – figure supplement 1A-D**). We seeded every profile in the Occi- and merged Eye/LabNvs (**Figure 5 – figure supplement 1C,D**). The Eye/LabNvs had a bundle of soma tracts from an SEZ interneuron hemilineage crossing the seed plane that was excluded from the seeding process based on the morphology of their initial segmentation (**Figure 5 – figure supplement 1C**). Previous studies reconstructed major portions of JONs in FAFB AntNv using the CATMAID platform (Hampel et al., 2020a; Kim et al., 2020). Because the FlyWire FAFB brain was locally realigned, we transformed those JONs into the FlyWire space using natverse version 0.2.4 (Bates et al., 2020). After overlaying these JONs onto the seed plane, they were excluded during the seeding effort to identify BMNs in the AntNv. This left a small ventral-medial area of the nerve with previously undocumented neurons that were seeded and reconstructed (**Figure 5 – figure supplement 1B**). We focused our reconstructions in the right hemisphere nerves. However, we also examined the OcciNv in the left hemisphere, given that it only contained a small number of neurons (**Figure 6 – figure supplement 4A-D**).

The segmentations of all seeded neurons were then fully proofread by a human annotator. This process involves splitting falsely merged parts and merging falsely missing parts of a neuron using the tools available in the FlyWire neuroglancer instance (flywire.ai). FlyWire neuroglancer was also used to examine the morphologies of neurons for classification purposes.

The neurons classified as sensory origin (no soma in the brain, only axonal projections and entering through a nerve) were skeletonized using natverse (skeletor in fafbseg package version 0.10.0). Skeletons were pruned to synapse rich areas to exclude the smooth axon in the nerve bundle. We created a three dimensional mesh of the synapses (for synapses see below) and pruned the skeletons to arbors within the mesh volume. We then compared their morphology using the NBLAST algorithm (Costa et al., 2016) and clustered the similarity scores with Ward (**Figure 6 – figure supplement 1A,B**). The skeletons of CATMAID reconstructions of JONs from (Hampel et al., 2020a; Kim et al., 2020) and skeletonizations of sensory neurons from this publication were transformed into JRC2018F standard brain space for plotting using natverse. The transformed skeletons, meshes from the FlyWire proofread segmentation and brain neuropil meshes were plotted with natverse in RStudio 2022.02.3. We used the standard brain transformations to analyze if BMNs crossed the midline in the brain. Defining the midline accurately is possible due to the symmetric nature of this brain space. If any skeleton node coordinates of a given BMN were located in the contralateral hemisphere (x of node > x of midline) we classed the BMN as midline-crossing.

FlyWire provides access to a synapse table imported from (Buhmann et al., 2021). We queried the table for pre- and postsynaptic sites belonging to the reconstructed sensory neurons for connectome analysis (**Figure 7 – figure supplements 1-3**). We used the cleft scores of the cleft prediction from (Heinrich et al., 2018) to filter synapses with scores below 50, which reliably excludes falsely predicted synapses.

We then analyzed the connectivity of BMNs with each other, and with other postsynaptic partners. First, we analyzed BMN type connectivity by adding up synaptic weights of BMN-to-BMN edges by type and normalizing by the number of possible edges between the groups (**Figure 8 – figure supplement 1B**). Graphs were plotted using Cytoscape version 3.9.1 and the RCy3 (version 2.17.1) and igraph (version 1.3.0) packages for Cytoscape control from R (Shannon et al., 2003). Further, we compared BMN types regarding their pre- and postsynaptic connection counts (**Figure 8 – figure supplement 1A**). We counted all entries in the FlyWire synapse table at which a given BMN was either the pre- and postsynaptic partner (not number of presynaptic sites, cleft scores ≥ 50). This revealed that BM-InOm neurons had fewer synaptic connections than other BMN types, which was not surprising given their small, non-complex axonic arbors in the brain. This posed a challenge when comparing BM-InOm neuron synaptic connectivity to other BMN types, as described below.

We calculated cosine similarity of BMNs to cluster them based on their connectivity similarity. Cosine similarity emphasizes the similarity of BMNs which have similar sets of postsynaptic targets. We took advantage of the good proofreading state of the FlyWire datasat to perform postsynaptic connectivity analysis (Dorkenwald et al., 2023, 2022). Note that this strategy is agnostic about partner types. A comprehensive typing of the postsynaptic partners will be included in a follow up study as it exceeds the focus of this study. For this analysis, we excluded synapses between BMNs and only considered postsynaptic connectivity to neuron partners of other types (non-BMNs). As mentioned, BM-InOm neurons have few connections to postsynaptic partners (pre counts in **Figure 8 – figure supplement 1A**), so we choose a low threshold of 3 synapses and excluded edges below that. When clustering the cosine similarity (ComplexHeatmap version 2.11.2 package in R) for all BMNs, we found that subsets of the BM-InOm neurons clustered together with other BMN types (data not shown), but the clustering failed to capture meaningful groups. Choosing a higher threshold resulted in most of the BM-InOm neuron connectivity being excluded, giving low cosine similarity scores even when compared to each other. We thus choose a higher threshold of 7 synapses to analyze the cosine similarity of the BMN types excluding BM-InOm neurons (**Figure 8 – figure supplement 2**) and the low synapse threshold of 3 for analysis of the BM-InOm neurons separately (**Figure 8 – figure supplement 3**). This analysis better captured the somatotopic mapping of the BMN types in the brain. From our preliminary analysis we expect BM-InOm neurons to share postsynaptic partners with other BMN types, but further analysis is required to investigate patterns of connectivity of all BMNs to postsynaptic targets.

Connections to postsynaptic partners were calculated as follows: We analyzed all postsynaptic partners of the BMNs (after applying the above mentioned cleft score) and summed the BMN input by BMN type. We assigned postsynaptic partners to the BMN type giving the highest input to them (e.g. if BM-Ant neurons contribute the highest synaptic input to a given postsynaptic neuron this neuron is termed Ant_post). We then plotted the connections from BMN types to the postsynaptic partner neurons grouped by their major input partner. To show only strong connections we applied a threshold (>5%) by normalizing the edges by the total output of a given BMN type (**Figure 8F**).

Matching EM reconstructed BMN projections with light microscopy imaged BMNs that innervate specific bristles

Manual categorization of the EM reconstructed sensory neurons revealed that they consist of BMNs, JONs, *taste peg mechanosensory neurons* (TPMNs), and *gustatory neurons* (GRNs). JONs and GRNs were previously identified and described in the EM volume using the CATMAID platform (Engert et al., 2022; Hampel et al., 2020a; Kim et al., 2020). The TPMNs were identified based on their morphological similarity to previous light microscopy descriptions (Jeong et al., 2016; Miyazaki and Ito, 2010; Zhou et al., 2019). 25 sensory neurons were reconstructed that could not be identified based on dye fill, MCFO, or published neurons. These neurons are referred to in this work as unknown and shown in **Figure 5 – figure supplement 2A-Y**. We also identified interneurons that were not classified because sensory neurons were the focus of this study. The BMNs, JONs, and TPMNs are shown in **Figure 5 – figure supplement 1A,E**. The GRNs and interneurons were excluded from further analysis in this study.

The 705 BMNs and 25 unknown sensory neurons were clustered based on NBLAST similarity scores as described above (**Figure 6 – figure supplement 1A,B**). We used these clusters in conjunction with manual anatomical inspection of light microscopy images to assign the BMNs to specific bristle populations. In particular, we compared the morphologies of the EM-reconstructed BMNs with dye-filled, stochastically-labeled (MCFO), and driver line-labeled BMNs (**Figure 6 – figure supplement 2A-N**). In some cases we did not have light microscopy images to enable direct matching of particular BMNs to their corresponding bristles. These BMNs were matched based on the morphology of BMNs innervating neighboring bristle populations (described for specific BMNs below). We also verified that the numbers of BMNs for each type were consistent with the numbers of their bristles (**Figure 6 – figure supplement 3B-F**). In the specific cases described below, we used additional evidence to match the different BMNs to their bristles, including comparing the reconstructed BMNs on both sides of the brain (OcciNv only, **Figure 6 – figure supplement 4A-D**) and based on common connectivity of the BMNs with their postsynaptic partners (**Figure 8A-C** and **Figure 8 – figure supplement 1**). A full list of the BMNs can be found in **Supplementary file 3**.

The BMNs have been referred to in some previous work as external sensilla (es neurons). We adopted BMN here because it was similar to the widely adopted nomenclature for different sensory modalities, such as GRNs, ORNs, JONs. Further, it more explicitly links the neurons to the bristles.

3 BMNs that innervate the InOc bristles (BM-InOc neurons, **Figure 6F**) were identified based on comparison with MCFO data (**Figure 6 – figure supplement 2C**). 1 BMN that innervates the Oc bristle (BM-Oc neuron, **Figure 6G**) was identified based on comparison with dye fill data (**Figure 6 – figure supplement 2D**). 6 BMNs are proposed to innervate the Fr bristles (BM-Fr neurons, **Figure 6H**). The Fr bristles are located near the midline, immediately above the Ant bristles and below the InOc and Oc bristles. BMNs that innervate the Ant, InOc, and Oc bristles show very similar morphology with the BM-Fr neurons, including the ipsilateral and midline projections. 20 BMNs that innervate the Ant bristles (BM-Ant neurons, **Figure 6I**) were identified based on comparison with dye fill data (**Figure 6 – figure supplement 2E**). 3 BMNs that innervate the Or bristles (BM-Or neurons, **Figure 6J**) were identified based on comparison with dye fill data (**Figure 6 – figure supplement 2F**). 6 BMNs are proposed to innervate the FrOr bristles (BM-FrOr neurons, **Figure 6K**). The FrOr bristles are located immediately ventral to the Or bristles. The BM-Or neurons show very similar morphology with the proposed BM-FrOr neurons, including an ipsilateral projection.

555 BMNs that innervate the InOm bristles (BM-InOm neurons, **Figure 6L**) were identified using previous descriptions of the projections of these neurons (Hampel et al., 2017; Zhang et al., 2020). The similarity of the collective projections of the BM-InOm neurons with those labeled by

the InOmBMN-LexA driver line are shown in **Figure 6 – figure supplement 2N**. Clustering based on NBLAST similarity scores revealed that there were morphologically distinct groups of BM-InOm neurons. However, in contrast to other BMN types, the BN-InOm neurons were small with few relatively simple branches, and the clusters were likely due to relatively minor differences in these branches. For example, at the selected cut height (H=5) resulted in 11 different clusters (**Figure 6 – figure supplement 1A,B**). Additionally, while the BM-InOm neurons showed some differential postsynaptic connectivity based on cosine clustering results, these differences were relatively low (**Figure 7 – figure supplement 3A,B**). Therefore, the BM-InOm neurons are treated as a single group that innervates eye bristles in this work, while a future study will further examine the heterogeneity of the BM-InOm neurons.

18 EyeNv-projecting BMNs that innervate the Vib bristles (BM-Vib neurons, **Figure 6M**) were identified based on comparison with dye fill data (**Figure 6 – figure supplement 2G**). This includes 3 BMNs that project through the AntNv (BM-Vib (AntNv) neurons) that are morphologically similar to the BM-Vib (EyeNv) neurons. Based on 52A06-GAL4 labeling of BMNs on the head, BM-Vib (AntNv) neurons innervate smaller anterior Vib bristles that are lateral to Vib 1 and 2 bristles. In total, 15 BMNs projecting through the EyeNv (BM-Vib (EyeNv)) and 3 projecting through the AntNv (BM-Vib (AntNv)) were identified in the EM dataset.

15 BMNs are proposed to innervate the MaPa bristles (BM-MaPa neurons, **Figure 6N**), as their morphology matches a previous description (Singh and Nayak, 1985). It was difficult to distinguish between BM-MaPa and BM-Vib neurons based on morphology or nerve projection. However, all BM-MaPa neurons showed high cosine similarity in their postsynaptic connectivity to non-BMN neurons, and clustered together (**Figure 8 – figure supplement 2**).

BMNs that innervate the Taste bristles (BM-Taste neurons, **Figure 6O**) were identified based on their similarity to the MCFO images (**Figure 6 – figure supplement 2H**). We did not have dye fill or MCFO images of the BMNs that innervate the Hau bristles (BM-Hau neurons). These BMNs were presumed to show similar morphology to the BM-Taste neurons, given their close proximity. Indeed, visual inspection revealed 5 BMNs that had similar, yet slightly different morphology (**Figure 6P**). The axons appeared larger in diameter and showed a dorsal midline-crossing branch that was not found in BM-Taste neurons. Further, the 5 BM-Hau neurons showed high cosine similarity in their postsynaptic connectivity with non-BMN neurons (**Figure 8 – figure supplement 2**).

5 BMNs that project through the OcciNv that could innervate the Vt bristles (BM-Vt neurons, **Figure 6Q**) were identified based on comparison with dye fill data (**Figure 6 – figure supplement 2I-K**). Because there are only 4 Vt bristles, the additional BMN in this group is proposed to innervate the PoOc bristle (BM-PoOc neuron). However, because we had no dye fills for the BM-PoOc neuron and limited dye fill examples of BM-Vt neurons, we included all 5 BMNs in the category BM-Vt/PoOc neurons. PoOc is hypothesized to project through the OcciNv and show similar morphology to the neighboring BM-Oc and -InOc neurons, and at least one BM-Vt/PoOc neuron has the expected morphology. Although the BM-InOc neuron is presumed to exist, we could not find evidence of a neuron innervating the PoOc bristle using any of the BMN driver lines reported in this study (**Figure 2 – figure supplement 1G**).

7 BMNs projecting through the OcciNv showed very similar morphology and were identified as innervating the dPoOr and dOcci bristles and named BM-dPoOr and BM-dOcci neurons, respectively. The morphology of the BM-dPoOr neurons was determined from MCFO experiments using dBMN-spGAL4 (**Figure 6 – figure supplement 2L**). MCFO experiments using pBMN-spGAL4 did not enable us to distinguish between BM-dPoOr and BM-dOcci neurons, as we could not tell which BMN came from which bristle population (**Figure 4S,T**, **Figure 4 – figure supplement 7B-D**). One difficulty in matching the reconstructed BM-PoOr and BM-dOcci neurons was that their numbers in the left brain hemisphere did not match what we expected

from the numbers of their corresponding bristles. For example, there were only 4 tentatively assigned BM-dPoOr neurons, while we expected between 5 and 9 (**Figure 6 – figure supplement 3E**). Because the OcciNv contains only a small number of BMNs, we also reconstructed BMNs in the right brain hemisphere OcciNv (**Figure 6 – figure supplement 4A-D**). This revealed 4 additional BMNs on the right than on the left for the BM-dPoOr neurons, which matched what we expected (**Figure 6 – figure supplement 4D**). The numbers of the other BMN types that project through the OcciNv (i.e. BM-Vt/PoOc and BM-dOcci neurons) were the same in both hemispheres and matched with the expected number of bristles.

26 BMNs projecting through the EyeNv show very similar morphology and were identified as innervating the vPoOr and vOcci bristles. The vOcci-innervating BMNs (BM-vOcci neurons) were matched with MCFO images (**Figure 6 – figure supplement 2M**). However, we did not obtain dye fill or MCFO images of BMNs innervating the vPoOr bristles (BM-vPoOr neurons). These neurons were expected to show similar morphology with the BM-vOcci neurons based on their close proximity. Because we could not distinguish between these BMNs, they were grouped together and named (BM-vOcci/vPoOr neurons, **Figure 6T**).

Acknowledgements

We thank Brian Chen's lab at McGill University Health Centre for essential feedback on the development of the dye labeling protocol from this study. We thank the Princeton FlyWire team and members of the Murthy and Seung labs for development and maintenance of FlyWire (supported by BRAIN Initiative grant MH117815 to Murthy and Seung), and the Princeton EM proofreading team for contributing neuronal edits. We thank FlyWire users who contributed >10% proofreading of individual neurons or identification of neurons: Mala Murthy group ((>10% of 31 neurons) Claire McKellar, Austin T Burke, Sarah Morejohn, Kyle Patrick Willie, Merlin Moore, Doug Bland, Ben Silverman, Jay Gager, Ryan Willie), Carlos Ribeiro group ((>10% of 35 neurons) Ibrahim Tastekin, Raquel Barajas), the *Drosophila* Connectomics Group, Cambridge University (leads: M. Costa and G. Jefferis) for contributing to the tracing of FlyWire neurons ((>10% of 20 neurons) Yijie Yin, Paul Brooks, Laia Serratosa Capdevila, Siqi Fang, A Javier, Paul Brooks), Rachel Wilson group ((>10% of 8 neurons) Peter Gibb), Julie Simpson group ((>10% of 2 neurons) Li Guo), Wolf Hütteroth group (>10% of 4 neurons), and Jinseop Kim group ((>10% of 753 neurons) Hyunsoo Yim, Senongbong Yu, Chan Hyuk Kang, Taehyun Choe, Yeonju Nam, Tae Kim, Jinmook Kim).

Research reported in this publication was supported by the National Institute Of Neurological Disorders And Stroke of the National Institutes of Health under Award Number RF1NS121911. The content is solely the responsibility of the authors and does not necessarily represent the official views of the National Institutes of Health. This work was also funded by the Whitehall Foundation (2017-12-69), Puerto Rico Science, Technology & Research Trust (2020-00195), NIMHD MD007600 (RCMI), NIGMS-NIH RISE (R25GM061838), NIGMS-NIH RISE (5R25GM061151), NIH NIGMS GM103642, and NSF (HRD-1736019).

Supplementary file 1. Quantification of bristle populations on male and female heads. Table 1. Bristles counted using white light-illuminated male and female heads. Results of a two-tailed t-test comparing male and female bristle numbers are also shown. Table 2 shows counts of PoOr bristles innervated by BMNs that project through the OcciNv (dPoOr bristles) or the EyeNv (vPoOr bristles). BMNs were labeled by R52A06-GAL4. Table 3 shows vOcci bristles counted based on having an associated BMN labeled in the pBMN-spGAL4 (R28D07-AD ⋂ VT050279-DBD) pattern (males). Table 4 shows a summary of published bristle numbers.

Supplementary file 2. Table of download links for light microscopy image stacks used in this manuscript. Image stacks are stored in the Brain Image Library (BIL), and were used to generate panels for **Figure 1**, **Figure 2**, **Figure 3**, **Figure 4**, and figure supplements for these

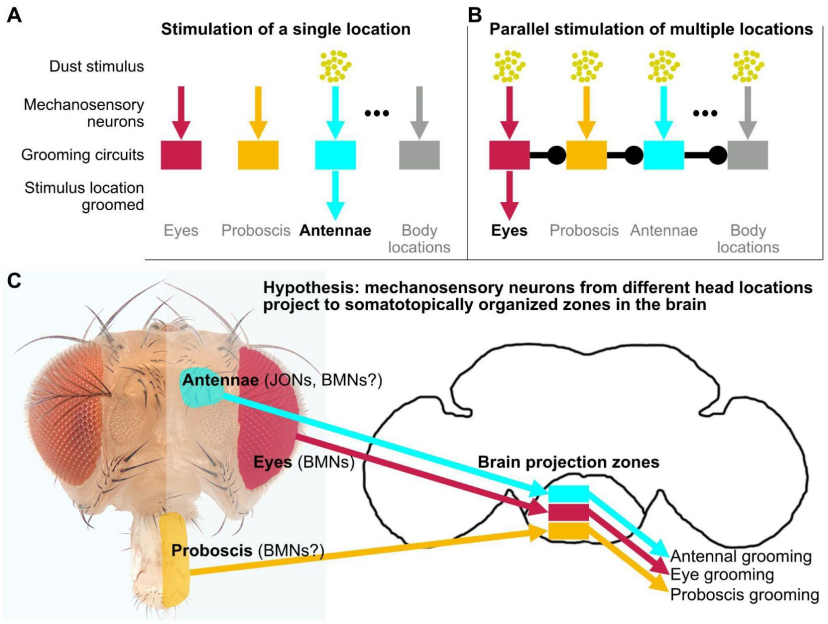

Figure 1 – figure supplement 1.

Hypothesized grooming circuit architecture features somatotopically organized parallel mechanosensory pathways.

(**A,B**) The architecture elicits aimed grooming of specific locations of the head and body (**A**) and exerts hierarchical suppression in the grooming sequence (**B**). (**A**) Stimulation of a single location (e.g. antennae) by a mechanical stimulus such as dust is detected by local mechanosensory neurons. These neurons connect with distinct postsynaptic circuits that elicit aimed grooming of their respective locations. We referred to these parallel mechanosensory pathways as “grooming modules” in Seeds *et al*., 2014. The present study focuses on the organization among bristle mechanosensory neurons (BMNs) that elicit aimed grooming of different locations on the head, such as the eyes (red), proboscis (orange), and antennae (aqua). The body locations grooming pathway (gray) represents a continuation of the parallel architecture for any given body location, such as the abdomen or wings. (**B**) Being coated in dust stimulates multiple locations, inducing competition among the pathways that elicit mutually exclusive grooming movements. These movements are prioritized through hierarchical suppression (unidirectional ball and stick connections between circuits). For illustration simplicity, only the nearest-neighbor connections are shown. In the hypothesized architecture, each circuit suppresses all the subordinate circuits in the hierarchy. For example, eye grooming occurs first in the sequence because it suppresses all later movements, such as grooming of the proboscis, antennae, and body locations. (**C**) We hypothesize that mechanosensory neurons from different head locations project to distinct somatotopically organized zones in the ventral brain. Mechanosensory neurons on the antennae (JONs) and eyes (BMNs) are reported to elicit aimed grooming, and BMNs at other locations are hypothesized to also elicit grooming. Mechanosensory neuron projections in the brain are hypothesized to connect with postsynaptic circuits (boxes) that elicit grooming through descending pathways that activate movement pattern generators in the ventral nerve cord.

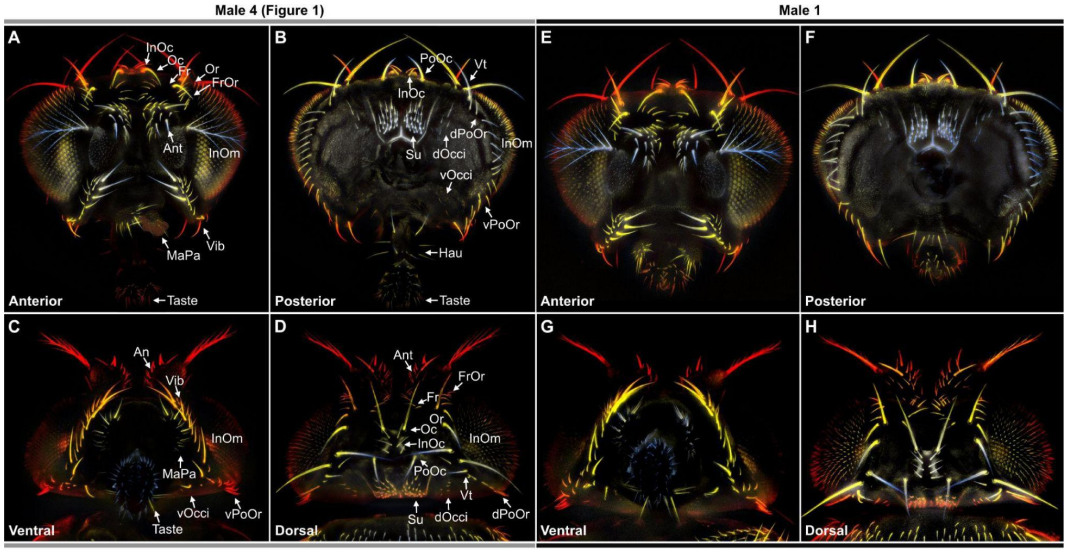

Figure 1 – figure supplement 2.

Color-coded depth maps of the head.

(**A-H**) Example depth maps that were constructed from image Z-stacks (see Materials and methods). Shown are the anterior (**A,E**), posterior (**B,F**), ventral (**C,G**), and dorsal (**D,H**) views of two different male heads. (**A-D**) Head shown in **Figure 1** (Male 4). (**E-H**) Example of a different male head (Male 1). Colors indicate closer features in light blue, and increasingly more distant features in white, yellow, and dark red. Bristle names are indicated using abbreviations, whose full names are listed in **Figure 1E**.

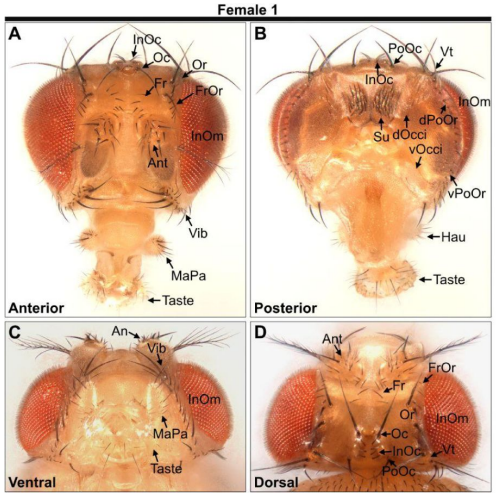

E

		Males			Females			t-test
Abv.	Bristle name	Range	Avg.	SD	Range	Avg.	SD	p-value
Ant	Antennal	18-22	20.6	0.9	16-23	21.0	1.3	0.465
Fr	Frontal	4-7	5.7	0.6	4-6	5.3	0.3	0.117
FrOr	Frontoorbital	4-6	4.9	0.4	4-6	5.1	0.5	0.418
Or	Orbital	3	3	0	3	3	0	1.000
Oc	Ocellar	1	1	0	1	1	0	1.000
InOc	Interocellar	3-4	3.4	0.3	3-5	3.9	0.3	0.033
Vib	Vibrissa	13-18	14.8	0.9	13-17	14.8	1.3	1.000
InOm	Interommatidial	ND	ND	ND	ND	ND	ND	ND
vOcci	Occipital (v)	12-18	15.2	0.9	ND	ND	ND	ND
PoOr	Postorbital (d + v)	18-22	19.9	1.2	20-23	21.5	0.4	0.006
Vt	Vertical	3-4	3.9	0.2	4	4	0	0.351
dOcci	Occipital (d)	2-5	4.2	0.5	4-8	5.0	0.8	0.140
MaPa	Maxillary palp	14-18	16.1	1.5	14-17	15.0	0.9	0.154
Hau	Haustellum	5	5	0	5	5	0	1.000
Taste	Taste	ND	ND	ND	ND	ND	ND	ND
PoOc	Postocellar	1	1	0	1	1	0	1.000
Su	Supracervical	14-22	18.3	1.5	18-23	20.4	1.0	0.023

Figure 1 – figure supplement 3.

Comparison of bristle numbers on male and female heads.

(**A-D**) Bristles on an anterior (**A**), posterior (**B**), ventral (**C**), and dorsal (**D**) female head (Female 1). (**E**) Table shows quantification of bristles on male and female heads and male/female comparisons (male N=8, female N=4). Bristle numbers for each population are for one half of the head. Range, Avg., and SD are shown as described in **Figure 1**. A student's t-test (2-tailed) was performed to compare the male/female bristle populations. InOc, PoOr (d+v), and Su bristles show a t-test $p \leq 0.05$, however the Bonferroni-adjusted α-value is 0.004 (14 comparisons). See **Supplementary file 1** for bristle counts for each head. Note that the PoOr (d+v) bristles were counted as a single group for comparing bristle numbers between males and females. Not determined (ND). See **Supplementary file 2** for image stack download links for each head used in this analysis.

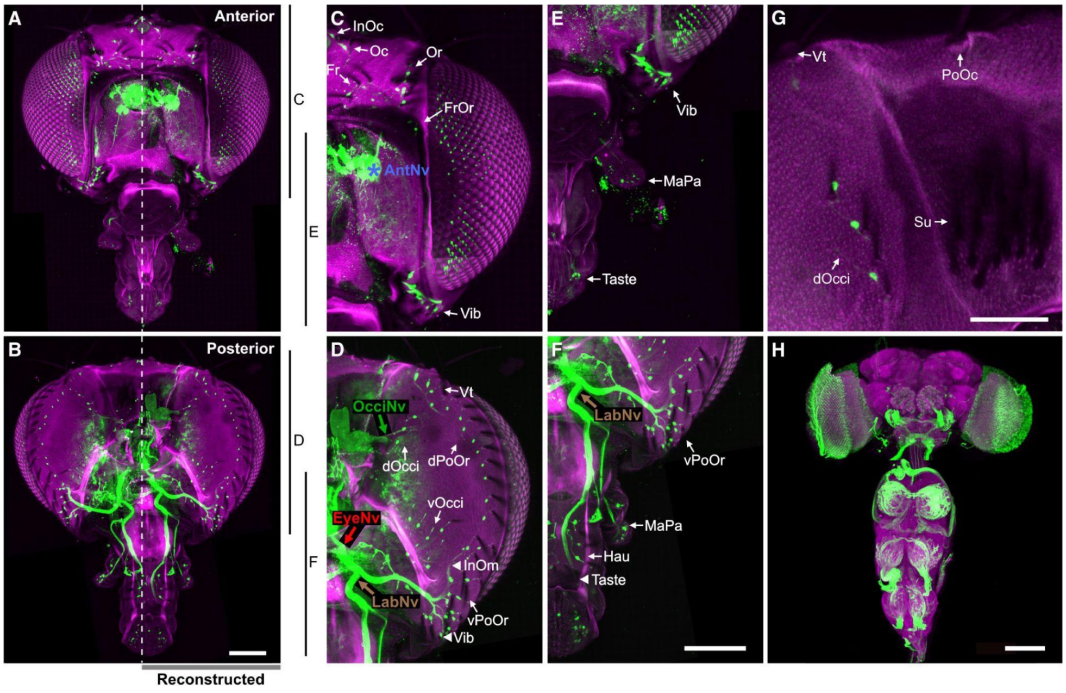

Figure 2 – figure supplement 1.

R52A06-GAL4 expression in head BMNs.

(**A,B**) Maximum intensity projections of the left and right halves of the anterior (**A**) and posterior (**B**) heads that are shown in **Figure 2C,D**. BMNs are green and the cuticle is magenta. The BMNs on the right side of the midline (dotted line) for either the anterior or posterior heads were reconstructed and shown in **Figure 2C,D** (right). Anterior and posterior images are from two different heads. (**C-F**) Magnified images of **A** and **B**. Magnified areas are indicated by the vertical lines. The different nerves are labeled with colored arrows. Location of unreconstructed portion of AntNv is indicated by an asterisk. Innervated bristles are indicated with white arrows. White arrowheads in **D** and **F** indicate partially reconstructed axons of BMNs innervating the InOm, Vib, and Taste bristles. (**G**) Posterior region of the head that includes the PoOc, Su, and dOcci bristes. Note that there are no GFP-labeled BMNs innervating the PoOc and Su bristles. (**H**) Brain and ventral nerve cord of R52A06-GAL4 expressing GFP and immunostained for GFP (green) and Bruchpilot (magenta) to label the neuropile. Scale bars all indicate 100 µm. **Supplementary file 2** provides confocal Z-stack download links.

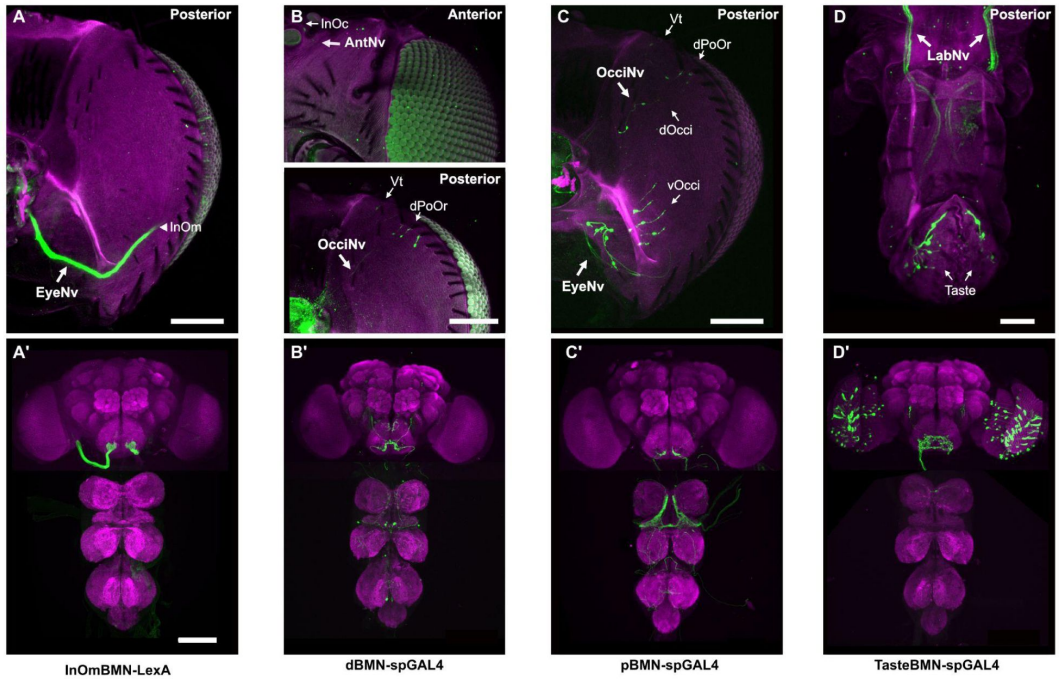

E

Driver line	Ant	Fr	FrOr	Or	Oc	InOc	Vlb	InOm	vOcci	vPoOr	dPoOr	Vt	dOcci	MaPa	Hau	Taste	PoOc	Su
dBMN-spGAL4						1.0 +/- 0					1.4 +/- 0.7	1.8 +/- 0.7						
pBMN-spGAL4									15.2 +/- 0.9		1.2 +/- 0.7	1.2 +/- 0.9	2.9 +/- 0.7					
TasteBMN-spGAL4																3.7 +/- 1.3		

Number of GFP positive BMNs that innervate each bristle population (Average +/- SD)

Figure 3 – figure supplement 1.

Driver line expression in head BMNs.

(**A-D'**) Maximum intensity projections of heads (**A-D**) and CNSs (**A'-D'**) expressing GFP in BMNs that innervate different bristles. **A-D** were produced from the same confocal Z-stacks that were used for the BMN reconstructions shown in **Figure 3D-G**. Magnified views of the SEZs in **A'-D'** are shown in **Figure 3D'-G'**. The expression patterns of the following driver lines are shown: InOmBMN-LexA (**A,A'**), dBMN-spGAL4 (**B,B'**), pBMN-spGAL4 (**C,C'**), and TasteBMN-spGAL4 (**D,D'**). Scale bars, 100 µm (**A-C**), 50 µm (**D**), 100 µm (**A'-D'**). (**E**) Table showing the average number of GFP positive BMNs (and SD) that innervate each bristle population from the indicated spGAL4 lines. **Supplementary file 2** provides confocal Z-stack download links.

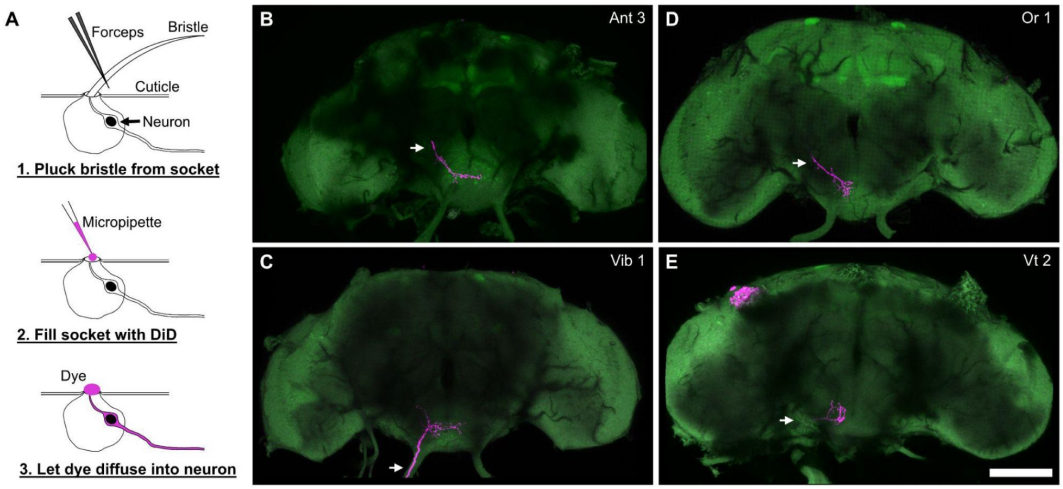

Figure 4 – figure supplement 1.

Overview of the dye filling technique and whole brain examples.

(**A**) Schematic of the dye filling technique used for labeling BMNs from specific bristles. BMNs were labeled with the anterograde dye, DiD. Each bristle was plucked from a head and DiD was pipetted onto the exposed socket to label the BMN innervating that bristle. (**B-E**) Whole brain examples of four fills shown in **Figure 4**. Examples are from Ant 3 (**B**), Vib 1 (**C**), Or 1 (**D**), and Vt 2 (**E**) bristle socket fills. Each filled BMN is magenta and the brain neuropile is labeled with pan neuronally expressed nSyb.GFP in green. Scale bar, 100 µm. **Supplementary file 2** provides confocal Z-stack download links.

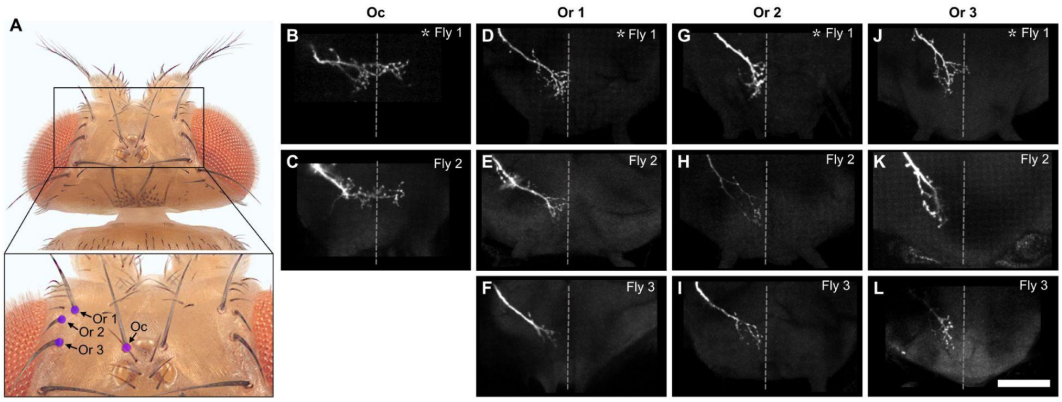

Figure 4 – figure supplement 2.

Different fill trials for Oc and Or bristles.

(**A**) Oc and Or bristles whose associated BMNs were labeled by dye filling are indicated with labeled dots (dorsal view). The boxed area in the top image is shown magnified in the bottom image. (**B-L**) Anterior view of the SEZ projections of individual BMNs that innervate the Oc (**B,C**), Or 1 (**D-F**), Or 2 (**G-I**), and Or 3 (**J-L**) bristles. Two or three different flies were tested for each bristle (fly number indicated in upper right corner). Asterisk indicates the BMN example that is shown in **Figure 4**. BMNs are oriented as if they are projecting from the right side of the head. Scale bar, 50 µm. Dotted line indicates approximate SEZ midline. **Supplementary file 2** provides confocal Z-stack download links.

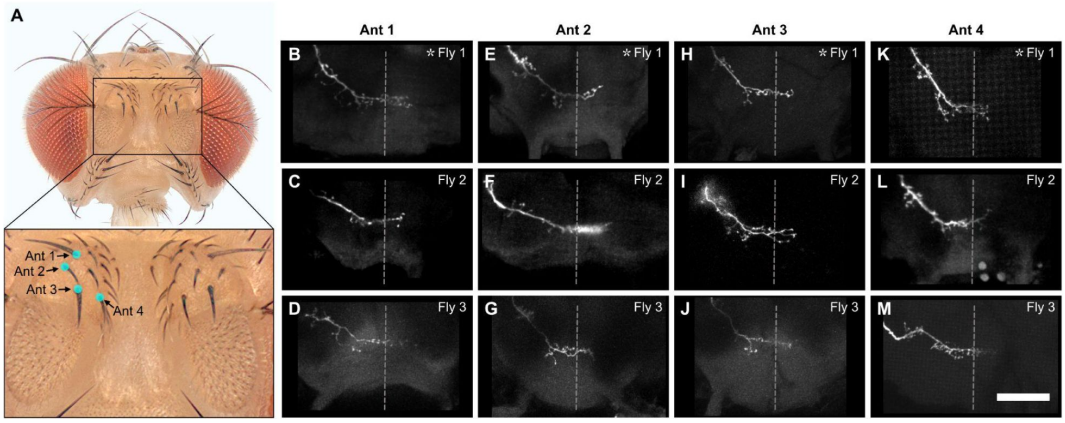

Figure 4 – figure supplement 3.

Different fill trials for Ant bristles.

(**A**) Ant bristles whose associated BMNs were labeled by dye filling are indicated with labeled dots (anterior view). The boxed area in the top image is shown magnified in the bottom image. (**B-M**) Anterior view of the SEZ projections of individual BMNs that innervate the Ant 1 (**B-D**), Ant 2 (**E-G**), Ant 3 (**H-J**), and Ant 4 (**K-M**) bristles. Three different flies were tested for each bristle (fly number indicated in upper right corner). Asterisk indicates the BMN example that is shown in **Figure 4**. Scale bar, 50 µm. Dotted line indicates approximate SEZ midline. **Supplementary file 2** provides confocal Z-stack download links.

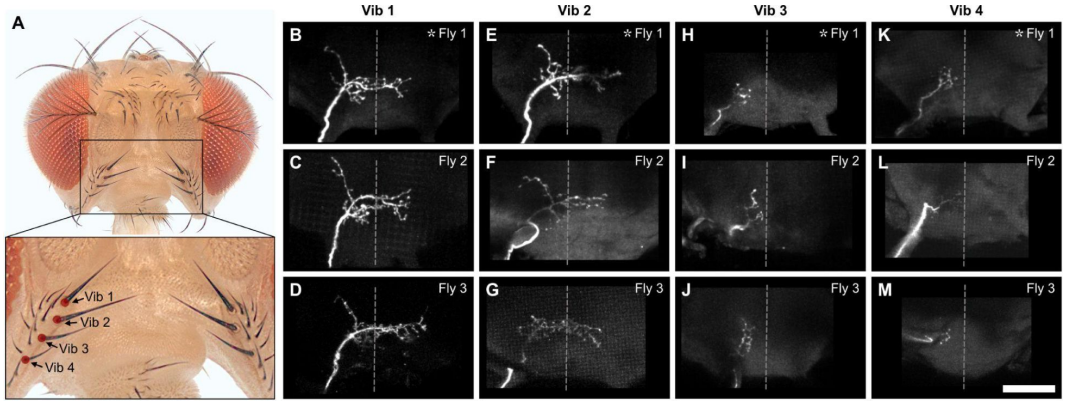

Figure 4 – figure supplement 4.

Different fill trials for Vib bristles.

(**A**) Vib bristles whose associated BMNs were labeled by dye filling are indicated with labeled dots (anterior view). The boxed area in the top image is shown magnified in the bottom image. (**B-M**) Anterior view of the SEZ projections of individual BMNs that innervate the Vib 1 (**B-D**), Vib 2 (**E-G**), Vib 3 (**H-J**), and Vib 4 (**K-M**) bristles. Three different flies were tested for each bristle (fly number indicated in upper right corner). Asterisk indicates the BMN example that is shown in **Figure 4**. Scale bar, 50 µm. Dotted line indicates approximate SEZ midline. **Supplementary file 2** provides confocal Z-stack download links.

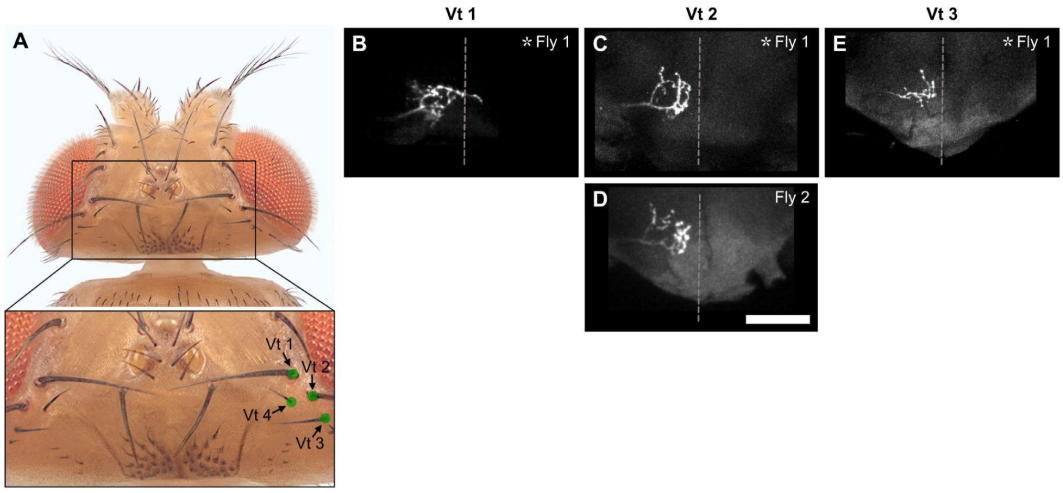

Figure 4 – figure supplement 5.

Different fill trials for Vt bristles.

(**A**) Vt bristles whose associated BMNs were labeled by dye filling are indicated with labeled dots (dorsal view). The boxed area in the top image is shown magnified in the bottom image. (**B-E**) Anterior view of the SEZ projections of individual BMNs that innervate the Vt 1 (**B**), Vt 2 (**C,D**), and Vt 3 (**E**) bristles. One or two different flies were tested for each bristle (fly number indicated in upper right corner). Asterisk indicates the BMN example that is shown in **Figure 4**. Scale bar, 50 µm. Dotted line indicates approximate SEZ midline. Note: Vt 4 was not filled. **Supplementary file 2** provides confocal Z-stack download links.

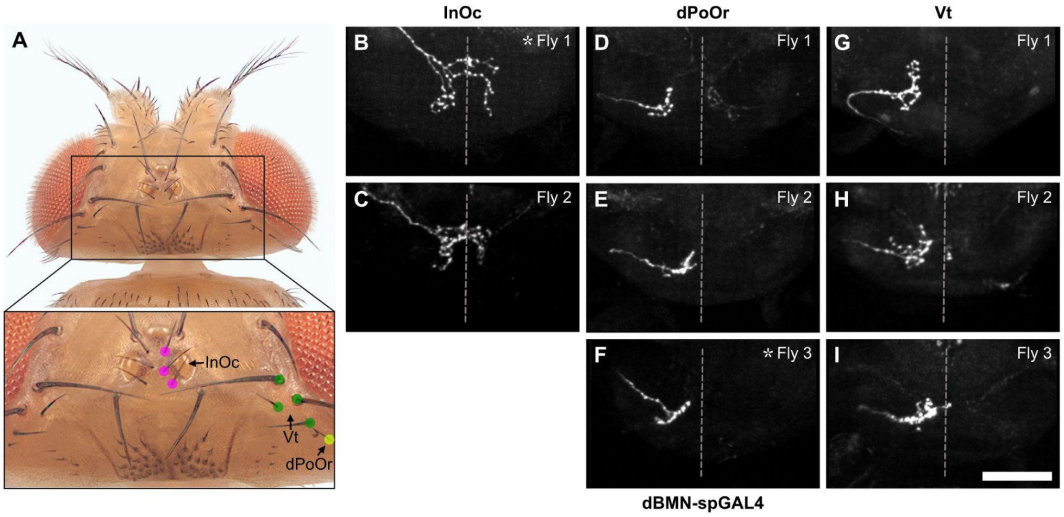

Figure 4 – figure supplement 6.

MCFO trials for BMNs innervating the InOc, dPoOr, and Vt bristles.

(**A**) Bristles whose associated BMNs were labeled by MCFO are indicated with labeled dots (dorsal view). The boxed area in the top image is shown magnified in the bottom image. (**B-I**) Anterior view of the SEZ projections of individual BMNs labeled by MCFO using dBMN-spGAL4. BMNs shown innervate the InOc (**B,C**), dPoOr (**D-F**), and Vt (**G-I**) bristles. At least two different flies were tested for each BMN (fly number indicated in upper right corner). Asterisk indicates the BMN example that is shown in **Figure 4**. Scale bar, 50 µm. Dotted line indicates approximate SEZ midline. **Supplementary file 2** provides confocal Z-stack download links.

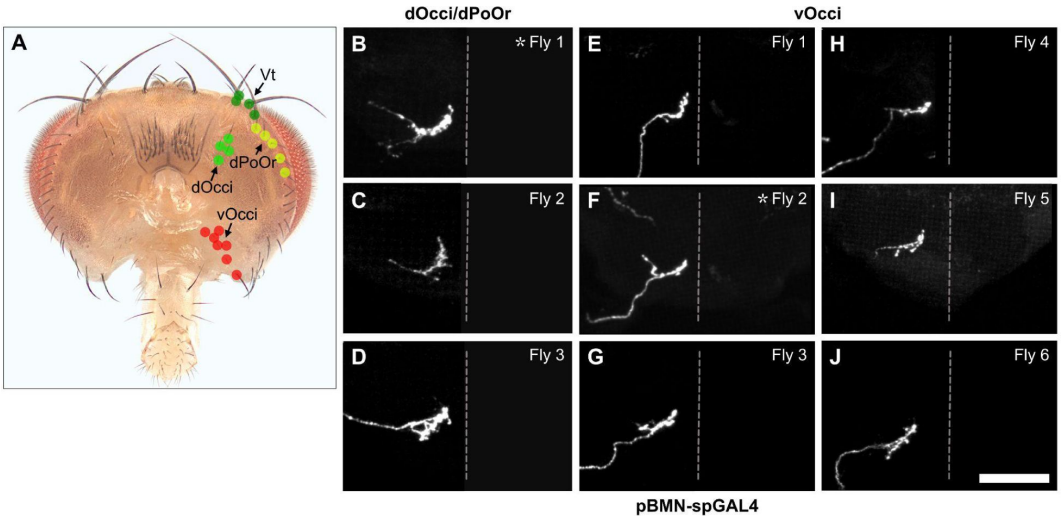

Figure 4 – figure supplement 7.

MCFO labeled trials for BMNs innervating the dOcci/dPoOr and vOcci bristles.

(**A**) Bristles whose associated BMNs were labeled by MCFO are indicated with labeled dots (posterior view). (**B-J**) Anterior view of the SEZ projections of individual BMNs labeled by MCFO using pBMN-spGAL4. BMNs shown innervate the dPoOr/dOcci (**B-D**) and vOcci (**E-J**) bristles. Three or six different flies were tested for each BMN (fly number indicated in upper right corner). Asterisk indicates the BMN example that is shown in **Figure 4**. Scale bar, 50 µm. Dotted line indicates approximate SEZ midline. **Supplementary file 2** provides confocal Z-stack download links.

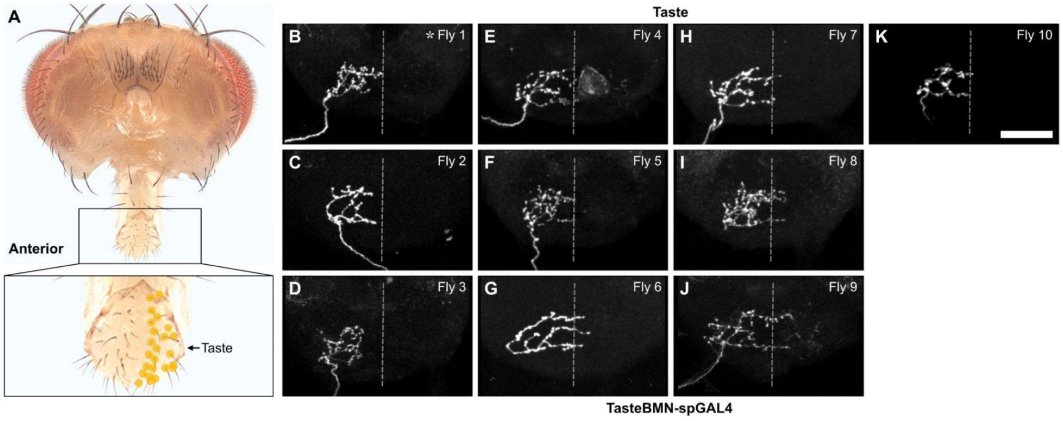

Figure 4 – figure supplement 8.

MCFO labeled trials for Taste bristles.

(**A**) Bristles whose associated BMNs were labeled by MCFO are indicated with labeled dots (posterior view). The boxed area in the top image is shown magnified in the bottom image. (**B-K**) Anterior view of the SEZ projections of individual BMNs labeled by MCFO using TasteBMN-spGAL4. BMNs shown innervate the Taste bristles. Ten different flies were tested (fly number indicated in upper right corner). Asterisk indicates the BMN example that is shown in **Figure 4**. Scale bar, 50 µm. Dotted line indicates approximate SEZ midline. **Supplementary file 2** provides confocal Z-stack download links.

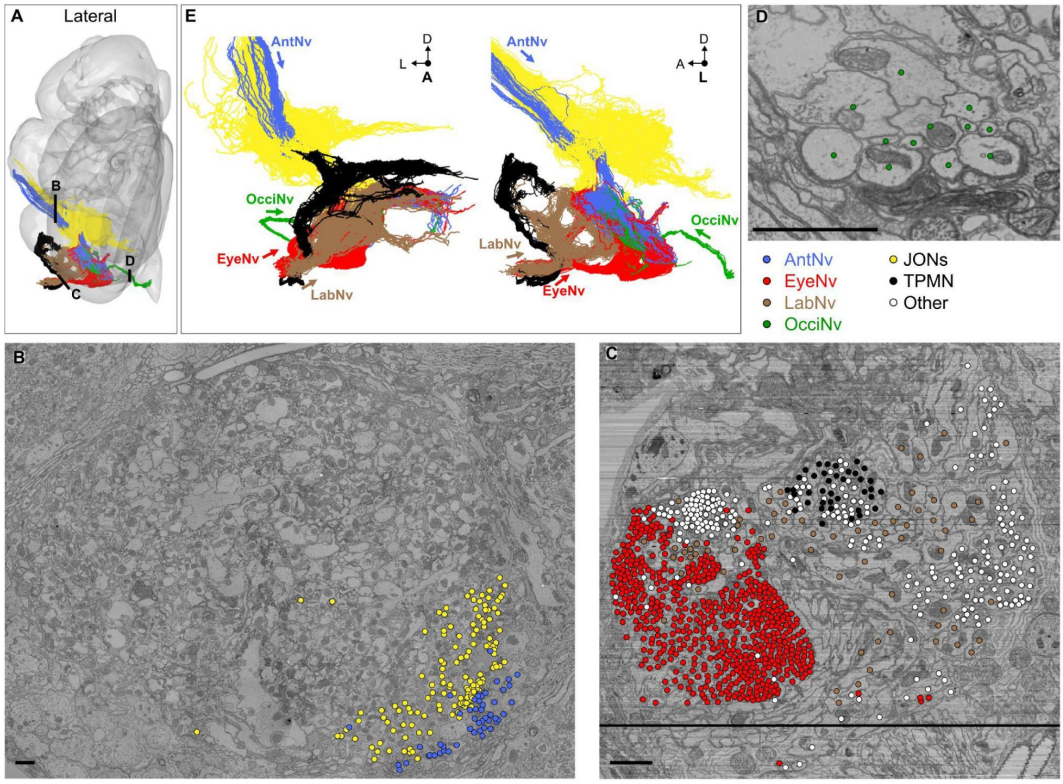

Figure 5 – figure supplement 1.

Reconstruction of mechanosensory neurons in different head nerves.

(**A**) Locations in each nerve where different segmented neurons in the EM volume were seeded for proofreading and editing (black lines). (**B-D**) EM sections through each nerve at the locations shown in **A** with seeded neurons indicated with dots. Shown are AntNv (**B**), EyeNv/LabNv (**C**), and OcciNv (**D**) sections. Dot colors indicate the seeded neuron type, including BMNs projecting through the AntNv (blue), EyeNv (red), LabNv (brown), OcciNv (green), JONs (yellow), TPMNs (black), or other neurons (white). All neuron segments were seeded for each nerve, with the following exceptions: 1) The Eye/LabNv had a bundle of soma tracts from an interneuron hemilineage crossing the seed plane that was excluded based on the morphology of their initial segmentation, and 2) Previously reconstructed JONs were excluded when seeding the AntNv (**B**, upper left), leaving a ventral-medial area of the nerve with previously undocumented neurons (bottom right). Scale bars, 2 µm. (**E**) Anterior (left) and lateral (right) views of all reconstructed head mechanosensory neurons, including BMNs, JONs, and TPMNs (colors same as **A-D**). Arrows for each incoming nerve indicate projection direction.

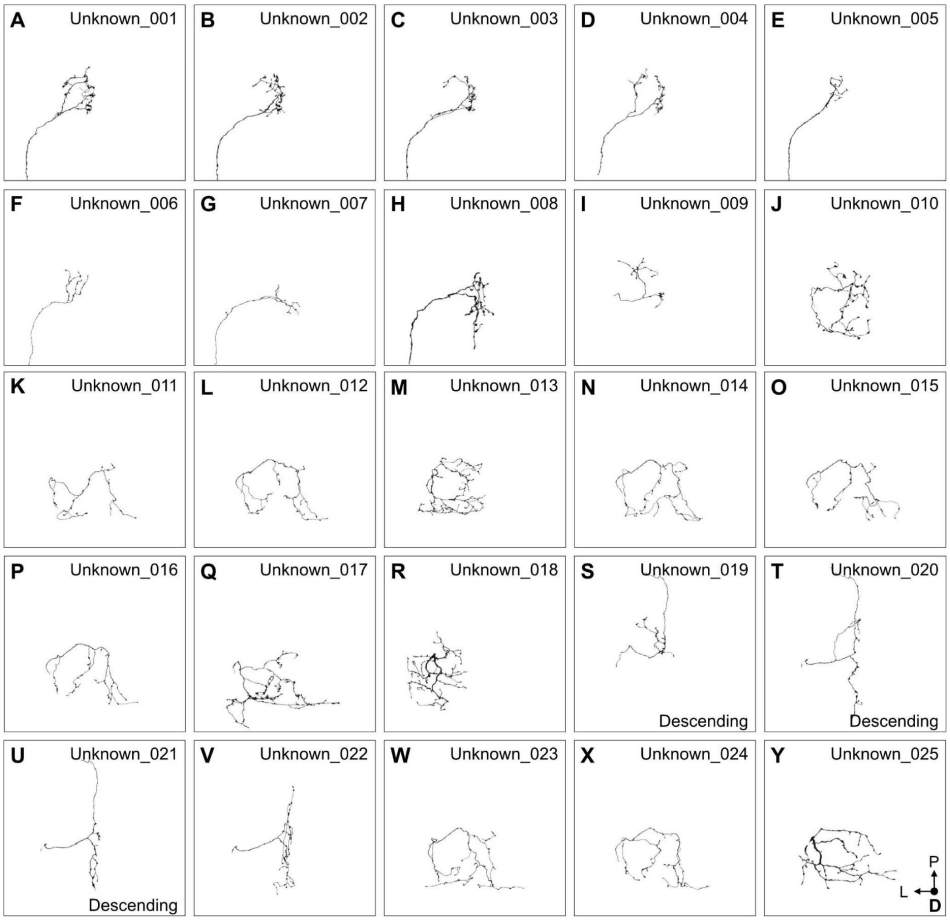

Figure 5 – figure supplement 2.

Reconstructed sensory neurons that could not be assigned an identity (unknown sensory neurons).

(**A-Y**) SEZ projections (dorsal views) of unknown sensory neurons 001 (**A**), 002 (**B**), 003 (**C**), 004 (**D**), 005 (**E**), 006 (**F**), 007 (**G**), 008 (**H**), 009 (**I**), 010 (**J**), 011 (**K**), 012 (**L**), 013 (**M**), 014 (**N**), 015 (**O**), 016 (**P**), 017 (**Q**), 018 (**R**), 019 (**S**), 020 (**T**), 021 (**U**), 022 (**V**), 023 (**W**), 024 (**X**), and 025 (**Y**). Unknown sensory neurons project through the AntNv (**A-H**) or the EyeNv/LabNv (**I-Y**). Unknown neurons in **S-U** send their axons into the neck connective, and possibly descend to the ventral nerve cord.

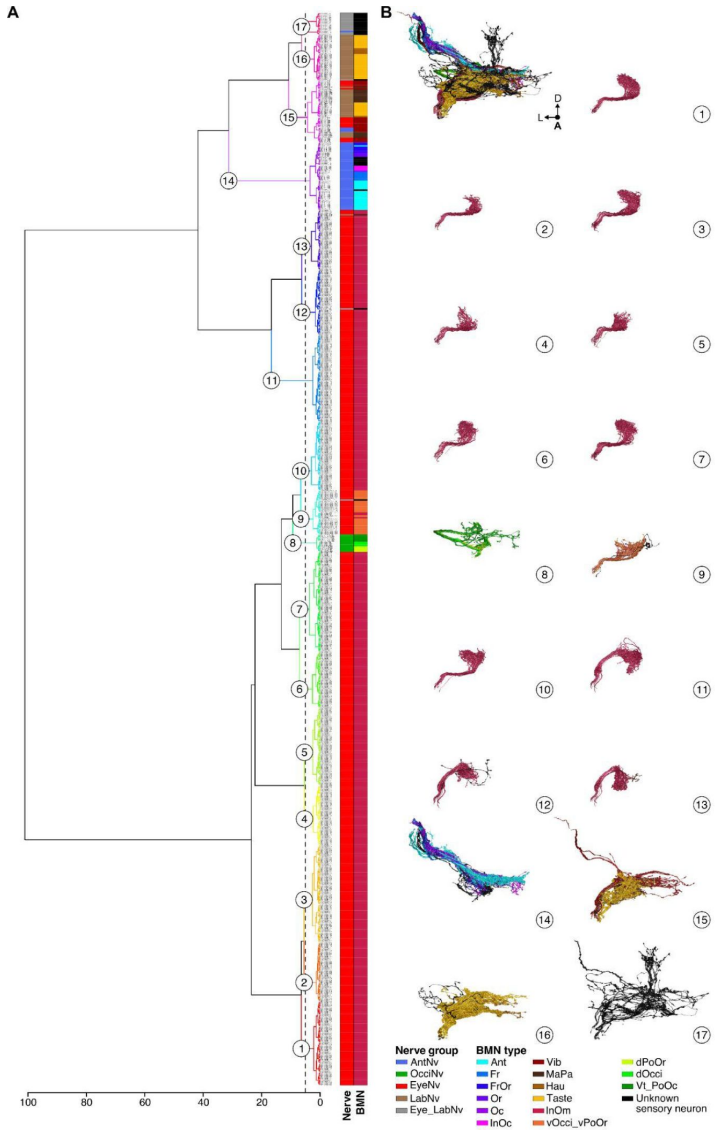

Figure 6 – figure supplement 1.

NBLAST clustering of BMNs.

(**A**) Dendrogram of Ward clustered NBLAST similarity scores of all reconstructed sensory neurons. Identified nerve projection groups and BMN type assignments are color coded in the bars to the right (color IDs shown in the bottom right corner). The dendrogram was cut at H=5, resulting in 17 clusters indicated by numbers on the dendrogram. **Supplementary file 3** shows the NBLAST clusters when the dendrogram was cut at H=1, at which most of the BMN types are clustered individually. (**B**) Morphology of the BMNs in each NBLAST cluster shown in **A**, indicated by the same number (color-coded by type).

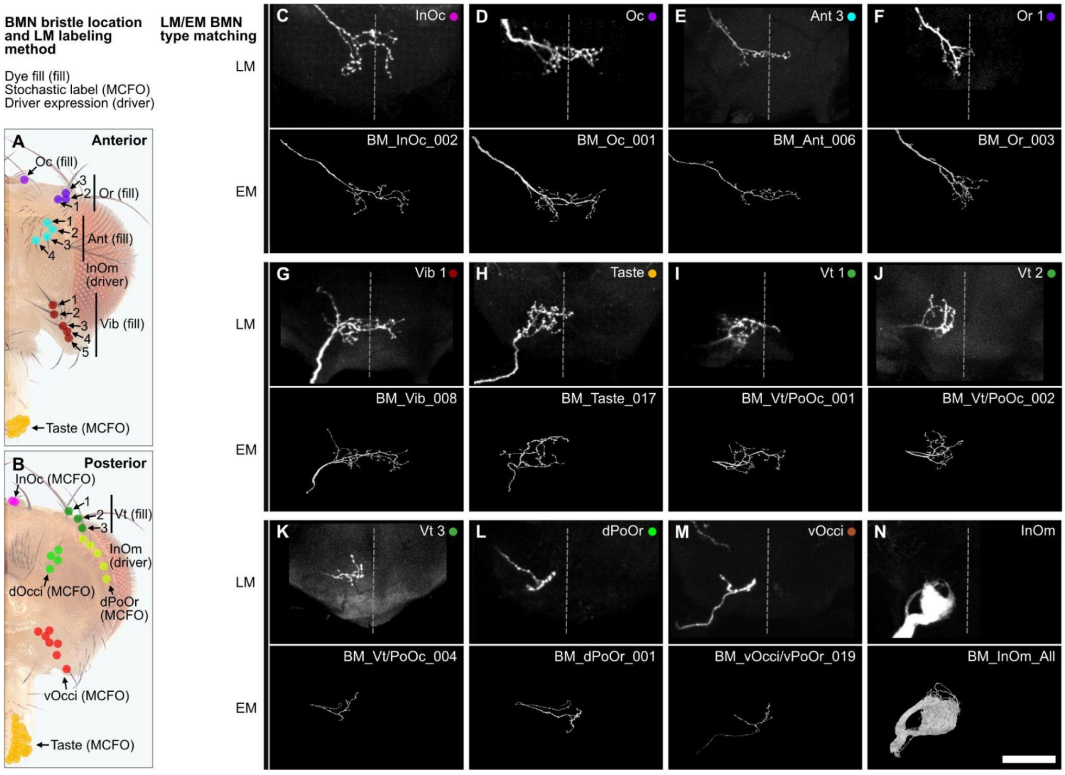

Figure 6 – figure supplement 2.

Matching EM reconstructed BMN projections with light microscopy (LM) imaged BMNs that innervate specific bristles.

(**A-B**) Bristles on the anterior (**A**) and posterior (**B**) head whose associated BMNs were labeled by dye filling (fill), stochastic labeling (MCFO), or full pattern driver line expression (driver). (**C-N**) Top panels show representative images of the SEZ projections of labeled and LM imaged BMNs that innervate the bristle indicated in the top right corner (anterior view). All fill and MCFO trials for the different bristles are shown in **Figure 4 – figure supplement 2**-**8**. Bottom panels show representative examples of the EM-reconstructed BMN types (types indicated in the top right corner). BMN types and their LM labeling methods are BM-InOc (MCFO) (**C**), BM-Oc (fill) (**D**), BM-Ant (fill) (**E**), BM-Or (fill) (**F**), BM-Vib (fill) (**G**), BM-Taste (MCFO) (**H**), BM-Vt/PoOc (fill) (**I**), BM-Vt/PoOc (fill) (**J**), BM-Vt/PoOc (fill) (**K**), BM-dPoOr (MCFO) (**L**), BM-vOcci/vPoOr (MCFO) (**M**), and BM-InOm (driver) (**N**). Note that the BM-InOm neurons shown in **N** (top panel) are those labeled in the full expression pattern of the driver line InOmBMN-LexA. The bottom panel of **N** includes all EM reconstructed BM-InOm neurons. Scale bar, 50 µm.

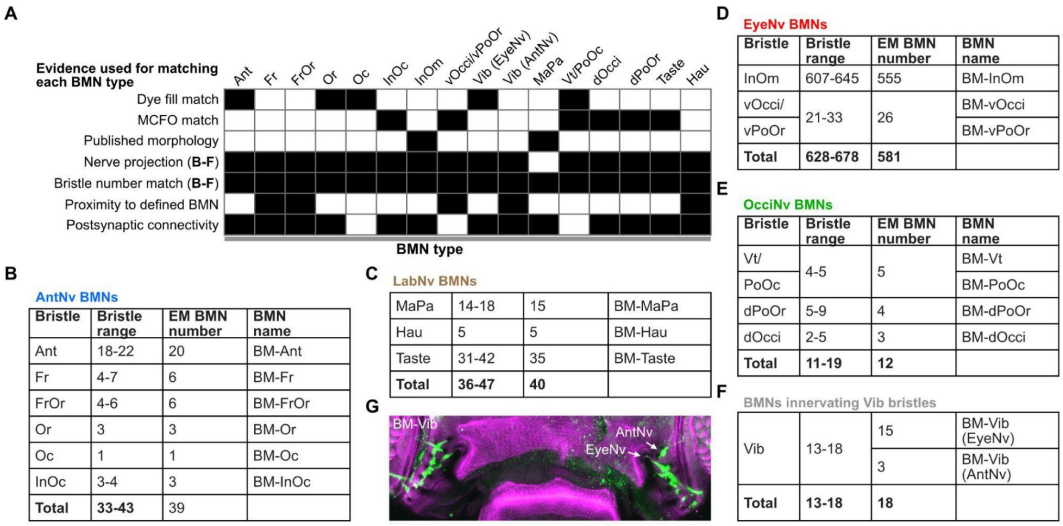

B AntNv BMNs

Bristle	Bristle range	EM BMN number	BMN name
Ant	18-22	20	BM-Ant
Fr	4-7	6	BM-Fr
FrOr	4-6	6	BM-FrOr
Or	3	3	BM-Or
Oc	1	1	BM-Oc
InOc	3-4	3	BM-InOc
Total	**33-43**	39	

C LabNv BMNs

MaPa	14-18	15	BM-MaPa
Hau	5	5	BM-Hau
Taste	31-42	35	BM-Taste
Total	**36-47**	**40**	

D EyeNv BMNs

Bristle	Bristle range	EM BMN number	BMN name
InOm	607-645	555	BM-InOm
vOcci/ vPoOr	21-33	26	BM-vOcci
			BM-vPoOr
Total	**628-678**	**581**	

E OcciNv BMNs

Bristle	Bristle range	EM BMN number	BMN name
Vt/ PoOc	4-5	5	BM-Vt
			BM-PoOc
dPoOr	5-9	4	BM-dPoOr
dOcci	2-5	3	BM-dOcci
Total	**11-19**	**12**	

F BMNs innervating Vib bristles

Vib	13-18	15	BM-Vib (EyeNv)
		3	BM-Vib (AntNv)
Total	**13-18**	**18**	

Figure 6 – figure supplement 3.

Evidence used to match the EM reconstructed BMNs with their bristles.

(**A**) NBLAST clusters were assigned as types that innervate particular bristle populations based on: 1) comparison of their morphology with images of dye-filled, MCFO-labeled, or published BMNs, 2) nerve projections, 3) proximity to BMNs with known morphology, and 4) common connectivity with postsynaptic partners. Postsynaptic connectivity clustering is shown in **Figure 7 – figure supplement 2**. The BMN types were validated because their numbers matched the numbers of their corresponding bristles. The mismatch between the reconstructed BM-InOm neurons and the number of InOm bristles is likely due to the latter being an estimate (shown in **D**). Black shaded boxes indicate which evidence was used to match each BMN type. Detailed descriptions of the evidence that was used for assigning each BMN type can be found in Materials and methods. (**B-F**) Head bristle counts for each population and the number of reconstructed BMNs for each type. Shown are BMNs projecting through the AntNv (**B**), LabNv (**C**), EyeNv (**D**), and OcciNv (**E**), and BMNs innervating the Vib bristles (**F**). (**G**) R52A06-GAL4 expression in BM-Vib neurons on the head (green). Maximum intensity projections of the ventral head. Cuticle is magenta. BM-Vib neurons (green) that project to the brain through the AntNv or EyeNv are labeled with arrows.

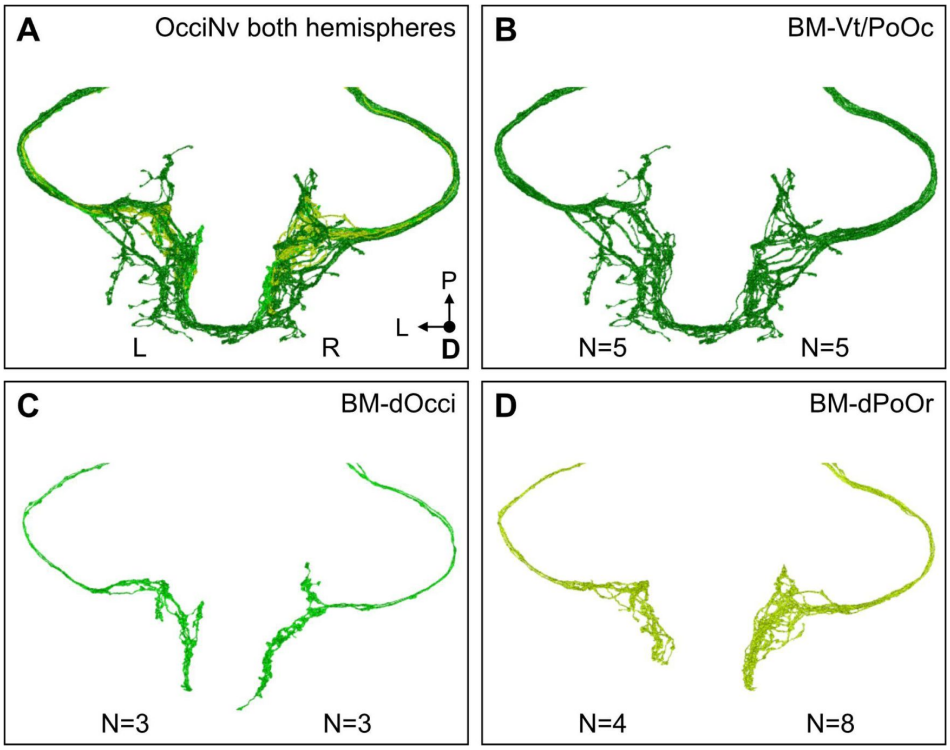

Figure 6 – figure supplement 4.

EM reconstruction of OcciNv BMNs from both brain hemispheres.

(**A**) All BMNs entering the brain through the right (R) and left (L) OcciNv, color-coded by the BMN type. (**B,C**) BMN numbers are consistent across hemispheres for the BM-Vt/PoOc (**B**) and BM-dOcci (**C**) neurons (indicated below each hemisphere). (**D**) Reconstruction of the full occipital nerve on both hemispheres revealed twice as many BM-dPoOr neurons on the right than on the left.

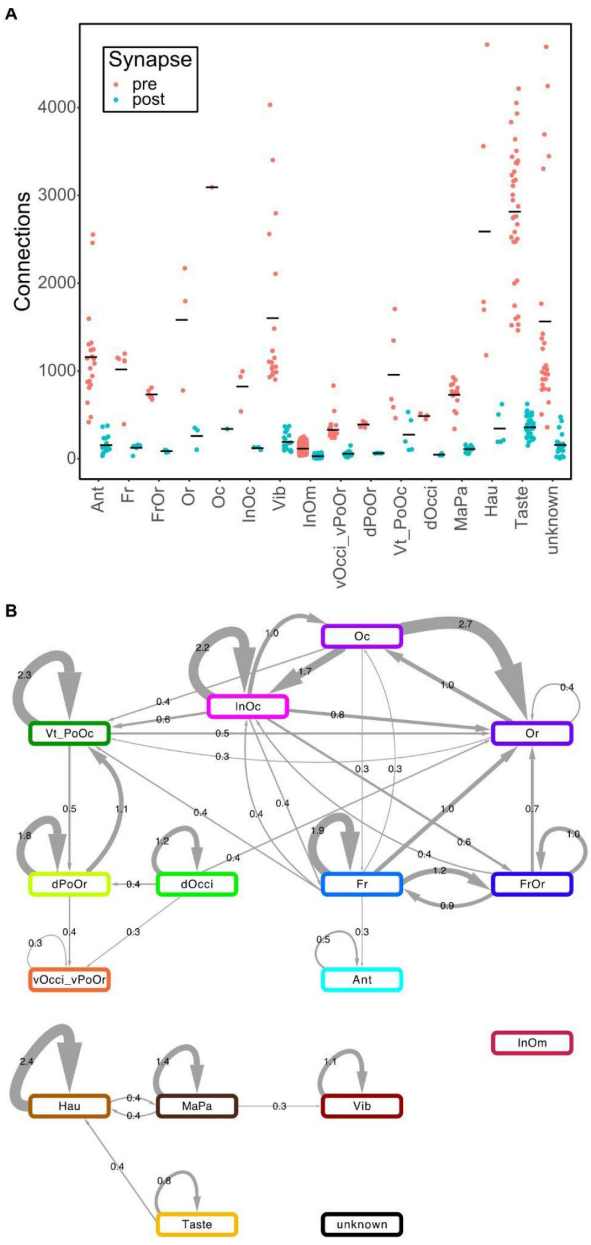

Figure 8 – figure supplement 1.

BMN type synaptic counts and BMN/BMN connectivity.

(**A**) Number pre- and postsynaptic connections for each BMN type. Black lines indicate mean synapse number. (**B**) Synaptic connectivity among BMN types. The average synaptic count for each edge is shown on arrows indicating directionality of the connection (arrow width corresponds to the count). Total count of synapses between two given types was divided by the number of possible edges between the two types.

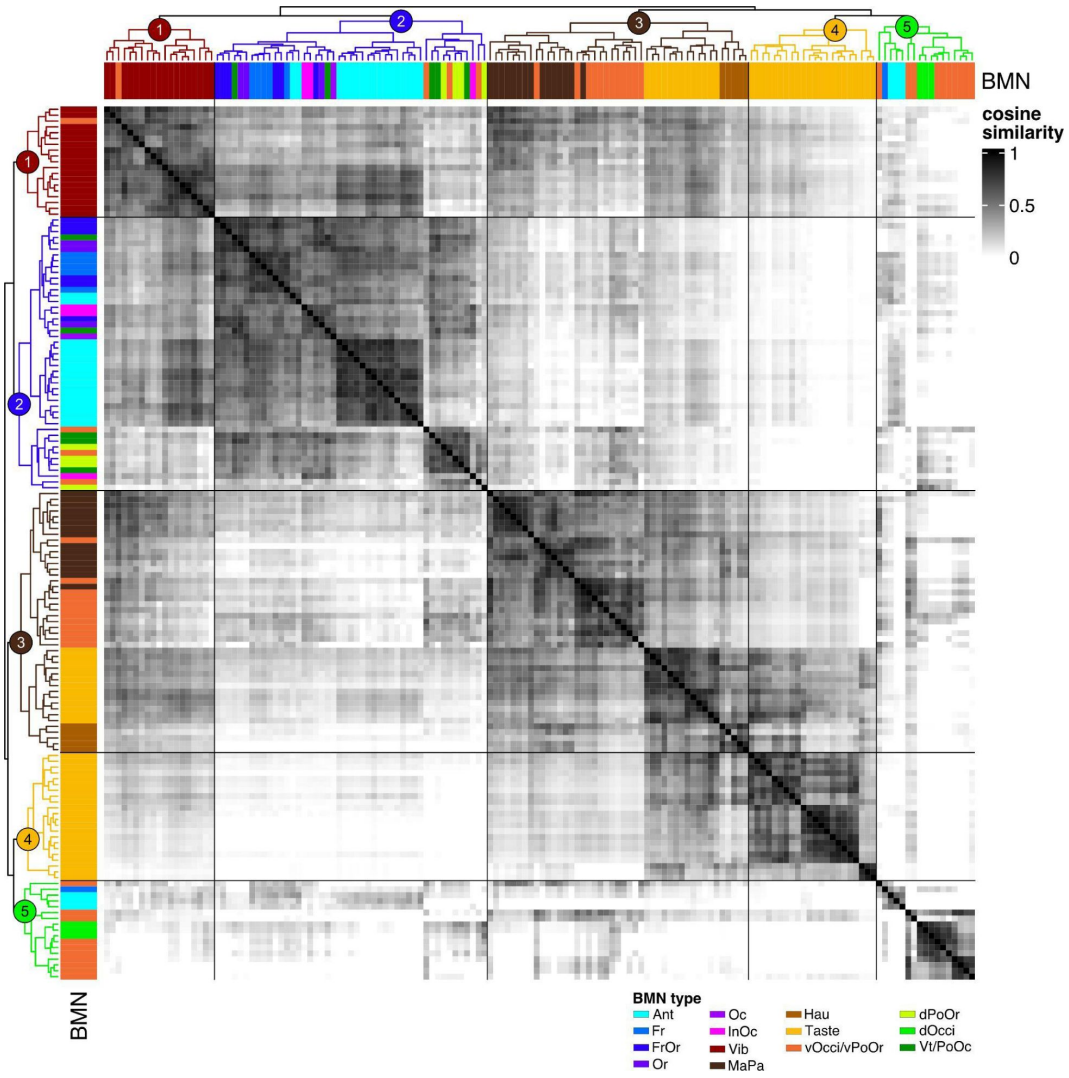

Figure 8 – figure supplement 2.

Cosine similarity clustering of BMN to non-BMN postsynaptic connectivity.

Heatmap of the cosine similarity among BMNs with the row and column order determined by clustering of the similarity scores. Postsynaptic partners excluded connections to other BMNs and connections with fewer than 6 synapses. Clustering of the rows and columns is the same as the dendrograms next to bars that indicate BMN type (color-code on bottom right). Dendrogram cut height 4.5 resulted in 5 clusters (indicated by numbers on the top dendrogram). Morphologies of the neurons in each cluster are shown in **Figure 8B**.

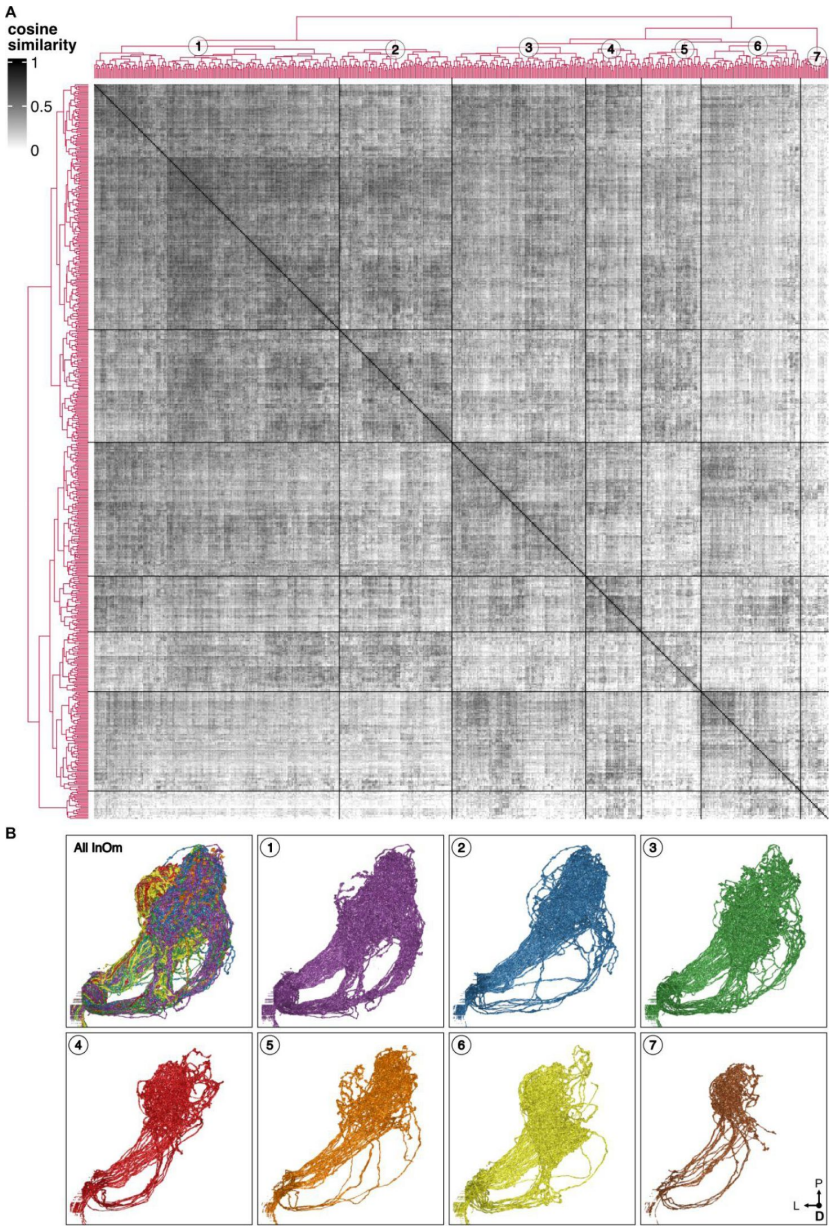

Figure 8 – figure supplement 3.

Cosine similarity clustering of BM-InOm neurons in their connectivity with non-BMN postsynaptic partners.

(**A**) Heatmap of BM-InOm neuron cosine similarity with the row and column order determined by clustering of the similarity scores. Postsynaptic partners excluded connections to other BMNs and connections with fewer than 2 synapses. Clustering of the rows and columns is the same with dendrograms shown on the left and top. Dendrogram cut height 5.6 resulted in 7 clusters (indicated by numbers on the top dendrogram). (**B**) Dorsal view of the neuron morphologies in each cluster (cluster number indicated at the top left), revealed tiling of the BM-InOm innervation area in the brain. Clusters 1-2 mainly innervate an area located medial-dorsally, while clusters 6-7 innervate a lateral-ventral area. Clusters 3-5 send branches to both areas.

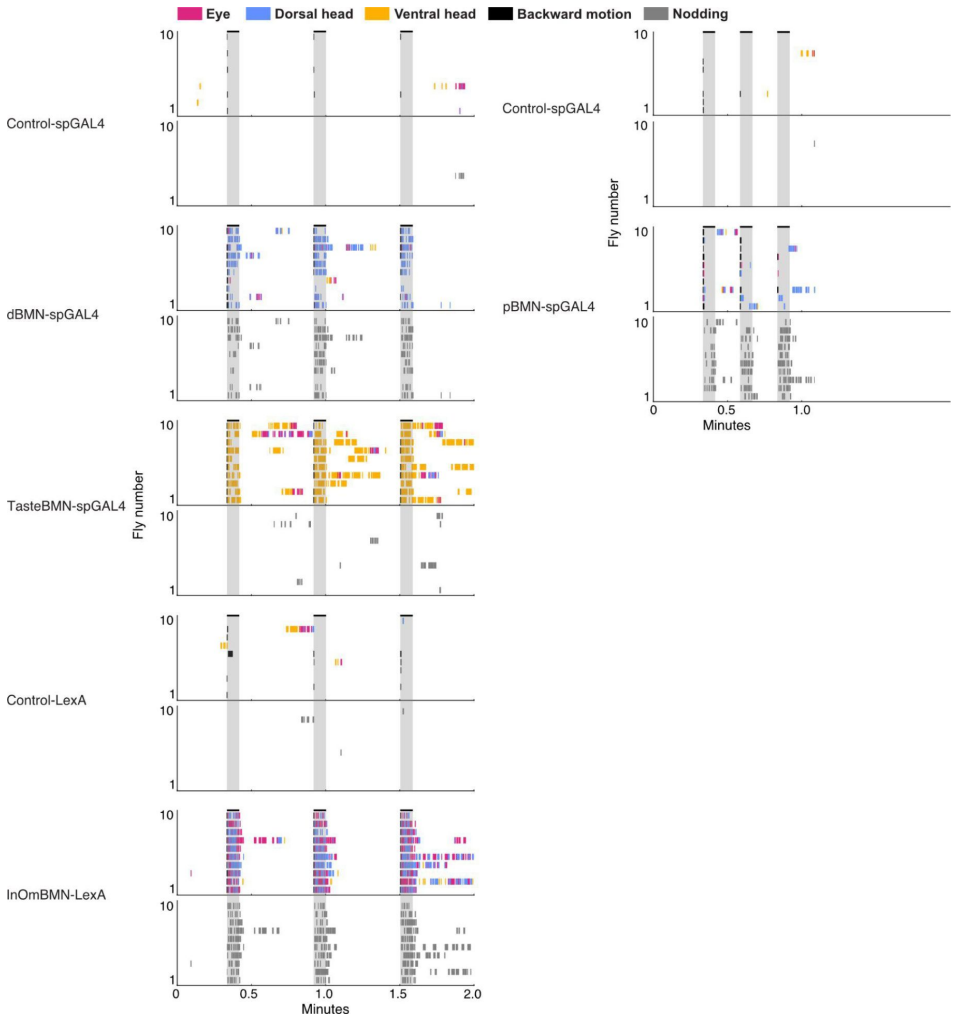

Figure 9 – figure supplement 1.

Ethograms of movements performed with activation of different BMNs.

Ethograms of manually scored videos showing the movements elicited with red-light induced activation. Ethograms of individual flies are stacked. Grooming movements (top plots) are indicated by different colors, including eye (magenta), dorsal head (blue), and ventral head (orange) grooming. Other elicited movements (bottom plots) include backward motion (black) and head nodding (gray). Gray bars indicate a 5 second red-light stimulus. Most driver lines were tested using 30 second interstimulus intervals, while pBMN-spGAL4 elicited more reliable behavior using 10 second intervals. Movements are mutually exclusive except head nodding. Gray bars indicate a 5 second red-light stimulus.

figures. Rows in the spreadsheet correspond to each image stack. Columns provide information about each stack including: figure panels that each image stack contributed to, image stack title, DOI for each stack (link provides metadata for each stack and file download link), image stack file name, genotype of imaged fly, and information about image stack.

Supplementary file 3. Table of EM-reconstructed BMNs, JONs, and TPMNs. Table includes FlyWire.ai neuron XYZ coordinates and IDs, nerve groups, names, types, NBLAST clusters, and cosine similarity clusters.

Figure 9 – source data 1. Numerical data used for producing each box plot. Rows correspond to individual flies. Columns indicate the percent time each fly spent performing different movements, including eye, dorsal, and ventral head grooming, nodding, and backward motions.

Video 1. Optogenetic activation of dorsal head BMNs elicits aimed dorsal head grooming. CsChrimson was expressed in BMNs targeted by the dBMN-spGAL4 driver line. Infrared light in the bottom right corner indicates when the red light was on to activate the targeted BMNs. Note that head nodding movements and backward motions are also elicited.

Video 2. Optogenetic activation of BM-Taste neurons elicits aimed proboscis and ventral head grooming. CsChrimson was expressed in BMNs targeted by the TasteBMN-spGAL4 driver line. Infrared light in the bottom right corner indicates when the red light was on to activate the targeted BMNs.

Video 3. Optogenetic activation of BM-InOm neurons elicits eye and dorsal head grooming. CsChrimson was expressed in BMNs targeted by the InOmBMN-LexA driver line. Infrared light in the bottom right corner indicates when the red light was on to activate the targeted BMNs. Note that head nodding movements and backward motions are also elicited.

Video 4. Optogenetic activation of posterior head BMNs elicits head nodding. CsChrimson was expressed in BMNs targeted by the pBMN-spGAL4 driver line. Infrared light in the bottom right corner indicates when the red light was on to activate the targeted BMNs. Note that dorsal head grooming movements are also elicited (not shown in video).

Video 5. Optogenetic stimulus in control flies. Control fly was exposed to the same red-light stimulus shown in **Videos 1-3**. The infrared light in the bottom right corner indicates when the red light was on.

References

Abraira VE, Ginty DD (2013) **The sensory neurons of touch** *Neuron* **79**:618–639 https://doi.org/10.1016/j.neuron.2013.07.051

Adibi M (2019) **Whisker-Mediated Touch System in Rodents: From Neuron to Behavior** *Frontiers Syst Neurosci* **13** https://doi.org/10.3389/fnsys.2019.00040

Averbeck BB, Chafee MV, Crowe DA, Georgopoulos AP (2002) **Parallel processing of serial movements in prefrontal cortex** *Proceedings of the National Academy of Sciences* **99**:13172–13177 https://doi.org/10.1073/pnas.162485599

Bates AS, Manton JD, Jagannathan SR, Costa M, Schlegel P, Rohlfing T, Jefferis GS (2020) **The natverse, a versatile toolbox for combining and analysing neuroanatomical data** *Elife* **9** https://doi.org/10.7554/elife.53350

Berkowitz A, Laurent G (1996) **Central generation of grooming motor patterns and interlimb coordination in locusts** *The Journal of Neuroscience* **16**:8079–8091

Bodenstein D, Miller A, Cooper KW, Poulson DF, Ferris GF, Sonnenblick BP, Spenser WP (1994) **Biology of Drosophila**

Bohland JW, Bullock D, Guenther FH (2010) **Bohland JW, Bullock D, Guenther FH. 2010. Neural representations and mechanisms for the performance of simple speech sequences. 22:1504–1529. doi:10.1162/jocn.2009.21306** *Neural representations and mechanisms for the performance of simple speech sequences* **22**:1504–1529 https://doi.org/10.1162/jocn.2009.21306

Brown AG, Rose PK, Snow PJ (1977) **The morphology of hair follicle afferent fibre collaterals in the spinal cord of the cat** *J Physiology* **272**:779–797 https://doi.org/10.1113/jphysiol.1977.sp012073

Buhmann J *et al.* (2021) **Automatic detection of synaptic partners in a whole-brain Drosophila electron microscopy data set** *Nat Methods* **18**:771–774 https://doi.org/10.1038/s41592-021-01183-7

Bullock D (2004) **Adaptive neural models of queuing and timing in fluent action** *Trends in Cognitive Sciences* **8**:426–433 https://doi.org/10.1016/j.tics.2004.07.003

Burg M, Wu C (1986) **Differentiation and central projections of peripheral sensory cells with action-potential block in Drosophila mosaics** *J Neurosci* **6**:2968–2976 https://doi.org/10.1523/jneurosci.06-10-02968.1986

Burg MG, Hanna L, Kim YT, Wu CF (1993) **Development and maintenance of a simple reflex circuit in small-patch mosaics of Drosophila: effects of altered neuronal function and developmental arrest** *Journal of Neurobiology* **24**:803–823 https://doi.org/10.1002/neu.480240608

Burg MG, Wu CF (1989) **Central projections of peripheral mechanosensory cells with increased excitability in Drosophila mosaics** *Developmental Biology* **131**:505–514 https://doi.org/10.1016/s0012-1606(89)80021-1

Cande J, Namiki S, Qiu J, Korff W, Card GM, Shaevitz JW, Stern DL, Berman GJ (2018) **Optogenetic dissection of descending behavioral control in Drosophila** *Elife* **7** https://doi.org/10.7554/elife.34275

Chen BE, Kondo M, Garnier A, Watson FL, Püettmann-Holgado R, Lamar DR, Schmucker D (2006) **The Molecular Diversity of Dscam Is Functionally Required for Neuronal Wiring Specificity in Drosophila** *Cell* **125**:607–620 https://doi.org/10.1016/j.cell.2006.03.034

Corfas G, Dudai Y (1990) **Adaptation and fatigue of a mechanosensory neuron in wild-type Drosophila and in memory mutants** *Journal of Neuroscience* **10**:491–499

Corfas G, Dudai Y (1989) **Habituation and dishabituation of a cleaning reflex in normal and mutant Drosophila** *The Journal of Neuroscience* **9**:56–62

Costa M, Manton JD, Ostrovsky AD, Prohaska S, Jefferis GSXE (2016) **NBLAST: Rapid, Sensitive Comparison of Neuronal Structure and Construction of Neuron Family Databases** *Neuron* https://doi.org/10.1016/j.neuron.2016.06.012

Dawkins R, Dawkins M (1976) **Hierarchical organization and postural facilitation: Rules for grooming in flies** *Animal Behaviour* **24**:739–755 https://doi.org/10.1016/s0003-3472(76)80003-6

Dionne H, Hibbard K, Cavallaro A, Kao JC, bioRxiv GR (2017) **2017. Genetic reagents for making split-GAL4 lines in Drosophila** *biorxiv.org* https://doi.org/10.1101/197509

Dorkenwald S *et al.* (2023) **Neuronal wiring diagram of an adult brain** *bioRxiv* https://doi.org/10.1101/2023.06.27.546656

Dorkenwald S *et al.* (2022) **FlyWire: online community for whole-brain connectomics** *Nat Methods* **19**:119–128 https://doi.org/10.1038/s41592-021-01330-0

Eckstein N, Bates AS, Du M, Hartenstein V, Jefferis GSXE, Funke J. (2020) **Neurotransmitter Classification from Electron Microscopy Images at Synaptic Sites in Drosophila** *Biorxiv* https://doi.org/10.1101/2020.06.12.148775

Engert S, Sterne GR, Bock DD, Scott K (2022) **Drosophila gustatory projections are segregated by taste modality and connectivity** *Elife* **11** https://doi.org/10.7554/elife.78110

Falk R, Bleiser-Avivi N, Atidia J. (1976) **Labellar taste organs of Drosophila melanogaster** *J Morphol* **150**:327–341 https://doi.org/10.1002/jmor.1051500206

Feng L, Zhao T, Kim J (2015) **neuTube 1.0: A New Design for Efficient Neuron Reconstruction Software Based on the SWC Format** *eNeuro* **2** https://doi.org/10.1523/eneuro.0049-14.2014

Galili DS, Jefferis GS, Costa M (2022) **Connectomics and the neural basis of behaviour** *Curr Opin Insect Sci* **54** https://doi.org/10.1016/j.cois.2022.100968

Ghysen A (1980) **The projection of sensory neurons in the central nervous system of Drosophila: choice of the appropriate pathway** *Developmental Biology* **78**:521–541 https://doi.org/10.1016/0012-1606(80)90351-6

Guo L, Zhang N, Simpson JH (2022) **Descending neurons coordinate anterior grooming behavior in Drosophila** *Curr Biol* https://doi.org/10.1016/j.cub.2021.12.055

Hagedorn J, Hailpern J, Karahalios KG (2008) **VCode and VData: illustrating a new framework for supporting the video annotation workflow** *Extended Abstracts of AVI* **317** https://doi.org/10.1145/1385569.1385622

Hampel S, Chung P, McKellar CE, Hall D, Looger LL, Simpson JH (2011) **Hampel S, Chung P, McKellar CE, Hall D, Looger LL, Simpson JH. 2011. Drosophila Brainbow: a recombinase-based fluorescence labeling technique to subdivide neural expression patterns 8:253–259. doi:10.1038/nmeth.1566** *Drosophila Brainbow: a recombinase-based fluorescence labeling technique to subdivide neural expression patterns* **8**:253–259 https://doi.org/10.1038/nmeth.1566

Hampel S, Eichler K, Yamada D, Bock D, Kamikouchi A, Seeds AM (2020) **Distinct subpopulations of mechanosensory chordotonal organ neurons elicit grooming of the fruit fly antennae** *Elife* **9** https://doi.org/10.7554/elife.59976

Hampel S, Eichler K, Yamada D, Kim H, Horigome M, Franconville R, Bock DD, Kamikouchi A, Seeds AM (2020) **Convergence of distinct subpopulations of mechanosensory neurons onto a neural circuit that elicits grooming** *Biorxiv* https://doi.org/10.1101/2020.06.08.141341

Hampel S, Franconville R, Simpson JH, Seeds AM (2015) **A neural command circuit for grooming movement control** *eLife* **4** https://doi.org/10.7554/elife.08758

Hampel S, McKellar CE, Simpson JH, Seeds AM (2017) **Simultaneous activation of parallel sensory pathways promotes a grooming sequence in Drosophila** *eLife* **6** https://doi.org/10.7554/elife.28804

Heinrich L, Funke J, Pape C, Nunez-Iglesias J, Saalfeld S (2018) **Synaptic Cleft Segmentation in Non-isotropic Volume Electron Microscopy of the Complete Drosophila Brain., Medical Image Computing and Computer Assisted Intervention – MICCAI 2018** *MICCAI 2018. Lecture Notes in Computer Science* https://doi.org/10.1007/978-3-030-00934-2_36

Homberg U, Christensen TA, Hildebrand JG (1989) **Structure and function of the deutocerebrum in insects** *Annual Review of Entomology* **34**:477–501 https://doi.org/10.1146/annurev.en.34.010189.002401

Honegger H-W (1977) **Interommatidial hair receptor axons extending into the ventral nerve cord in the cricket Gryllus campestris** *Cell and tissue research*

Honegger HW, Reif H, Müller W (1979) **Sensory mechanisms of eye cleaning behavior in the cricket Gryllus campestris** *Journal of Comparative Physiology A: Neuroethology, Sensory, Neural, and Behavioral Physiology* **129**:247–256

Houghton G, Hartley T (1995) **Parallel models of serial behavior: Lashley revisited** *Psyche* **2**:1–25

Ishikawa Y, Okamoto N, Nakamura M, Kim H, Kamikouchi A (2017) **Anatomic and Physiologic Heterogeneity of Subgroup-A Auditory Sensory Neurons in Fruit Flies** *Frontiers in neural circuits* **11** https://doi.org/10.3389/fncir.2017.00046

Jefferis GSXE, Potter CJ, Chan AM, Marin EC, Rohlfing T, Luo L. (2007) **Comprehensive Maps of Drosophila Higher Olfactory Centers: Spatially Segregated Fruit and Pheromone Representation** *Cell* **128**:1187–1203 https://doi.org/10.1016/j.cell.2007.01.040

Jenett AA *et al.* (2012) **A GAL4-driver line resource for Drosophila neurobiology** *Cell Reports* **2**:991–1001 https://doi.org/10.1016/j.celrep.2012.09.011

Jeong YT, Oh SM, Shim J, Seo JT, Kwon JY, Moon SJ (2016) **Mechanosensory neurons control sweet sensing in Drosophila** *Nature communications* **7** https://doi.org/10.1038/ncomms12872

Johnson SE, Murphey RK (1985) **The afferent projection of mesothoracic bristle hairs in the cricket** *Acheta domesticus. J Comp Physiology* **156**:369–379 https://doi.org/10.1007/bf00610729

Kaas JH (1997) **Topographic maps are fundamental to sensory processing** *Brain Research Bulletin* **44**:107–112 https://doi.org/10.1016/s0361-9230(97)00094-4

Kamikouchi A, Inagaki HK, Effertz T, Hendrich O, Fiala A, Göpfert MC, Ito K (2009) **The neural basis of Drosophila gravity-sensing and hearing** *Nature* **458**:165–171 https://doi.org/10.1038/nature07810

Kamikouchi A, Shimada T, Ito K (2006) **Comprehensive classification of the auditory sensory projections in the brain of the fruit fly Drosophila melanogaster** *The Journal of Comparative Neurology* **499**:317–356 https://doi.org/10.1002/cne.21075

Kays I, Cvetkovska V, Chen BE (2014) **Structural and functional analysis of single neurons to correlate synaptic connectivity with grooming behavior** *Nature protocols* **9**:1–10 https://doi.org/10.1038/nprot.2013.157

Kent KS, Levine RB (1988) **Neural control of leg movements in a metamorphic insect: Sensory and motor elements of the larval thoracic legs in Manduca sexta** *J Comp Neurol* **271**:559–576 https://doi.org/10.1002/cne.902710407

Kim H, Horigome M, Ishikawa Y, Li F, Lauritzen JS, Card G, Bock DD, Kamikouchi A (2020) **Wiring patterns from auditory sensory neurons to the escape and song-relay pathways in fruit flies** *J Comp Neurol* https://doi.org/10.1002/cne.24877

Klapoetke NC *et al.* (2014) **Klapoetke NC, Murata Y, Kim SS, Pulver SR, Birdsey-Benson A, Cho YK, Morimoto TK, Chuong AS, Carpenter EJ, Tian Z, Wang J, Xie Y, Yan Z, Zhang Y, Chow BY, Surek B, Melkonian M, Jayaraman V, Constantine-Paton M, Wong GK-S, Boyden ES. 2014. Independent optical excitation of distinct neural populations 11:338–346. doi:10.1038/nmeth.2836** *Independent optical excitation of distinct neural populations* **11**:338–346 https://doi.org/10.1038/nmeth.2836

Lashley KS (1951) **Cerebral mechanisms in behavior**

Lehnert BP, Baker AE, Gaudry Q, Chiang A-S, Wilson RI (2013) **Distinct roles of TRP channels in auditory transduction and amplification in Drosophila** *Neuron* **77**:115–128 https://doi.org/10.1016/j.neuron.2012.11.030

Li J, Zhang W, Guo Z, Wu S, Jan LY, Jan YN (2016) **A Defensive Kicking Behavior in Response to Mechanical Stimuli Mediated by Drosophila Wing Margin Bristles** *Journal of Neuroscience* **36**:11275–11282 https://doi.org/10.1523/jneurosci.1416-16.2016

Luan H, Peabody NC, Vinson CR, White BH (2006) **Refined spatial manipulation of neuronal function by combinatorial restriction of transgene expression** *Neuron* **52**:425–436 https://doi.org/10.1016/j.neuron.2006.08.028

Mamiya A, Dickinson MH (2015) **Antennal mechanosensory neurons mediate wing motor reflexes in flying Drosophila** *Journal of Neuroscience* **35**:7977–7991 https://doi.org/10.1523/jneurosci.0034-15.2015

Mamiya A, Straw AD, Tómasson E, Dickinson MH (2011) **Active and passive antennal movements during visually guided steering in flying Drosophila** *Journal of Neuroscience* **31**:6900–6914 https://doi.org/10.1523/jneurosci.0498-11.2011

Matheson T (1997) **Hindleg targeting during scratching in the locust** *The Journal of experimental biology* **200**:93–100

Matsuo E, Yamada D, Ishikawa Y, Asai T, Ishimoto H, Kamikouchi A (2014) **Identification of novel vibration- and deflection-sensitive neuronal subgroups in Johnston's organ of the fruit fly** *Frontiers in Physiology* **5** https://doi.org/10.3389/fphys.2014.00179

Melzig J, Buchner S, Wiebel F, Wolf R, Buchner E, Burg M, Pak WL (1996) **Genetic depletion of histamine from the nervous system of Drosophila eliminates specific visual and mechanosensory behavior** *Journal of Comparative Physiology A* **179**:763–773

Merritt DJ, Murphey RK (1992) **Projections of leg proprioceptors within the CNS of the fly Phormia in relation to the generalized insect ganglion** *The Journal of Comparative Neurology* **322**:16–34 https://doi.org/10.1002/cne.903220103

Mitchell BK, Itagaki H, Rivet MP (1999) **Peripheral and central structures involved in insect gustation** *Microscopy Research and Technique* **47**:401–415 https://doi.org/10.1002/(sici)1097-0029(19991215)47:6<401::aid-jemt4>3.0.co;2-7

Miyazaki T, Ito K (2010) **Neural architecture of the primary gustatory center of Drosophila melanogaster visualized with GAL4 and LexA enhancer-trap systems** *Journal of comparative neurology* **518**:4147–4181 https://doi.org/10.1002/cne.22433

Mueller JM, Ravbar P, Simpson JH, Carlson JM (2019) **Drosophila melanogaster grooming possesses syntax with distinct rules at different temporal scales** *Plos Comput Biol* **15** https://doi.org/10.1371/journal.pcbi.1007105

Murphey RK, Possidente D, Pollack G, Merritt DJ (1989) **Modality-specific axonal projections in the CNS of the flies Phormia and Drosophila** *The Journal of Comparative Neurology* **290**:185–200 https://doi.org/10.1002/cne.902900203

Murphey RK, Possidente DR, Vandervorst P, Ghysen A (1989) **Compartments and the topography of leg afferent projections in Drosophila** *Journal of Neuroscience* **9**:3209–3217

Mushiake H, Saito N, Sakamoto K, Itoyama Y, Tanji J (2006) **Activity in the lateral prefrontal cortex reflects multiple steps of future events in action plans** *Neuron* **50**:631–641 https://doi.org/10.1016/j.neuron.2006.03.045

Nayak SV, Singh RN (1983) **Sensilla on the tarsal segments and mouthparts of adult Drosophila melanogaster meigen (Diptera : Drosophilidae)** *Int J Insect Morphol Embryology* **12**:273–291 https://doi.org/10.1016/0020-7322(83)90023-5

Nern A, Pfeiffer BD, Rubin GM (2015) **Optimized tools for multicolor stochastic labeling reveal diverse stereotyped cell arrangements in the fly visual system** *Proceedings of the National Academy of Sciences* **112**:E2967–76 https://doi.org/10.1073/pnas.1506763112

Newland PL (1991) **Morphology and somatotopic organisation of the central projections of afferents from tactile hairs on the hind leg of the locust** *J Comp Neurol* **312**:493–508 https://doi.org/10.1002/cne.903120402

Newland PL, Burrows M (1997) **Processing of tactile information in neuronal networks controlling leg movements of the locust** *Journal of insect physiology* **43**:107–123

Newland PL, Rogers SM, Gaaboub I, Matheson T (2000) **Parallel somatotopic maps of gustatory and mechanosensory neurons in the central nervous system of an insect** *The Journal of Comparative Neurology* **425**:82–96 https://doi.org/10.1002/1096-9861(20000911)425:1<82::aid-cne8>3.0.co;2-5

Page KLK, Matheson TT (2004) **Wing hair sensilla underlying aimed hindleg scratching of the locust** *Journal of Experimental Biology* **207**:2691–2703 https://doi.org/10.1242/jeb.01096

Patella P, Wilson RI (2018) **Functional Maps of Mechanosensory Features in the Drosophila Brain** *Current biology : CB* **28**:1189–1203 https://doi.org/10.1016/j.cub.2018.02.074

Pfeiffer BD *et al.* (2008) **Tools for neuroanatomy and neurogenetics in Drosophila** *Proceedings of the National Academy of Sciences* **105**:9715–9720 https://doi.org/10.1073/pnas.0803697105

Pfeiffer BD, Ngo T-TB, Hibbard KL, Murphy C, Jenett A, Truman JW, Rubin GM (2010) **Refinement of tools for targeted gene expression in Drosophila** *Genetics* **186**:735–755 https://doi.org/10.1534/genetics.110.119917

Pflüger H-J (1980) **The Function of Hair Sensilla on the Locust's Leg: the Role Of tibial hairs** *J Exp Biol* **87**:163–176 https://doi.org/10.1242/jeb.87.1.163

Phelps JS *et al.* (2021) **Reconstruction of motor control circuits in adult Drosophila using automated transmission electron microscopy** *Cell* **184**:759–774 https://doi.org/10.1016/j.cell.2020.12.013

Phillis RW, Bramlage AT, Wotus C, Whittaker A, Gramates LS, Seppala D, Farahanchi F, Caruccio P, Murphey RK (1993) **Isolation of mutations affecting neural circuitry required for grooming behavior in Drosophila melanogaster** *Genetics* **133**:581–592

Ready DF, Hanson TE, Benzer S (1976) **Development of the Drosophila retina, a neurocrystalline lattice** *Dev Biol* **53**:217–240 https://doi.org/10.1016/0012-1606(76)90225-6

Salvaterra PM, Kitamoto T (2001) **Drosophila cholinergic neurons and processes visualized with Gal4/UAS–GFP** *Gene expression patterns* **1**:73–82 https://doi.org/10.1016/s1567-133x(01)00011-4

Sánchez-Alcañiz JA, Zappia G, Marion-Poll F, Benton R (2017) **A mechanosensory receptor required for food texture detection in Drosophila** *Nature communications* **8** https://doi.org/10.1038/ncomms14192

Seeds AM, Ravbar P, Chung P, Hampel S, Midgley FM, Mensh BD, Simpson JH (2014) **A suppression hierarchy among competing motor programs drives sequential grooming in Drosophila** *eLife* **3**

Shanbhag S, Park S-K, Pikielny C, Steinbrecht R (2001) **Gustatory organs of Drosophila melanogaster: fine structure and expression of the putative odorant-binding protein PBPRP2** *Cell Tissue Res* **304**:423–437 https://doi.org/10.1007/s004410100388

Shannon P, Markiel A, Ozier O, Baliga NS, Wang JT, Ramage D, Amin N, Schwikowski B, Ideker T (2003) **Cytoscape: A Software Environment for Integrated Models of Biomolecular Interaction Networks** *Genome Res* **13**:2498–2504 https://doi.org/10.1101/gr.1239303

Singh RN, Nayak SV (1985) **Fine structure and primary sensory projections of sensilla on the maxillary palp of Drosophila melanogaster Meigen (Diptera : Drosophilidae)** *Int J Insect Morphol Embryology* **14**:291–306 https://doi.org/10.1016/0020-7322(85)90044-3

Smith SA, Shepherd D (1998) **Central afferent projections of proprioceptive sensory neurons in Drosophila revealed with the enhancer-trap technique** *The Journal of Comparative Neurology* **364**:311–323

Steyskal GC (1976) **THE TERMINOLOGY OF BRISTLES ON THE UPPER BACK OF THE HEAD IN THE HIGHER DIPTERA** *Journal of the Kansas Entomological Society* **49**:55–159

Stocker RF (1994) **The organization of the chemosensory system in Drosophila melanogaster: a review** *Cell and tissue research* **275**:3–26

Stocker RF, Schorderet M (1981) **Cobalt filling of sensory projections from internal and external mouthparts in Drosophila** *Cell Tissue Res* **216**:513–523 https://doi.org/10.1007/bf00238648

Suver MP, Matheson AMM, Sarkar S, Damiata M, Schoppik D, Nagel KI (2019) **Encoding of Wind Direction by Central Neurons in Drosophila** *Neuron* **102**:828–842 https://doi.org/10.1016/j.neuron.2019.03.012

Szebenyi AL (1969) **Cleaning behaviour in Drosophila melanogaster** *Animal Behaviour* **17**:641–651 https://doi.org/10.1016/s0003-3472(69)80006-0

Thei J (1979) **Mechanoreceptive bristles on the head of the blowfly: Mechanics and electrophysiology of the macrochaetae** *Journal of Comparative Physiology A* **132**:55–68 https://doi.org/10.1007/bf00617732

Thivierge J-P, Marcus GF (2007) **The topographic brain: from neural connectivity to cognition** *Trends in Neurosciences* **30**:251–259 https://doi.org/10.1016/j.tins.2007.04.004

Tirián L, Dickson B. (2017) **The VT GAL4, LexA, and split-GAL4 driver line collections for targeted expression in the Drosophila nervous system** *bioRxiv* https://doi.org/10.1101/198648

Tootoonian SS, Coen PP, Kawai RR, Murthy MM (2012) **Neural representations of courtship song in the Drosophila brain** *Journal of Neuroscience* **32**:787–798 https://doi.org/10.1523/jneurosci.5104-11.2012

Tsubouchi A, Yano T, Yokoyama TK, Murtin C, Otsuna H, Ito K (2017) **Topological and modality-specific representation of somatosensory information in the fly brain** *Science* **358**:615–623 https://doi.org/10.1126/science.aan4428

Tuthill JC, Wilson RI (2016) **Parallel Transformation of Tactile Signals in Central Circuits of Drosophila** *Cell* **164**:1046–1059 https://doi.org/10.1016/j.cell.2016.01.014

Tuthill JC, Wilson RI (2016) **Mechanosensation and Adaptive Motor Control in Insects** *Current biology : CB* **26**:R1022–R1038 https://doi.org/10.1016/j.cub.2016.06.070

Tyrer NM, Bacon JP, Davies CA (1979) **Sensory projections from the wind-sensitive head hairs of the locust Schistocerca gregaria. Distribution in the central nervous system** *Cell and tissue research* **203**:79–92

Usui-Ishihara AA, Ghysen A, Kimura K-I (1995) **Peripheral Axonal Pathway and Cleaning Behavior Are Correlated in Drosophila Microchaetes** *Developmental Biology* **167**:398–401 https://doi.org/10.1006/dbio.1995.1034

Vandervorst P, Ghysen A (1980) **Genetic control of sensory connections in Drosophila** *Nature* **286**:65–67 https://doi.org/10.1038/286065a0

Vaughan AG, Zhou C, Manoli DS, Baker BS (2014) **Neural pathways for the detection and discrimination of conspecific song in D. melanogaster** *Current biology : CB* **24**:1039–1049 https://doi.org/10.1016/j.cub.2014.03.048

Walker RG (2000) **A Drosophila Mechanosensory Transduction Channel** *Science* **287**:2229–2234 https://doi.org/10.1126/science.287.5461.2229

Yang T, Yuan Z, Liu C, Liu T, Zhang W (2021) **A neural circuit integrates pharyngeal sensation to control feeding** *Cell Reports* **37** https://doi.org/10.1016/j.celrep.2021.109983

Yasuyama K, Salvaterra PM (1999) **Localization of choline acetyltransferase-expressing neurons in Drosophila nervous system** *Microscopy Research and Technique* **45**:65–79 https://doi.org/10.1002/(sici)1097-0029(19990415)45:2<65::aid-jemt2>3.0.co;2-0

Yorozu S, Wong A, Fischer BJ, Dankert H, Kernan MJ, Kamikouchi A, Ito K, Anderson DJ (2009) **Distinct sensory representations of wind and near-field sound in the Drosophila brain** *Nature* **458**:201–205 https://doi.org/10.1038/nature07843

Zack SS, Bacon JJ (1981) **Interommatidial sensilla of the praying mantis: their central neural projections and role in head-cleaning behavior** *Journal of Neurobiology* **12**:55–65 https://doi.org/10.1002/neu.480120105

Zhang N, Guo L, Simpson JH (2020) **Spatial Comparisons of Mechanosensory Information Govern the Grooming Sequence in Drosophila** *Curr Biol* **30**:988–1001 https://doi.org/10.1016/j.cub.2020.01.045

Zhang YV, Aikin TJ, Li Z, Montell C (2016) **The Basis of Food Texture Sensation in Drosophila** *Neuron* **91**:863–877 https://doi.org/10.1016/j.neuron.2016.07.013

Zheng Z *et al.* (2018) **A Complete Electron Microscopy Volume of the Brain of Adult Drosophila melanogaster** *Cell* **174**:730–743 https://doi.org/10.1016/j.cell.2018.06.019

Zhou Y, Cao L-H, Sui X-W, Guo X-Q, Luo D-G (2019) **Mechanosensory circuits coordinate two opposing motor actions in Drosophila feeding** *Science advances* **5** https://doi.org/10.1126/sciadv.aaw5141

Article and author information

Katharina Eichler
Institute of Neurobiology, University of Puerto Rico-Medical Sciences Campus, San Juan, Puerto Rico
ORCID iD: 0000-0002-7833-8621

Stefanie Hampel
Institute of Neurobiology, University of Puerto Rico-Medical Sciences Campus, San Juan, Puerto Rico
For correspondence: stef.hampel@gmail.com
ORCID iD: 0000-0001-8287-549X

Adrián Alejandro-García
Institute of Neurobiology, University of Puerto Rico-Medical Sciences Campus, San Juan, Puerto Rico

Steven A. Calle-Schuler
Institute of Neurobiology, University of Puerto Rico-Medical Sciences Campus, San Juan, Puerto Rico
ORCID iD: 0000-0003-1304-585X

Alexis Santana-Cruz
Institute of Neurobiology, University of Puerto Rico-Medical Sciences Campus, San Juan, Puerto Rico

Lucia Kmecova
Institute of Neurobiology, University of Puerto Rico-Medical Sciences Campus, San Juan, Puerto Rico

Jonathan M. Blagburn
Institute of Neurobiology, University of Puerto Rico-Medical Sciences Campus, San Juan, Puerto Rico
ORCID iD: 0000-0002-7681-2764

Eric D. Hoopfer
Neuroscience Program, Carleton College, Northfield, Minnesota
ORCID iD: 0000-0002-5888-0173

Andrew M. Seeds
Institute of Neurobiology, University of Puerto Rico-Medical Sciences Campus, San Juan, Puerto Rico
For correspondence: seeds.andrew@gmail.com
ORCID iD: 0000-0002-4932-6496

Copyright

© 2023, Eichler et al.

This article is distributed under the terms of the Creative Commons Attribution License, which permits unrestricted use and redistribution provided that the original author and source are credited.

Editors

Reviewing Editor
Sonia Sen
Tata Institute for Genetics and Society, Bangalore, India

Senior Editor
K VijayRaghavan
National Centre for Biological Sciences, Tata Institute of Fundamental Research, Bangalore, India

Reviewer #2 (Public Review):

The authors combine genetic tools, dye fills and connectome analysis techniques to generate a "first-of-its-kind", near complete, synaptic resolution map of the head bristle neurons of Drosophila. While some of the BMN anatomy was already known based on previous work by the authors and other researchers, this is the first time a near complete map has been created for the head BMNs at electron microscopy resolution.

Strengths:

(1) The authors cleverly use techniques that allow moving back and forth between periphery (head bristle location) and brain, as well as moving between light microscopy and electron microscopy data. This allows them to first characterize the pathways taken by different head BMNs to project to the brain and also characterize anatomical differences among individual neurons at the level of morphology and connectivity.
(2) The work is very comprehensive and results in a near complete map of all head BMNs.
(3) Authors also complement this anatomical characterization with a first-level functional analysis using optogenetic activation of BMNs that results in expected directed grooming behavior.

Weaknesses:
(1) While not strictly needed here, it could help provide context if authors revealed some of the important downstream pathways that could explain optogenetics behavioral phenotypes: This point was addressed by authors in the revisions and I agree a detailed description of downstream circuits is not needed at this point.
(2) In contrast to the rigorous quantitative analysis of the anatomical data, the behavioral data is analyzed using much more subjective methods. While I do not think it is necessary to perform a rigorous analysis of behaviors in this anatomy focused manuscript, the conclusions based on behavioral analysis should be treated as speculative in the current form e.g. calling "nodding + backward motions" as an avoidance response is not justified as it currently stands. Strong optogenetic activation could lead to sudden postural changes that due to purely biomechanical constraints could lead to a couple of backward steps as seen in the example videos. Moreover since the quantification is manual, it is not clear what the analyst interprets as backward walking or nodding. Interpretation is also concerning because controls show backward walking (although in fewer instances based on subjective quantification): This point was addressed by the authors during revisions and I'm mostly satisfied with their response, where authors agree that the behavioral results are currently used to speculate about the role of BMNs in aversive behaviors. Still, the fact that controls show some "backward motions" is a bit concerning when talking about "significant differences" between control and test groups based on manual annotations and I would recommend future studies focusing on these behaviors to use more unbiased quantitative analysis wherever possible.

Summary:

The authors end up generating a near-complete map of head BMNs that will serve as a long-standing resource to the Drosophila research community. This will directly shape future experiments aimed at modeling or functionally analyzing the head grooming circuit to understand how somatotopy guides behaviors. I appreciate the authors taking the time to revise the manuscript and address reviewer concerns.

https://doi.org/10.7554/eLife.87602.2.sa1

Reviewer #3 (Public Review):

Eichler et al. set out to catalog the mechanosensory bristles of the fly head in an effort to understand the extent to which their organization is consistent with the parallel model of hierarchical suppression in the context of grooming behavior. They map the locations of the mechanosensory bristles on the fly head, examine the axonal morphology of the bristle mechanosensory neurons (BMNs) that innervate them, and match these to electron microscopy reconstructions of the same BMNs in a previously published EM volume of the female adult fly brain. They use BMN synaptic connectivity information to create clusters of BMNs that they show occupy different regions of the subesophageal zone brain region and use optogenetic activation of subsets of BMNs to evaluate the behaviors evoked by specific activation of BMN subpopulations innervating the head.

The authors have beautifully cataloged the mechanosensory bristles and the projection paths and patterns of the corresponding BMN axons in the brain using detailed and painstaking methods. The result is a neuroanatomy resource that will be an important community resource. To match BMNs reconstructed in an electron microscopy volume of the adult fly brain, the authors matched clustered reconstructed BMNs with light-level BMN classes observed using precise dye-fills and stochastic labeling techniques. The authors then employ a variety of clustering methods to demonstrate that BMN populations that innervate different regions of the head project into the subesophageal zone and terminate in distinctive yet, in some cases, partially overlapping zones. By clustering BMNs on the basis of their synaptic partners, the authors find that BMNs from distant areas of the head have non-overlapping synaptic partners while those from neighbor areas have overlapping synaptic partners. This result calls into question the scale at which the parallel model of hierarchical suppression may be operating. Finally, the authors use tools that were generated during the light-level characterization of BMN projections to show that activating BMNs that innervate specific areas of the head leads to grooming of the innervated regions and neighboring regions, consistent with the observed overlap in downstream circuits between BMNs innervating neighboring regions of the head. This result suggests that while the parallel model could be operating on a broad scale, additional circuit mechanisms may be operating on a finer scale to produce grooming of the area surrounding the source of mechanosensory input.

This work will have a positive impact on the field by contributing a complete accounting of the mechanosensory bristles of the fruit fly head, describing the brain projection patterns of the BMNs that innervate them, and linking them to BMN sensory projections in an electron microscopy volume of the adult fly brain. It will also have a positive impact on the field by providing genetic tools to help functionally subdivide the contributions of different BMN populations to circuit computations and behavior. This contribution will pave the way for further mechanistic study of central circuits that subserve grooming circuits.

https://doi.org/10.7554/eLife.87602.2.sa0

Author Response

The following is the authors' response to the original reviews.

> ***eLife assessment***
>
> *This valuable work provides a near-complete description of the mechanosensory bristles on the Drosophila melanogaster head and the anatomy and projection patterns of the bristle mechanosensory neurons that innervate them. The data presented are solid. The study has generated numerous invaluable resources for the community that will be of interest to neuroscientists in the field of circuits and behaviour, particularly those interested in mechanosensation and behavioural sequence generation.*

We express our gratitude to the Reviewers for their valuable suggestions, which significantly enhanced the manuscript. The revisions were undertaken, not with the expectation of acceptance, but rather driven by our sincere belief that these revisions would enhance the manuscript's impact for future readers.

> ***Public Reviews:***
>
> ***Reviewer #1 (Public Review):***
>
> *Sensory neurons of the mechanosensory bristles on the head of the fly project to the sub esophageal ganglion (SEZ). In this manuscript, the authors have built on a large body of previous work to comprehensively classify and quantify the head bristles. They broadly identify the nerves that various bristles use to project to the SEZ and describe their region-specific innervation in the SEZ. They use dye-fills, clonal labelling, and electron microscopic reconstructions to describe in detail the phenomenon of somatotopy - conserved peripheral representations within the central brain - within the innervation of these neurons. In the process they develop novel tools to access subsets of these neurons. They use these to demostrate that groups of bristles in different parts of the head control different aspects of the grooming sequence.*
>
> ***Reviewer #2 (Public Review):***
>
> *The authors combine genetic tools, dye fills and connectome analysis techniques to generate a "first-of-its-kind", near complete, synaptic resolution map of the head bristle neurons of Drosophila. While some of the BMN anatomy was already known based on previous work by the authors and other researchers, this is the first time a near complete map has been created for the head BMNs at electron microscopy resolution.*
>
> *Strengths:*
>
> *(1) The authors cleverly use techniques that allow moving back and forth between periphery (head bristle location) and brain, as well as moving between light microscopy and electron microscopy data. This allows them to first characterize the pathways taken by different head BMNs to project to the brain and also characterize anatomical differences among individual neurons at the level of morphology and connectivity.*
>
> *(2) The work is very comprehensive and results in a near complete map of all I'm head BMNs.*
>
> *(3) Authors also complement this anatomical characterization with a first-level functional analysis using optogenetic activation of BMNs that results in expected directed grooming behavior.*
>
> *Weaknesses:*

> *(1) The clustering analysis is compelling but cluster numbers seem to be arbitrarily chosen instead of by using some informed metrics.*

We made revisions to the manuscript that address this concern. Please see our response to “recommendations for authors” for a description of these revisions.

> *(2) It could help provide context if authors revealed some of the important downstream pathways that could explain optogenetics behavioral phenotypes and previously shown hierarchical organization of grooming sequences.*

We made revisions to the manuscript that address this recommendation. Please see our response to “recommendations for authors” for a description of these revisions.

> *(3) In contrast to the rigorous quantitative analysis of the anatomical data, the behavioral data is analyzed using much more subjective methods. While I do not think it is necessary to perform a rigorous analysis of behaviors in this anatomy focused manuscript, the conclusions based on behavioral analysis should be treated as speculative in the current form e.g. calling "nodding + backward walking" as an avoidance response is not justified as it currently stands. Strong optogenetic activation could lead to sudden postural changes that due to purely biomechanical constraints could lead to a couple of backward steps as seen in the example videos. Moreover since the quantification is manual, it is not clear what the analyst interprets as backward walking or nodding. Interpretation is also concerning because controls show backward walking (although in fewer instances based on subjective quantification).*

While unbiased machine vision-based methods would nicely complement the present work, this type of analysis is not yet working to distinguish between different head grooming movements. Therefore, we are currently limited to manual annotation for our behavioral analysis. That said, we do not believe that our manual annotation is subjective. The grooming movements that we examine in this work are distinguishable from each other through frame-by-frame manual annotation of video at 30 fps. Our annotation of the grooming and backward motions performed by flies are based on previous publications that established a controlled vocabulary defining each movement (Hampel et al., 2020a, 2017, 2015; Seeds et al., 2014). In this work, we added head nodding to this controlled vocabulary that is described in the Materials and methods. We have added additional text to the third paragraph of the Material and methods section entitled “Behavioral analysis procedures” that we hope better describes our behavioral analysis. This description now reads:

Head nodding was annotated when the fly tilted its head downward by any amount until it returned its head back in its original position. This movement often occurred in repeated cycles. Therefore, the “start” was scored at the onset of the first forward movement and the “stop” when the head returned to its original position on the last nod.

We do not make any firm conclusions about the head movements (nodding) and backwards motions. We refer to nodding as a descriptive term that would allow the reader to better understand what the behavior looks like. We make no firm conclusions about any behavioral functional role that either the nodding or the backward motions might have, with the exception of nodding in the context of grooming. We only suggest that the behaviors appear to be avoidance responses. Furthermore, backward walking was not mentioned. Instead we refer to backward motions. We are only reporting our annotations of these movements that do occur, and are significantly different from controls. We speculate that these could be avoidance responses based on support from the literature. Future studies will be required to understand whether these movements serve real behavioral roles.

Summary:

The authors end up generating a near-complete map of head BMNs that will serve as a long-standing resource to the Drosophila research community. This will directly shape future experiments aimed at modeling or functionally analyzing the head grooming circuit to understand how somatotopy guides behaviors.

Reviewer #3 (Public Review):

Eichler et al. set out to map the locations of the mechanosensory bristles on the fly head, examine the axonal morphology of the bristle mechanosensory neurons (BMNs) that innervate them, and match these to electron microscopy reconstructions of the same BMNs in a previously published EM volume of the female adult fly brain. They used BMN synaptic connectivity information to create clusters of BMNs that they show occupy different regions of the subesophageal zone brain region and use optogenetic activation of subsets of BMNs to support the claim that the morphological projections and connectivity of defined groups of BMNs are consistent with the parallel model for behavioral sequence generation.

The authors have beautifully cataloged the mechanosensory bristles and the projection paths and patterns of the corresponding BMN axons in the brain using detailed and painstaking methods. The result is a neuroanatomy resource that will be an important community resource. To match BMNs reconstructed in an electron microscopy volume of the adult fly brain, the authors matched clustered reconstructed BMNs with light-level BMN classes using a variety of methods, but evidence for matching is only summarized and not demonstrated in a way that allows the reader to evaluate the strength of the evidence. The authors then switch from morphology-based categorization to non-BMN connectivity as a clustering method, which they claim demonstrates that BMNs form a somatotopic map in the brain. This map is not easily appreciated, and although contralateral projections in some populations are clear, the distinct projection zones that are mentioned by the authors are not readily apparent. Because of the extensive morphological overlap between connectivity-based clusters, it is not clear that small projection differences at the projection level are what determines the post-synaptic connectivity of a given BMN cluster or their functional role during behavior. The claim the somatotopic organization of BMN projections is preserved among their postsynaptic partners to form parallel sensory pathways is not supported by the result that different connectivity clusters still have high cosine similarity in a number of cases (i.e. Clusters 1 and 3, or Clusters 1 and 2). Finally, the authors use tools that were generated during the light-level characterization of BMN projections to show that specifically activating BMNs that innervate different areas of the head triggers different grooming behaviors. In one case, activation of a single population of sensory bristles (lnOm) triggers two different behaviors, both eye and dorsal head grooming. This result does not seem consistent with the parallel model, which suggests that these behaviors should be mutually exclusive and rely on parallel downstream circuitry.

We made revisions to the manuscript that address this recommendation. Please see our response to “recommendations for authors” for a description of these revisions.

This work will have a positive impact on the field by contributing a complete accounting of the mechanosensory bristles of the fruit fly head, describing the brain projection patterns of the BMNs that innervate them, and linking them to BMN sensory projections in an electron microscopy volume of the adult fly brain. It will also have a positive impact on the field by providing genetic tools to help functionally subdivide the contributions of different BMN populations to circuit computations and behavior. This contribution will

> *pave the way for further mechanistic study of central circuits that subserve grooming circuits.*
>
> ***Recommendations for the authors:***
>
> *All three reviewers appreciated the work presented in this manuscript. There were also a few overlapping concerns that were raised that are summarised below, should the authors wish to address them:*
>
> *Somatotopy: We recommend that the authors describe the extent of prior knowledge in more detail to highlight their contribution better.*

We made revisions that better highlight the extent of prior knowledge about somatotopy. We describe how previous studies showed bristle mechanosensory neurons in insects are somatotopically organized, but these studies were not comprehensive descriptions of complete somatotopic maps for the head or body. To our knowledge, our study provides the first comprehensive and synaptic resolution somatotopic map of a head for any animal. This sets the stage for the complete definition of the interface between somatotopically-organized mechanosensory neurons and postsynaptic circuits, which has broad implications for future studies on aimed grooming, and mechanosensation in general. Below we itemize revisions to the Introduction, Discussion, and Figures to provide a clearer statement of the significance of our study as it relates to somatotopy.

(1) Newly added Figure 1 – figure supplement 1 more explicitly grounds the study in somatotopy, providing a working model of the organization of the circuit pathways that produce the grooming sequence. This model features somatotopy as shown in Figure 1 – figure supplement 1C.

(2) Figure 1 – figure supplement 1 is incorporated into the Introduction in the second, third, and fourth paragraphs, the first paragraph of the Results section titled “Somatotopically-organized parallel BMN pathways”, and the second and third paragraphs of the last Discussion section titled “Parallel circuit architecture underlying the grooming sequence”.

(3) We added text to the end of the fourth paragraph of the Introduction that now reads: “In this model, parallel-projecting mechanosensory neurons that respond to stimuli at specific locations on the head or body could connect with somatotopically-organized parallel circuits that elicit grooming of those locations (Figure 1 – figure supplement 1A-C). The previous discovery of a mechanosensory-connected circuit that elicits aimed grooming of the antennae provides evidence of this organization (Hampel 2015). However, the extent to which distinct circuits elicit grooming of other locations is unknown, in part, because the somatotopic projections of the mechanosensory neurons have not been comprehensively defined for the head or body.”

(4) There is a Discussion section that further explains the extent of prior knowledge and our contributions on somatotopy that is titled “A synaptic resolution somatotopic map of the head BMNs”. Additionally, the previous version of this section had a paragraph on the broader implications of our work as it relates to somatotopy across species. In light of the reviewer comments, we decided to make this paragraph into its own Discussion section to better highlight the broader significance of our work. This section is titled “First synaptic resolution somatotopic map of the head”.

> *The somatotopy isn't overtly obvious - perhaps they could try mapping presynaptic sites and provide landmarks to improve visualisation.*

We made the following revisions to better highlight the head BMN somatotopy. One point of confusion from the previous manuscript version stemmed from us not explicitly defining the

somatotopic organization that we observed. There seemed to be confusion that we were defining the head somatotopy based only on the small projection differences among BMNs from neighboring head locations. While we believe that these small differences indeed correspond to somatotopy, we failed to highlight that there are overt differences in the brain projections of BMNs from distant locations on the head. For example, Figure 5B (right panel) shows the distinct projections between the LabNv (brown) and AntNv (blue) BMNs that innervate bristles on the ventral and dorsal head, respectively. Thus, BMN types innervating neighboring bristles show overlapping projections with small projection differences, whereas those innervating distant bristles show non overlapping projections into distinct zones.

Our analysis of postsynaptic connectivity similarity also shows somatotopic organization among the BMN postsynaptic partners, as BMN types innervating the same or neighboring bristle populations show high connectivity similarity (Figure 8, old Figure 7). Below we highlight major revisions to the text and Figures that hopefully better reveal the head somatotopy.

(1) In the last paragraph of the Introduction we added text that explicitly frames the experiments in terms of somatotopic organization: “This reveals somatotopic organization, where BMNs innervating neighboring bristles project to the same zones in the CNS while those innervating distant bristles project to distinct zones. Analysis of the BMN postsynaptic connectome reveals that neighboring BMNs show higher connectivity similarity than distant BMNs, providing evidence of somatotopically organized postsynaptic circuit pathways.”

(2) We mention an example of overt somatotopy from Figure 5 in the Results section titled “EM-based reconstruction of the head BMN projections in a full adult brain”. The text reads “For example, BMNs from the Eye- and LabNv have distinct ventral and anterior projections, respectively. This shows how the BMNs are somatotopically organized, as their distinct projections correspond to different bristle locations on the head (Figure 5B,C).”

(3) In new Figure 8 (part of old Figure 7), we modified panels that correspond to the cosine similarity analysis of postsynaptic connectivity. The major revision was to plot the cosine similarity clusters onto the head bristles so that the bristles are now colored based on their clusters (C). This shows how neighboring BMNs cluster together, and therefore show similar postsynaptic connectivity. We believe that this provides a nice visualization of somatotopic organization in BMN postsynaptic connectivity. We also added the clustering dendrogram as recommended by Reviewer #2 (Figure 8A).

(4) In new Figure 8, we added new panels (D-F) that summarize our anatomical and connectomic analysis showing different somatotopic features of the head BMNs. Different BMN types innervate bristles at neighboring and distant proximities (D). BMNs that innervate neighboring bristles project into overlapping zones (E, example of reconstructed BM-Fr and -Ant neurons with non-overlapping BM-MaPa neurons) and show postsynaptic connectivity similarity (F, example connectivity map of three BM types on cosine similarity data).

(5) To accompany the new Figure 8D-F panels, we added a paragraph to summarize the different somatotopic features of the head BMNs that were identified based on our anatomical and connectomic analysis. This is the last paragraph in the Results section titled “Somatotopically-organized parallel BMN pathways”:

Our results reveal head bristle proximity-based organization among the BMN projections and their postsynaptic partners to form parallel mechanosensory pathways. BMNs innervating neighboring bristles project into overlapping zones in the SEZ, whereas those innervating distant bristles project to distinct zones (example of BM-Fr, -Ant, and -MaPa neurons shown in Figure 8D,E). Cosine similarity analysis of BMN postsynaptic connectivity revealed that BMNs innervating the same bristle populations (same types) have the highest connectivity similarity. Figure 8F shows example parallel connections for BM-Fr, -Ant, and -MaPa neurons

(vertical arrows), where the edge width indicates the number of synapses from each BMN type to their major postsynaptic partners. Additionally, BMNs innervating neighboring bristle populations showed postsynaptic connectivity similarity, while BMNs innervating distant bristles show little or none. For example, BM-Fr and -Ant neurons have connections to common postsynaptic partners, whereas BM-MaPa neurons show only weak connections with the main postsynaptic partners of BM-Fr or -Ant neurons (Figure 8F, connections under 5% of total BMN output omitted). These results suggest that BMN somatotopy could have different possible levels of head spatial resolution, from specific bristle populations (e.g. Ant bristles), to general head areas (e.g. dorsal head bristles).

We also refer to Figure 8D-F to illustrate the different somatotopic features in the Discussion. These references can be found in the following Discussion sections titled “A synaptic resolution somatotopic map of the head BMNs (fourth paragraph)”, and “Parallel circuit architecture underlying the grooming sequence (second paragraph)”.

(6) In addition to improving the Figures, we provide additional tools that enable readers to explore the BMN somatotopy in a more interactive way. That is, we provide 5 different FlyWire.ai links in the manuscript Results section that enable 3D visualization of the different reconstructed BMNs (e.g. FlyWire.ai link 1).

Note: In working on old Figure 7 to address this Reviewer suggestion, we also reordered panels A-E. We believe that this was a more logical ordering than in the previous draft. These panels are now the only data shown in Figure 7, as the cosine similarity analysis is now in Figure 8. We hope that splitting these panels into two Figures will improve manuscript readability.

> *Light EM Mapping: A better description of methods by which this mapping was done would be helpful. Perhaps the authors could provide a few example parallel representations of the EM and light images in the main figure would help the reader better appreciate the strength of their approach.*

We have done as the Reviewers suggested and added panels to Figure 6 that show examples of the LM and EM image matching (Figure 6A,B). We added two examples that used different methods for labeling the LM imaged BMNs, including MCFO labeling of an individual BM-InOc neuron and driver line labeling of a major portion of BM-InOm neurons using InOmBMN-LexA. These panels are referred to in the first paragraph of the Results section titled “Matching the reconstructed head BMNs with their bristles”. Note that examples for all LM/EM matched BMN types are shown in Figure 6 – figure supplement 2.

We had provided Figure 6 – figure supplement 2 in the reviewed manuscript that shows all the above requested “parallel representations of the EM and light images”. However, the Reviewer critiques made us realize that the purpose of this figure supplement was not clearly indicated. Therefore, we have revised Figure 6 – figure supplement 2 and its legend to make its purpose clearer. First, we changed the legend title to better highlight its purpose. The legend is now titled: “Matching EM reconstructed BMN projections with light microscopy (LM) imaged BMNs that innervate specific bristles”. Second, we added label designations to the figure panel rows that highlight the LM and EM comparisons. That is, the rows for light microscopy images of BMNs are indicated with LM and the rows for EM reconstructed BMN images are labeled with EM. Reviewer #3 had indicated that it was not clear what labeling methods were used to visualize the LM imaged BM-InOm neurons in Figure 6 – figure supplement 2N. Therefore, we added text to the figure and the legend to better highlight the different methods used. Panels A and B were also cropped to accommodate the above mentioned revisions.

The manuscript also provides an extensive Materials and methods section that describes the different lines of evidence that were used to assign the reconstructed BMNs as specific types.

We changed the title to better highlight the purpose of this methods section to “Matching EM reconstructed BMN projections with light microscopy imaged BMNs that innervate specific bristles”. The evidence used to support the assignment of the different BMN types is also summarized in Figure 6 – figure supplement 3.

> *Parallel circuit model: The authors motivate their study with this. We're recommending that they define expectations of such circuitry, its alternatives (including implications for downstream pathways), and behavior before they present their results. We're also recommending that they interpret their behavioural results in the context of these circuits.*

Our primary motivation for doing the experiments described in this manuscript was to help define the neural circuit architecture underlying the parallel model that drives the Drosophila grooming sequence. This manuscript provides a comprehensive assessment of the first layer of this circuit architecture. A byproduct of this work is a contribution that offers immediate utility and significance to the Drosophila connectomics community. Namely, the description of the majority of mechanosensory neurons on the head, with their annotation in the recently released whole brain connectome dataset (FlyWire.ai). In writing this manuscript, we tried to balance both of these things, which was difficult to write. We very much appreciate the Reviewers' comments that have highlighted points of confusion in our original draft. We hope that the revised draft is now clearer and more logically presented. We have made revisions to the text and provided a new figure supplement (Figure 1 - figure supplement 1) and new panels in Figure 8. Below we highlight the major revisions.

(1) The Introduction was revised to more explicitly ground the study in the parallel model, while also removing details that were not pertinent to the experiments presented in the manuscript.

The first paragraph introduces different features of the parallel model. To better focus the reader on the parts of the model that were being assessed in the manuscript, we removed the following sentences: “Performance order is established by an activity gradient among parallel circuits where earlier actions have the highest activity and later actions have the lowest. A winner-take-all network selects the action with the highest activity and suppresses the others. The selected action is performed and then terminated to allow a new round of competition and selection of the next action.” Note that these sentences are included in the third and fourth paragraphs of the last Discussion section titled “Parallel circuit architecture underlying the grooming sequence”.

The first paragraph of the Introduction now introduces a bigger picture view of the model that emphasizes the two main features: 1) a parallel circuit architecture that ensures all mutually exclusive actions to be performed in sequence are simultaneously readied and competing for output, and 2) hierarchical suppression among the parallel circuits, where earlier actions suppress later actions.

(2) Newly added Figure 1 – figure supplement 1 provides a working model of grooming (Reviewer # 1 suggestion). We now more strongly emphasize that the study aimed to define the parallel neural circuit architecture underlying the grooming sequence, focusing on the mechanosensory layer of this architecture. In particular, we refer to the new Figure 1 – figure supplement 1 that has been added to better convey the hypothesized grooming neural circuit architecture. Figure 1 – figure supplement 1 is incorporated into the Introduction (paragraphs two, three, and four), Results section titled “Somatotopically-organized parallel BMN pathways (first paragraph)”, and last Discussion section titled “Parallel circuit architecture underlying the grooming sequence (second and third paragraphs)”.

(3) New panels in Figure 8 update the model of parallel circuit organization as it relates to somatotopy (D-F). These panels show the parallel circuits hypothesized by the model, but also

indicate convergence, with different possible levels of head resolution for these circuits. We describe above where these panels are referenced in the text.

(4) We added a new paragraph in the last Discussion section titled “Parallel circuit architecture underlying the grooming sequence” that better incorporates the results from this manuscript into the working model of grooming. This paragraph is shown below.

Here we define the parallel architecture of BMN types that elicit the head grooming sequence that starts with the eyes and proceeds to other locations, such as the antennae and ventral head. The different BMN types are hypothesized to connect with parallel circuits that elicit grooming of specific locations (described above and shown in Figure 1 – figure supplement 1A,C). Indeed, we identify distinct projections and connectivity among BMNs innervating distant bristles on the head, providing evidence supporting this parallel architecture (Figure 8D-F). However, we also find partially overlapping projections and connectivity among BMNs innervating neighboring bristles. Further, optogenetic activation of BMNs at specific head locations elicits grooming of both those locations and neighboring locations (Figure 9). These findings raise questions about the resolution of the parallel architecture underlying grooming. Are BMN types connected with distinct postsynaptic circuits that elicit aimed grooming of their corresponding bristle populations (e.g. Ant bristles)? Or are neighboring BMN types that innervate bristles in particular head areas connected with circuits that elicit grooming of those areas (e.g. dorsal or ventral head)? Future studies of the BMN postsynaptic circuits will be required to define the resolution of the parallel pathways that elicit aimed grooming.

> *Aside from this summary of major concerns, the detailed recommendations are attached below.*
>
> ***Reviewer #1 (Recommendations For The Authors):***
>
> *I appreciate the quality and exhaustive body of work presented in this manuscript. I have a few comments that the authors may want to consider:*
>
> *(1) The authors motivate this study by posing that it would allow them to uncover whether the complex grooming behaviour of flies followed a parallel model of circuit function. It would have been nice to have been introduced to what the alternative model might be and what each would mean for organisation of the circuit architecture. Some guiding schematics would go a long way in illustrating this point. Modifying the discussion along these lines would also be helpful.*

We made several revisions to the manuscript that address this recommendation. Among these revisions, we added Figure 1 – figure supplement 1 that includes a working model for grooming. Please see above for a description of these revisions.

> *(2) The authors mention the body of work that has mapped head bristles and described somatotopy. It would be useful to discuss in more detail what these studies have shown and highlight where the gaps are that their study fills.*

We made several revisions to the manuscript that address this recommendation. Please see above for a description of these revisions.

> *(3) The dye-fills and reconstructions that are single colour could use a boundary to demarcate the SEZ. This would help in orienting the reader.*

We agree with Reviewer #1 that Figure 4 and its supplements could use some indicator that would orient the reader with respect to the dye filled or stochastically labeled neurons. The images are of the entire SEZ in the ventral brain, and in the case of some panels, the

background staining enables visualization of the brain (e.g. Figure 4H,M,N. To help orient the reader in this region, we added a dotted line to indicate the approximate SEZ midline. This also enables the reader to more clearly see which of the BMN types cross the midline.

Midline visual guides were added for Figure 4, Figure 4 – figure supplement 2, Figure 4 – figure supplement 3, Figure 4 – figure supplement 4, Figure 4 – figure supplement 5, Figure 4 – figure supplement 6, Figure 4 – figure supplement 7, Figure 4 – figure supplement 8, Figure 6 – figure supplement 2.

> *(4) The comparison between the EM and the fills/clones are not obvious. And particularly because they are not directly determined, it would be nice to have the EM reconstruction alongside the dye-fills. This would work very nicely in the supplementary figure with the multiple fills of the same bristles. I think this would really drive home the point.*

We made several revisions to the manuscript that address this recommendation. Please see above for a description of these revisions.

> *(5) Are there unnoticed black error-bars floating around in many of the gray-scale images?*

The black bars were masking white scale bars in the images. We have removed the black bars and remade the images without scale bars. This was done for the following Figures: Figure 4, Figure 4 – figure supplement 2, Figure 4 – figure supplement 3, Figure 4 – figure supplement 4, Figure 4 – figure supplement 5, Figure 4 – figure supplement 6, Figure 4 – figure supplement 7, Figure 4 – figure supplement 8, Figure 6 – figure supplement 2.

> ***Reviewer #2 (Recommendations For The Authors):***
>
> *(1) The only point in the paper I found myself going back and forth between methods/supp and text was when authors discuss about the clustering. I think it would help the reader if a few sentences about cosine clustering used for connectivity based clustering were included in the main text. Also, for NBLAST hierarchical clustering, it would help if some informed metrics could be used for defining cluster numbers (e.g. Braun et al, 2010 PLOS ONE shows how Ward linkage cost could be used for hierarchical clustering).*

Depending on where the cut height is placed on the dendrogram for cosine similarity of BMNs, different features of the BMN type postsynaptic connectivity are captured. As the number of clusters is increased (lower cut height), clustering is mainly among BMNs of the same type, showing that these BMNs have the highest connectivity similarity. As the number of clusters is reduced (higher cut height), BMNs innervating neighboring bristles on the head are clustered, revealing three general clusters corresponding to the dorsal, ventral, and posterior head. This reveals somatotopy based clustering among same and neighboring BMN types. The cut height shown in Figure 8 and Figure 8 – figure supplement 2 was chosen because it highlighted both of these features.

The NBLAST clustering shows similar results to the connectivity based clustering with respect to neighboring and distant BMN types. As the number of clusters increases BMNs of the same type are clustered, and these types can be further subdivided into morphologically distinct subtypes. As the number of clusters is reduced, the clustering captures neighboring BMNs. Thus, neighboring BMN types showed high morphology similarity (and proximity) with each other, and low similarity with distant BMN types.

Please see our responses to a Reviewer #3 critique below for further description of the clustering results.

> *On the same lines it would help if the clustering dendrograms were included in the main figure.*

We thank Reviewer #2 for this comment. We have added the dendrogram to Figure 8A, a change that we feel makes this Figure much easier to understand.

> *(2) It could help provide intuition if the authors revealed some of the downstream targets and their implication in explaining the behavioral phenotypes.*

While this will be the subject of at least two forthcoming manuscripts, we have added text to the present manuscript that provides insight into BMN postsynaptic targets. Our previous work (Hampel et al. 2015) described a mechanosensory connected neural circuit that elicits grooming of the antennae. While this previous study demonstrated that the Johnston's organ mechanosensory neurons are synaptically and functionally connected with this circuit, our preliminary analysis indicates that it is also connected with BM-Ant neurons. We hypothesize that there are additional such circuits that are responsible for eliciting grooming of other head locations.

To better highlight potential downstream targets in the manuscript, we now mention the antennal circuit in the Introduction. This text reads: In this model, parallel-projecting mechanosensory neurons that respond to stimuli at specific locations on the head or body could connect with somatotopically-organized parallel circuits that elicit grooming of those locations (Figure 1 – figure supplement 1A-C). The previous discovery of a mechanosensory-connected circuit that elicits aimed grooming of the antennae provides evidence of this organization (Hampel 2015). However, the extent to which distinct circuits elicit grooming of other locations is unknown, in part, because the somatotopic projections of the mechanosensory neurons have not been comprehensively defined for the head or body.

There is also text in the Discussion that addresses this Reviewer comment. It describes the antennal circuit and mentions the possibility that other similar circuits may exist. This can be found in the third paragraph of the section titled "Circuits that elicit aimed grooming of specific head locations".

> *(3) Authors find that opto activation of BMNs leads to grooming of targeted as well as neighboring areas. Is there any sequence observed here? i.e. first clean targeted area and then clean neighboring area? I wonder if the answer to this is something as simple as common post-synaptic targets which is essentially reducing the resolution of the BMN sensory map. Some more speculation on this interesting result could be helpful.*

We appreciate and agree with this point from Reviewer #2, and have tried to better emphasize the possible implications for grooming that the overlapping projections and connectivity among BMNs innervating neighboring bristles may have. This is now better addressed in the Results and Discussion sections. Below we highlight where this is addressed:

(1) In the second paragraph of the Results section titled "Activation of subsets of head BMNs elicits aimed grooming of specific locations" we added text that suggests the possibility that grooming of the stimulated and neighboring locations could be due to the overlapping projections and connectivity. This text reads: This suggested that head BMNs elicit aimed grooming of their corresponding bristle locations, but also neighboring locations. This result is consistent with our anatomical and connectomic data indicating that BMNs innervating neighboring bristles show overlapping projections and postsynaptic connectivity similarity (see Discussion).

(2) In the fourth paragraph of the Discussion section titled “A synaptic resolution somatotopic map of the head BMNs”, we added a sentence to the end of the fourth paragraph that alludes to further discussion of this topic. This sentence reads: This overlap may have implications for aimed grooming behavior. For example, neighboring BMNs could connect with common neural circuits to elicit grooming of overlapping locations (discussed more below).

(3) In the fourth paragraph of the Discussion section titled “Circuits that elicit aimed grooming of specific head locations” there is a paragraph that mentions the possibility of mechanosensory convergence onto common postsynaptic circuits to promote grooming of the stimulated area, along with neighboring areas. This paragraph is below.

We find that activation of specific BMN types elicits both aimed grooming of their corresponding bristle locations and neighboring locations. This suggests overlap in the locations that are groomed with the activation of different BMN types. Such overlap provides a means of cleaning the area surrounding the stimulus location. Interestingly, our NBLAST and cosine similarity analysis indicates that neighboring BMNs project into overlapping zones in the SEZ and show common postsynaptic connectivity. Thus, we hypothesize that neighboring BMNs connect with common neural circuits (e.g. antennal grooming circuit) to elicit overlapping aimed grooming of common head locations.

(4) In the new second paragraph of the Discussion section titled “Parallel circuit architecture underlying the grooming sequence” we further discuss the issue of the BMN “sensory map. This paragraph is below.

Here we define the parallel architecture of BMN types that elicit the head grooming sequence that starts with the eyes and proceeds to other locations, such as the antennae and ventral head. The different BMN types are hypothesized to connect with parallel circuits that elicit grooming of specific locations (described above and shown in Figure 1 – figure supplement 1A,C). Indeed, we identify distinct projections and connectivity among BMNs innervating distant bristles on the head, providing evidence supporting this parallel architecture (Figure 8D-F). However, we also find partially overlapping projections and connectivity among BMNs innervating neighboring bristles. Further, optogenetic activation of BMNs at specific head locations elicits grooming of both those locations and neighboring locations (Figure 9). These findings raise questions about the resolution of the parallel architecture underlying grooming. Are BMN types connected with distinct postsynaptic circuits that elicit aimed grooming of their corresponding bristle populations (e.g. Ant bristles)? Or are neighboring BMN types that innervate bristles in particular head areas connected with circuits that elicit grooming of those areas (e.g. dorsal or ventral head)? Future studies of the BMN postsynaptic circuits will be required to define the resolution of the parallel pathways that elicit aimed grooming.

> *(4) If authors were to include a summary table that shows all known attributes about BMN type as columns that could be very useful as a resource to the community. Table columns could include attributes like "bristle name", "nerve tract", "FlyWire IDs of all segments corresponding to the bristle class". "split-Gal4 line or known enhancer" , etc.*

We provided a table that includes much of this information after the manuscript had already gone out for review. We regret that this was not available. This is now provided as Supplementary file 3. This table provides the following information for each reconstructed BMN: BMN name, bristle type, nerve, flywire ID, flywire coordinates, NBLAST cluster (cut height 1), NBLAST cluster (cut height 5), and cosine cluster (cut height 4.5). Note that the driver line enhancers for targeting specific BMN types are shown in Figure 3I.

> *Specific Points:*

> *Figure 4C-V:*
>
> - *I find it a bit difficult to distinguish ipsi- from contra-lateral projections. Maybe indicate the midline as a thin, stippled line?*

We thank the Reviewer #2 for this suggestion. We have now added lines in the panels in Figure 4C-V to indicate the approximate location of the midline. We also added lines to the Figure 4 – figure supplements as described above.

> *I think this Fig reference is wrong "the red-light stimulus also elicited backward motions with control flies (Figure 6B,C, control, black trace, Video 5)." should be Fig 8B,C*

We have fixed this error.

> ***Reviewer #3 (Recommendations For The Authors):***
>
> *Introduction:*
>
> *Motivating this study in terms of understanding the neural mechanisms that execute the parallel model seems to overstate what you will achieve with the current study. If you want to motivate it this way, I suggest focusing on the grooming sequence of the head along (eyes, antennae, proboscis).*

We made several revisions to the manuscript that address this recommendation. Please see above for a description of these revisions. Please note that many of the revisions focus on the head grooming sequence. We also made minor revisions to the Introduction that further emphasize the focus on head grooming.

> *Results:*
>
> *Figure 1. Please indicate that this is a male fly in either the figure title or in the figure itself.*

We added a male symbol to Figure 1A.

> *Figure 3. Panel J is referenced in the main body text and in the figure caption, but there is no Fig 3J.*

Panel J is shown in the upper right corner of Figure 3. We realize that the placement of this panel is not ideal, but this was the only place that we could fit it. Additionally, the panel works nicely at that location to better enable comparison with panel C. We have revised the text in the Figure 3 legend to better highlight the location of this Figure panel: “Shown in the upper right corner of the figure are the aligned expression patterns of InOmBMN-LexA (red), dBMN-spGAL4 (green), and TasteBMN-spGAL4 (brown).”

We also added text to a sentence in the results section entitled “Head BMNs project into discrete zones in the ventral brain” that indicates the panel location. This text reads: To further visualize the spatial relationships between these projections, we computationally aligned the expression patterns of the different driver lines into the same brain space (Figure 3J, upper right corner).

> *Matching the BMNs to EM reconstructions: why cut the dendrogram at H=5? Would be better to determine cluster number using an unbiased method.*

To match the morphologically distinct EM reconstructed BMNs to their specific bristles, we relied on different lines of evidence, including NBLAST results (discussed more below), dye fill/stochastic labeling/driver line labeling matches, published morphology, nerve projection, bristle number, proximity to other BMNs, and postsynaptic connectivity (summarized in Figure 6 – figure supplement 3). The following Materials and methods section provides a detailed description of the evidence used to assign each BMN type in "Matching EM reconstructed BMN projections with light microscopy imaged BMNs that innervate specific bristles". In many cases, BMN type could be assigned with confidence solely based on morphological comparisons with our light level data (e.g. dye fills), in conjunction with bristle counts to indicate an expected number of BMNs showing similar morphology. Thus, the LM/EM matches and NBLAST clustering were largely complementary.

The EM reconstructed BMNs were matched as particular BMN types, in part based on examination of the NBLAST data at different cut heights. NBLAST clustering of the BMNs revealed general trends at higher and lower cut heights (Figure 6 – figure supplement 1A, Supplementary file 3). The lowest cut heights included mostly BMNs of the same type innervating the same bristle populations, and smaller clusters that subdivided into morphologically distinct subtypes (see Supplementary file 3 for clusters produced at cut height 1). This revealed that BMNs of the same type tended to show the highest morphological similarity with each other, but they also showed intratype morphological diversity. Higher cut heights produced clusters of BMNs innervating neighboring bristles populations (e.g. ventral head BMNs), showing high morphological similarity among neighboring BMN types.

We selected the cut height 5 shown in Figure 6 – figure supplement 1A,B because it captures examples of both same and neighboring type clustering. For example, it captures a cluster of mostly BM-Taste neurons (Cluster 16), and neighboring BMN types, including those from the dorsal head (Cluster 14) or ventral head (Cluster 15).

Based on reviewer comments, we realized that the way we wrote the BMN matching section in the Results indicated more reliance on the NBLAST clustering than what was actually necessary, distorting the way we actually matched the BMNs. Therefore, we softend the first couple of sentences to place less emphasis on the importance of the NBLAST. We also indicated that the readers can find the resulting clusters at different cut heights, referring to Figure 6 – figure supplement 1A and Supplementary file 3. The first two sentences of the first paragraph in the Results section titled "Matching the reconstructed head BMNs with their bristles" now read:

The reconstructed BMN projections were next matched with their specific bristle populations. The projections were clustered based on morphological similarity using the NBLAST algorithm (example clustering at cut height 5 shown in Figure 6 – figure supplement 1A,B, Supplementary file 3, FlyWire.ai link 2) (Costa et al., 2016). Clusters could be assigned as BMN types based on their similarity to light microscopy images of BMNs known to innervate specific bristles.

> *The number of reconstructed BMNs is remarkably similar to what is expected based on bristle counts for each group except for lnOm. Why do you think there is such a large discrepancy there?*

We believe that there is a discrepancy between the number of reconstructed BM-InOm neurons and the number expected based on InOm bristle counts because these bristle counts were based on few flies and these numbers appear to be variable. We did not further investigate the numbers of InOm bristles in this manuscript because we only needed an estimate of their numbers, given that there is over an order of magnitude difference in the eye bristles versus any other head bristle population. Therefore, we could relatively easily

conclude that the head BMNs were related to the InOm bristles, based on their sheer numbers and their morphology.

> *Figure 6 - figure supplement 2N, please describe these panels better. Main text says the upper image is from lnOmBMN-LexA, but the figure legend doesn't agree.*

We have added text to the figure legend that now makes the contents of panel 2N clear to the reader. Further, we now indicate in the figure legend for each panel, the method used to obtain the labeled neurons (i.e. fill, MCFO, driver), to avoid similar confusion for the other panels.

> *Figure 6 - figure supplement 4D. How frequently is there a mismatch between the number of BMNs for a given type across hemispheres?*

Although the full reconstruction of the BMNs on both sides of the brain was beyond the scope of this work, the BMNs on both sides have since been reconstructed and annotated (Schlegal et al. 2023). We plan to provide more analysis of BMNs on both sides of the brain in a forthcoming manuscript. However, the BMN numbers tend to show agreement on both sides of the brain. The table below shows a comparison between the two sides:

Author response table 1.

Type	LM counts	EM left side	EM right side
Ant	18-22	20	21
Fr	4-7	6	7
FrOr	4-6	6	7
Or	3	3	3
Oc	1	1	1
InOc	3-4	3	3
Vib	13-18	18	19
InOm	607-645	555	557
vOcci/vPoOr	21-33	26	26
MaPa	14-18	15	15
Hau	5	5	5
Taste	31-42	35	29
Vt/PoOc	4-5	5	5
dPoOr	5-9	4	8
dOcci	2-5	3	3

> *Figures 6 and 7. It would be helpful to include a reference brain in all panels that show cluster morphology. Without landmarks there is nothing to anchor the eye to allow the reader to see the described differences in BMN projection zones and patterns.*

While we apologize for not making this specific change, we have made revisions to other parts of the manuscript to better highlight the somatotopic organization among the BMNs (revisions described above). Please note that we now provide FlyWire.ai publicly available links that enable readers to view the BMN projections in 3D. They can also toggle a brain mesh on and off to provide spatial reference.

> *"BMN somatotopic map": It would be helpful to show or describe in more detail what the unique branch morphology for each zone is. It is quite difficult to appreciate, as the groups also have a lot of overlap. Would the unique regions that the BMN groups innervate be easier to see if you plotted presynaptic sites by group? I am left unsure about whether there is a somatotopic map here.*

We made several revisions to the manuscript that address this recommendation. Please see above for a description of these revisions. Please note that we did not examine the fine branch morphological differences between BMN types having overlapping projections. Showing these differences would require more extensive anatomical analysis that is beyond the scope of this work. For showing definitive somatotopy, we focused on the overt differences between BMNs innervating bristles at distant locations on the head.

> *Overall the strict adherence to the parallel model impacts the interpretation of the data. It would be helpful for the authors to discuss which aspects of the current study are consistent with the parallel model and which results are not consistent.*

We made several revisions to the manuscript that address this recommendation. Please see above for a description of these revisions.

> *Discussion:*
>
> *"Circuits that elicit aimed grooming of specific head locations": In the previous paragraph you mention "BMN types innervating neighboring bristle populations have overlapping projections into zones that correspond roughly to the dorsal, ventral, and posterior head. The overlap is likely functionally significant, as cosine similarity analysis revealed that neighboring head BMN types have common postsynaptic partners. However, overlap between neighboring BMN types is only partial, as they show differing projections and postsynaptic connectivity." Then in this paragraph, you say, "How do the parallel-projecting head BMNs interface with postsynaptic neural circuits to elicit aimed grooming of specific head locations? Different evidence supports the hypothesis that the BMNs connect with parallel circuits that each elicit a different aimed grooming movement (Seeds et al., 2014)." The overlapping postsynaptic BMN connectivity seems in conflict with the claim that the circuits are parallel.*

We apologize for this confusion. We now better describe this apparent discrepancy between our results and the parallel model of grooming behavior. We made several revisions to the manuscript that address this recommendation. Please see above for a description of these revisions.

We have made additional changes to the manuscript:

(1) We added Supplementary file 2 that includes links for downloading the image stacks used to generate panels in Figure 1, Figure 2, Figure 3, Figure 4, and figure supplements for these figures. These image stacks are stored in the Brain Image Library (BIL). Rows in the spreadsheet correspond to each image stack. Columns provide information about each stack including: figure panels that each image stack contributed to, image stack title, DOI for each stack (link provides metadata for each stack and file download link), image stack file name, genotype of imaged fly, and information about image stack. References to this file have been made at different locations throughout the text and Figure legends. We also added a section on the BIL data in the Materials and methods entitled “Light microscopy image stack storage and availability”. Old Supplementary file 2 has been renamed Supplementary file 3.

(2) We added a new reference for FlyWire.ai (Dorkenwald et al. 2023) that was posted as a preprint during the revision of this manuscript.